Doctoral Dissertation
Doctoral Program in Material Science and Technology (33th Cycle)

Photo-responsive polymer networks for the design of polymer coatings with light-tunable properties

Angelo Romano

Supervisors:

- Prof. Marco Sangermano, Supervisor - Politecnico di Torino, Department of Applied Science and Technology (Torino, Italy)
- Prof. Sandra Schlögl, Co-Supervisor - Polymer Competence Center Leoben (Leoben, Austria)
- Dr. Ignazio Roppolo, Co-Supervisor - Politecnico di Torino, Department of Applied Science and Technology (Torino, Italy)

Doctoral Examination Committee:

- Dr. Paula Bosch - Spanish National Research Council, Institute of Polymer Science and Technology (Madrid, Spain) (Reviewer)
- Prof. Mats Johansson - KTH Royal Institute of Technology, Department of Fibre & Polymer Technology, School of Chemical Science and Engineering (Stockholm, Sweden) (Reviewer)
- Prof. Thomas Grießer - Montanuniversität Leoben (Leoben, Austria)
- Prof. Eva Blasco - Ruprecht-Karls-Universität Heidelberg (Heidelberg, Germany)
- Dr. Yves Leterrier - École Polytechnique Fédérale de Lausanne (Lausanne, Switzerland)

Politecnico di Torino
2021

Declaration

I hereby declare that, the contents and organization of this dissertation constitute my own original work and does not compromise in any way the rights of third parties, including those relating to the security of personal data.

……

Angelo Romano
Torino 2021

Acknowledgments

I would like to dedicate this thesis to my aunt Ilsa, without her I wouldn't have come to Turin in 2009 and started all this incredible adventure that lasted almost 12 years. I would like to express my gratitude from the deepest of my heart to my supervisor Prof. Marco Sangermano for giving me this opportunity and for supporting me during these years of PhD. He was really patient with me, and I appreciate a lot the freedom he gives to everyone in the group, and how he cares for every PhD student. I would also like to express my deepest thanks to Prof. Sandra Schlögl that wrote my PhD project, and of course for the pure kindness she always showed me during these years. Without her I wouldn't probably have started a PhD. I would also love to deeply thanks Dr. Ignazio Roppolo that with his talent and friendship gave me huge support in this experience. Different ideas and solutions behind my works came from him. A deep thanks also to Prof. Thomas Grießer and Prof. Wolfgang Kern for hosting me in the university lab in Leoben.

I would love to thank all my friends and colleagues, the list will be huge but I will try. I would like to thank Luigi for all the friendship he showed me and for helping me in the most difficult moments. Thanks to Matteo for the long conversations we had during this last period we lived together. Thanks to Nicolò for the help and suggestions, and for all the great moments we spent together in the conference in Cancùn. Thanks to Duccio, I am happy this PhD gave me you as a friend. Thanks to my colleagues for the patience to handle my disorganization, for the lunches together: Simone, Gustavo, Parnian, Giuseppe, Camilla, Andrea, Lollo, Michael, Diana, Annalisa, Luisa, Andrea. Thanks to Carlos for all the ideas and the brainstorming we had in every different fields and to Maitè for the afternoons spent together in Turin. I will miss it a lot.

I would also like to thank all my friends and colleagues I have met during the periods spent in Leoben. Santhosh for his welcoming when I arrived the first year and for all the moments together. Thanks to Hojabr for his hospitality and friendship during this last year. Thanks to Ines for the friendship she always showed to me, to Ata and Walter for the barbeque, tea and conversations we had in mineroom. Thanks to all my friends and colleagues I have met there: Elisabeth, Paul, Krzysztof, Delara, Daniel, Michael, Luis, Chiara, Elisa, Simon, Nastia, Lara. I had very cool dinners and hiking tours with you, I will miss it a lot. Thanks also to Catharina, Boris, Simone, Evelyne, Gema, Romana, Rita and Jakob for the welcoming and help in the laboratory. Thanks to you I was feeling more than home in the lab and in the city during these years.

Finally, I would love to give a special thanks to my girlfriend Maya. I have met her also during (and thanks) to this PhD and in different ways she was

fundamental during these years. Thanks for being so close to me even when we were thousands of miles away. Thanks to my sister and my parents to be next to me during all these university years. Thanks to my friend Vito, without your motivation and your example I think I would have not done many choices that took me here. Thanks also to my historical friends: Nicolo, Valentino and Rocco. I think without our conversations and your advices it would have been different. I would finally love to express my gratitude to whoever took me here, I really think it was the best period of my life and I will always keep it moment by moment inside the deepest part of me.

Abstract

Stimuli-responsive or “smart” polymers refer to a class of macromolecules that undergo physical changes or chemical reactions upon certain stimuli such as temperature, magnetic field, pH or light. Among this class of macromolecules, light-responsive ones have gained increased attention in the design of functional materials, as they allow changes in polymers properties, on demand, and simply by light exposure. For instance, compared to other stimuli, light offers many advantages such as high temporal and spatial control of the photo-triggered reaction, and furthermore the irradiation parameters, such as light intensity, wavelength and irradiation time, can be remotely controlled and easily modulated to adequately comply with the system. For these reasons, in the last years, several photosensitive moieties were introduced in various polymer networks in order to achieve light responsive properties. Among photo-responsive molecules, ortho-nitrobenzyl ester (o-NBE) chemistry has become a common route in the design of polymer networks with photo-responsive properties. Upon UV irradiation, o-NBE groups undergo a cleavage reaction yielding carboxylic acids and o-nitrosobenzaldehyde as primary photoproducts, therefore promoting physical and chemical changes in the polymer networks in which they are applied.

In this thesis, the light responsive properties of o-NBE chemistry were exploited for the fabrication of photo-responsive polymer coatings and silica microparticles. The idea beyond each experimental contribution was to demonstrate how light triggers can be a convenient and a powerful tool for both the synthesis and the post-modification of polymer networks, ensuring hight reaction yields and fast reaction rate within mild reaction conditions.

Following this purpose, monomers containing o-NBE groups and with different end functionalities, such as epoxy, vinyl and acrylate, were first synthesized and then polymerized by means of photo-triggered reaction. Once the network was formed, the photo-responsive nature of o-NBE moieties was conveniently exploited for changing bulk and surface properties of the synthesized systems.

In a first work, photo-responsive thiol-epoxy networks were prepared following a photobase-catalyzed nucleophilic ring opening reaction among epoxy monomers with photolabile o-nitrobenzyl ester (o-NBE) groups and tri-functional thiols. In order to not promote the o-NBE cleavage reaction while curing, isopropylthioxanthone derivatives were employed as photosensitizer for shifting the photoinduced curing reaction to visible light region. Once the network has been formed, the o-NBE moieties were used for a well-defined network degradation upon UV exposure. Sol-gel analysis evidenced the formation of soluble species, which were exploited to inscribe positive tone micropatterns by photolithography technique. Along with the localized tuning of network structure, the irreversible o-NBE photoreaction was exploited to change the surface wettability of the thiol-

epoxy networks. The water contact angle significantly decreased upon UV exposure due to the photo-induced formation of hydrophilic cleavage products, enabling the inscription of domains with different surface wettability.

In a following work, it was proposed a novel method for the polymer coatings photopatterning, which employed a direct laser beam irradiation of the coatings surface instead of classical photomasking techniques. In this aim, photo-responsive thiol-ene polymer networks containing o-NBE moieties were first photopolymerized upon visible light irradiation, and subsequently cleaved with an UV laser beam. Compared to the commonly used photomasking techniques, direct laser beam irradiation gave many advantages such as the formation of sharp and defined 2.5D structures, that were developed directly through laser surface ablation and without the use of harsh solvents. Along with the fabrication of dry-developable micropatterns, the chemical surface composition of the exposed areas was conveniently adjusted and different domains with a tailored content of carboxylic groups, as o-NBE reaction products, were obtained simply by modulating the laser energy dose. In a following step, those groups were activated and exploited as anchor points for attaching an Alexa-546 conjugated Protein A, showing high linearity between laser energy dose and the amount of grafted proteins. Therefore, laser writer technique combined with the synthetized light-responsive networks demonstrated to be a convenient method for the fabrication of positive tone patterns, opening also future prospective for a wide range of biosensing applications.

In a last contribution, silica microparticles with light responsive polymer brushes were synthetized. For the polymer brush synthesis, two different procedures were followed and respectively; a photo-grafting from and an amino-epoxy coupling reaction. For the photochemical grafting path, BAPO photo-initiators derivatives with alkoxy-silane ending groups were anchored onto the silanol groups of silica microparticles. Light responsive polymer brushes were then grown upon visible light irradiation, exploiting a radical mediated reaction among the BAPO surface anchored photo-initiators and a synthesized acrylate monomer with o-NBE pendant groups. In a second procedure, the photo-responsive polymer brushes were synthetized trough an amino-epoxy coupling reaction among the primary amine of surface anchored trimethoxy silanes and a photo-responsive epoxy monomer containing o-NBE groups. Compared to the amino-epoxy reaction, the photochemical synthesis ensured higher grafting efficiency in terms of grafted polymer (about 3 mg/m^2) versus reaction time (4 hours), employing milder reaction conditions. Once the polymer brushes were formed, the o-NBE pending groups were exploited in order to change the particles surface properties upon UV light exposure. Zeta potential measurements and XPS spectroscopy demonstrated that physical and chemical surface properties of the silica particles were successfully modified due to the formation of carboxylic acids groups. Eventually, the presence of the photo-deprotected carboxylic acids onto silica particles were confirmed by conjugating an Alexa-546 fluorescent Protein. Confocal microscopy images proved the selective anchoring of the fluorescent protein only onto the UV irradiated particles, showing how ortho-nitrobenzyl chemistry can be efficiently exploited for the fabrication of light responsive particles.

"The important thing is not to stop questioning. Curiosity has its own reason for existence. One cannot help but be in awe when he contemplates the mysteries of eternity, of life, of the marvelous structure of reality. It is enough if one tries merely to comprehend a little of this mystery each day"

Albert Einstein: LIFE Magazine 2 May 1955

Contents

1.Introduction

Stimuli-responsivity can be defined as the ability of matter to change its properties, interactions, structure and/or dimensions once exposed to a well-defined chemical or physical stimulus (e.g. light, pressure, pH, humidity, temperature, magnetic field) [1].

Stimuli-responsiveness is a characteristic of paramount importance, especially for living matter. Biological functions rely on macromolecular structures that are responsive to exogenous or endogenous triggers [2,3]. Several examples can be given to such systems, as for instance the all involved light-triggered reactions in photosynthesis, or the electro-chemical stimuli employed in muscle fibres contraction [2–7].

Since the development of scientific method, understanding how and why molecules, materials, and/or complex systems behave has become the goal of scientists working in all the different fields. For instance, the interpretation of underlying matter's mechanisms is not only of biological interest but also paves the way for the development of materials that can replicate and exploit similar properties into synthetic materials [3,6,7].

On the other hand, development of chemistry led to the synthesis of synthetic molecules which show controllable behaviour under determined stimuli.

Therefore, employing stimuli-responsive or adaptive materials, whose properties can be controlled in a specific and predictable manner upon exposure to a certain stimulus, is fundamental for imparting features in artificial structures, and synthesize the so-called "smart materials" [8,9].

In this regards, responsive molecules that undergo changes in their structure or properties upon the application of external stimuli nowadays represent one of the most ambitious research areas in many scientific fields such as nanomedicine, biology, and functional coatings [10–13]. Typical external stimuli include both physical stimuli such as temperature, light, or magnetic field and chemical stimuli such as redox or pH value [14–16].

Among these stimuli, light has undoubted advantages in terms of spatial and temporal accuracy, including the possibility to be activated and deactivated on demand. Furthermore, photo-triggered reactions proceed under mild reaction conditions and are remotely controllable [17,18].

First documented scientific investigations of photo-triggered chemical reactions were carried out since 1790 by Joseph Priestley, which is considered one of the "fathers" of photo chemistry [19]. He gave important contributions in the study of nitric acid colour change and decomposition in presence of sunlight, and he was one of the first scientist to study the photosynthesis processes[19].

During the 19th century more and more photochemical reactions were described. For instance, Döbereiner explored inorganic photo-reactions of iron(III) oxide and oxalic acid that upon visible light and in aqueous solutions generate

carbon dioxide and iron(II) oxide. This reaction with appropriate modifications became the starting point for ferrioxalate actinometry [19–21]. Besides inorganic reactions, Trommsdorff, Sestini and Cannizzaro investigated the photochemical induced rearrangement of santonin, which is the longest known photoreaction of an organic compound, widely used at that time as active ingredient in medicine [19,22]. In the same years, Peter Griess conducted important works on Diazo and Diazonium Compounds that are still widely adopted as dyes and/or photo-responsive molecules in many applications [19,23].

During last decades of 19th century and the beginning of 20th century, the studies of Giacomo Ciamician and Paul Silber were remarkable as they carried out pioneering works on coumarin and nitrobenzyl compounds [19,24,25]. In 1912, Ciamician held a "visionary" lecture on "The photochemistry of the future" at the international congress of Applied Chemistry in New York, predicting the important role of photo-chemistry for future applications [26]. In this lesson he mentioned inventions that would have been made in the following decades, such as solar home heating or batteries based on photochemical processes [26].

In the second half of 20th century the enhanced possibility to synthesize and to characterize chemical structures, allowed a deeper study of light-responsive mechanisms, therefore driving more and more fundamental applications for these molecules in different fields of material science. For these reasons, in last decades several photo-responsive molecules were synthetized and exploited in numerous areas ranging from organic synthesis to polymer chemistry [17,18,27,28]

In a further distinction, light-responsive molecules may undergo through reversible or irreversible reactions, depending on the possibility or not for the molecules to recover their initial structures [17,18,29–31]. Prominent chromophores enabling reversible reactions are azobenzene groups (cis-trans isomerization), coumarin and anthracene derivatives (reversible cycloaddition reactions) (Figure 1.1) [29,31].

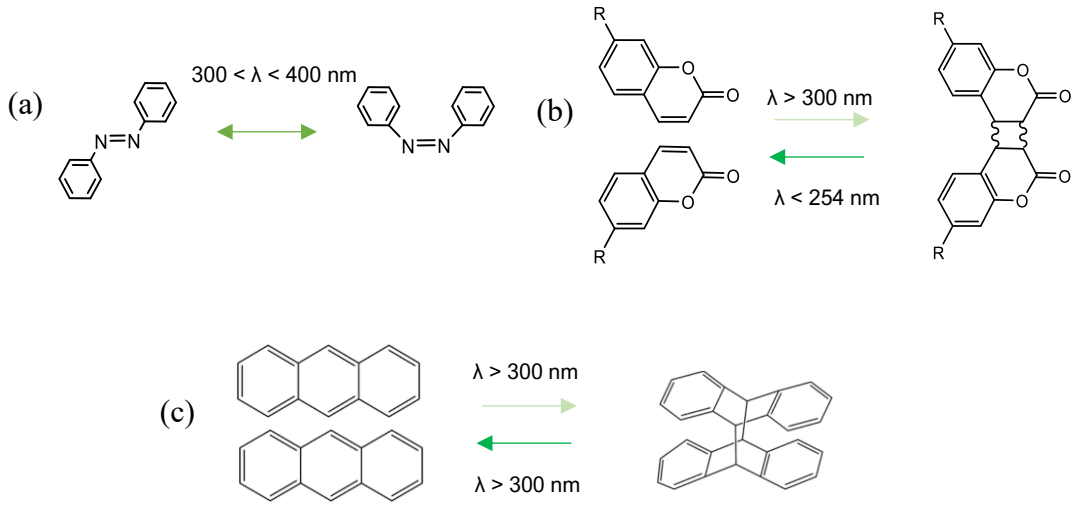

Figure 1.1 Reversible photoreactions mechanism of a) cis-trans isomerization of azobenzene groups, reversible cycloaddition reactions of b) coumarin derivates, c) anthracene derivatives

In the class of irreversible photo-responsive molecules, ortho-nitrobenzyl alcohol derivatives have become one of the most investigated groups in polymer science, for their versatility in being included in many different polymer networks and applications [32–36]. Those molecules, o-nitrobenzyl compounds, are still nowadays employed in photo-responsive systems, including all the investigations reported in this thesis and in my studies.

Initially, they were used as photo-protected groups in organic chemistry. A first application in this direction was presented in the work of Barltrop and co-workers in 1966, in which ortho-nitro benzyl ester groups (o-NBE) were employed as photo-protected groups for carboxylic acid [37]. The photo-deprotection under UV light occurs following this reaction mechanism (Figure 1.2).

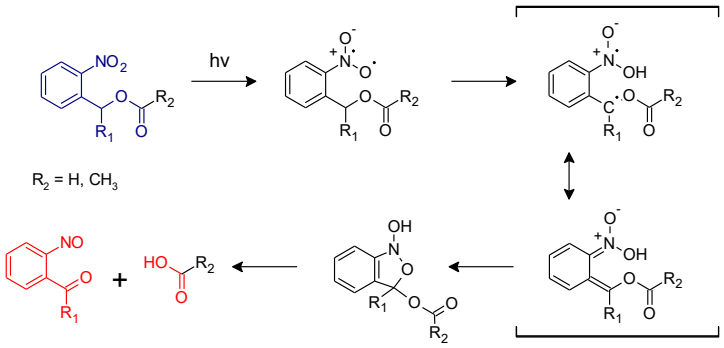

Figure 1.2 Photoreactions of ortho-nitro benzyl esters (Reproduced by [38] published by the Royal Society of Chemistry).

Upon UV irradiation (300–365 nm) the excited o-NBE chromophore abstracts a hydrogen from the methylene or methine carbon in γ-position with the formation of aci-nitro tautomers. This is followed by a molecular rearrangement, with the formation of a benzoisoxaline derivative that subsequently cleaves, yielding a carboxylic acid and an o-nitrosobenzaldehyde as primary photoproducts. Secondary photoreactions involve the formation of azobenzene groups by dimerization of the o-nitrosobenzaldehyde [32–36].

Along with carboxylic acids, the idea of employing o-nitrobenzyl alcohol derivatives as photo-protected groups was extended to several other functional groups such as carbamates and peptides [39–42]. Various strategies were pursued in order to shift the absorption window of the o-NB chromophores to longer wavelengths, to increase the quantum yield and to prevent the formation of photo-dimerized by-products [33,43–47]. These strategies include chemical modification either on the aromatic ring or at the benzyl position of the linker, and photo-sensitization mechanism [48,49]. The possibility to induce the cleavage of the o-NBE with near infrared light via 2 photon absorption mechanism opened an interesting opportunity for deep-tissue biomedical applications [50–52].

A first adoption of o-nitrobenzyl alcohol moieties as photolabile groups in polymer chemistry is reported in the work of Petropoulos in 1977 [53]. They were initially introduced in polymer networks for the fabrication of UV-sensitive photoresists and then progressively adopted as photocleavable crosslinkers for light-triggered drug delivery or as photocleavable junctions in copolymer blocks [54–66]. Advancing from bulk properties, the photo-sensitive nature of o-NB groups was used to opto-regulate the surface chemistry [67–69]. Examples are the fabrication of polyelectrolyte multilayers or the photopatterning of micro and nano arrays for spatially controlled protein immobilization and cell culture [70–73]. Other interesting applications include photocleavable self-assembled monolayers (SAMs) and optical devices [74–77].

In this thesis, I studied the use of o-NBE in different photocurable systems. Throughout this manuscript, in a first chapter (chapter 2) it is reviewed the state of the art of photo-responsive systems based on o-NBE chemistry. Although there are numerous studies and applications of o-NBE groups reported in literature, this chapter highlights the literature in which o-NBE chromophores are applied as photosensitive moieties in thin polymeric films, and in micro and nanoparticles structures. The literature was divided into five main categories, according to the polymer matrix and substrate, which included (i) methacrylate and acrylates, (ii) thiol-click networks, (iii) epoxy-based networks, (iv) polydimethylsiloxane and (v) micro and nanoparticles.

In the following chapters (3,4 and 5) the experimental activities in the field of photo-responsive polymer networks based on o-NBE chemistry are reported. Photo-responsive polymer networks containing o-NBE moieties were first synthetized through use of visible light source and further modified upon UV light irradiation, exploiting o-NBE isomerization reaction (Figure 1.2).

In Chapter 3, thiol-epoxy photo-responsive polymer networks containing o-NBE groups were achieved by employing a visible light source, aiming at avoiding the o-NBE isomerization reaction while curing. Once the photo-responsive network was formed, the o-NBE moieties were cleaved upon UV-light irradiation, showing how light trigger can be conveniently employed for changing coating surface wettability and for the fabrication of positive-tone photoresists.

In chapter 4, vinyl monomers containing o-NBE moieties were photo-polymerized with trifunctional thiols by exploiting a thiol-ene click reaction. In a subsequent step, a laser beam source, instead of conventional photolithographic techniques, was used in order to promote the photo-cleavage reaction of o-NBE moieties (Figure 1.2), therefore improving the resolution and the fabrication of positive-tone photoresists. Moreover, it was further shown how laser stimulus represents a powerful tool not only for the design of 2.5D patterns with high resolution and light-modulable profiles, but also for locally changing the surface properties by tuning the presence carboxylic acids as primary reaction products.

In chapter 5, photo-responsive polymer brushes containing o-NBE groups were grafted onto silica particles. The synthetic path followed two different procedures; a *photo-grafting from* photo-induced synthesis and an amino-epoxy coupling

reaction. In a further step, the photo-responsive formed brushes were cleaved upon UV light irradiation, aiming at changing the silica particles surface properties.

Although *o*-nitrobenzyl derivatives are a well-known and employed class of photo responsive molecules since their discovery more than a century ago, they still represent a valid and interesting route to impart stimuli responsive properties to different substrates, ranging from polymer coatings to the surface of micro and nanoparticles.

Chapter 2

State of the art

Part of the work described in this chapter was published in [78] : "Romano, A.; Roppolo, I.; Rossegger, E.; Schlögl, S.; Sangermano, M. Recent Trends in Applying Ortho-Nitrobenzyl Esters for the Design of Photo-Responsive Polymer Networks. *Materials (Basel).*, **2020**, *13*, 1–26".

2.1 Photo-Responsive Acrylate and Methacrylate Polymers

Because of their versatile properties and their commercial availability, acrylate and methacrylate monomers have been widely used in the fabrication of polymers since decades [79]. By carefully selecting monomer structure and their functionalities, polymers can be synthesized for a plethora of industrial applications such as industrial coatings, adhesives, inks, and biomaterials [80–83]. The high reactivity of the carbon-carbon double bonds together with the possibility to be photo-initiated made (meth) acrylic monomers also the most used compounds in new technologies such as light-activated 3D printing technologies [84,85].

The possibility to combine acrylate or methacrylate polymer networks with photolabile groups could give further advantages in terms of "smart" properties and in 4D printing strategies [86]. In the last decades, o-NB alcohol derivatives were employed in several applications based on methacrylate and acrylate networks and the first interest in thin polymer films arose for the fabrication of photoresists [57].

A photoresist is a light sensitive polymeric compound, whose solubility properties are locally changed through mask-mediated irradiation [87]. In particular, photolithographic techniques are typically applied to inscribe patterns in thin films of the photoresists. In a subsequent step, the pattern is developed with a proper solvent that either dissolves the irradiated (positive tone photoresist) or the non-irradiated area (negative tone photoresist), leaving the desired architecture that could be then used for further processes (metal deposition, epitaxial growth, surface functionalization, etc.) [88].

Different approaches were adopted in literature in order to exploit o-NBE chemistry for the development of photoresists.

One of the first work in this sense was made by Reichmanis et al. [89] in the early 80s. They introduced o-nitrobenzyl cholate ester in a polymeric matrix of poly-co-(methyl methacrylate-methacrylic acid) in order to inhibit the network's solubility. Upon UV light irradiation, the o-nitrobenzyl cholate ester was cleaved into soluble species allowing a selective extraction of the irradiated area in an aqueous alkali developer. Results showed higher resolution (1 micron) compared to other photopatterning techniques. The authors also demonstrated the possibility to increase the reaction quantum yield, by proper substitutions on the o-nitro-benzyl chromophore.

In another work [90], Reinhold Schwalm compared different co-polymers containing o-nitrobenzyl (meth)acrylates as solution inhibitor, in terms of quantum yields (referred to the isomerization reaction of the nitro groups), resist sensitivity,

and contrast. In this study the high influence of the network's glass transition temperature (T_g) on the ortho-nitro reaction was evidenced, that is a consequence of the high free volume that the o-nitrobenzyl group requires for the photoisomerization reaction. In fact, o-nitrobenzyl isomerization proceeds via some intermediates, which require at least rotational motions of the nitro and benzyl moieties. Thus, relatively high free volume is necessary in order to obtain high quantum yields. This property is also common in other Norrish type II reactions [91]. Consequently, in order to have high cleavage conversion of the nitro groups, the system should be irradiated above its T_g. According to this logic, the author selected appropriate co-polymer films, optimized the reaction parameters, and was able to fabricate micro-resists with a resolution between 0.75 and 1 μm.

In the late 1980s, particular interest was also focused on the exploitation of this photocleavage reaction in chemical amplification concepts. Willson and co-workers synthetized poly(carbonate)s with o-nitrobenzyl pendant groups, which form free hydroxymethyl pendant groups upon UV exposure [92]. Chemically amplified depolymerization of the illuminated polymer was then obtained during a post-baking step in the presence of a photo acid. A route towards positive chemical amplification was pursued by Wilkins et al. who described the synthesis of an o-NB ester of cholic acid [93]. The ester acts as photosensitive dissolution inhibitor for copolymers of methyl methacrylate and methyl acrylic acid. Deep UV exposure changed the solubility characteristics of the inhibitor since the cleavage products were highly soluble in alkaline solutions and positive tone patterns with a resolution of 0.5 μm were accomplished.

These works highlight the advantages of o-NBE links in photoresists compared to conventional ones that employed moieties that are unusable at wavelength shorter than 300 nm, such as novolak-quinone diazine [89,94]. Instead, with nitrobenzyl groups, being active to shorter wavelengths, it is possible to reduce light diffraction effect, thus, increasing the definition and resolution of the photoresist [95]. The high reaction quantum yields of o-NB isomerization reduces also the necessity to use high light energy doses that could degrade the matrix producing poor profiles [90].

More recently, o-NBE-based photoresists were successfully adopted for the patterning of organic light-emitting diode (OLED) displays and organic thin-film transistors (OTFTs). An interesting work in this context was reported by Taylor and co-workers in 2009 [96]. They synthetized a photoresist based on a co-polymer that contains perfluoro polyesters or nitrobenzyl ester as pendant groups (Figure 2.1).

After photolysis of the o-nitrobenzyl ester moieities, the co-polymer became insoluble in hydrofluoroethers solvents allowing a selective network dissolution. Taking advantages of the photo-switchable solubility properties, the synthetized photoresist was employed as photo-pattern system on PEDOT: PSS films. The results showed a sub-micrometer patterning, and, generally higher performance compared to other chemically amplified techniques for PEDOT: PSS photo-patterning. As a further application, they were able to fabricate a field-effect transistor, in which an organic semiconductor material (pentacene) was patterned on the PEDOT: PSS coating.

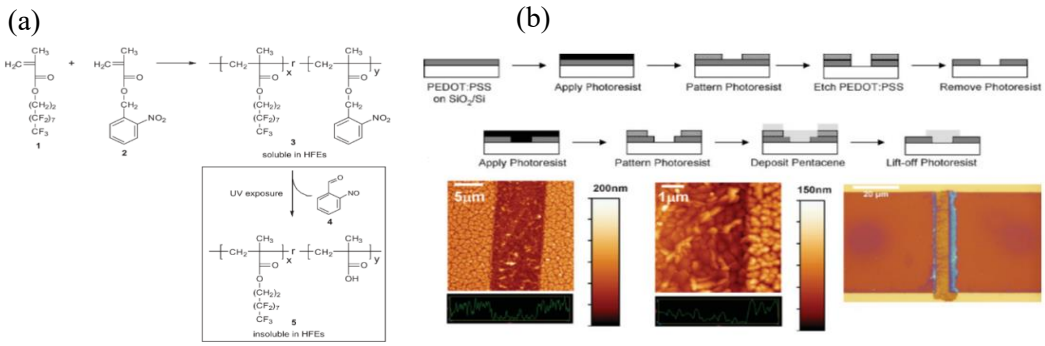

Figure 2.1 (a) Synthesis of the UV-sensitive acid-stable polymer resist (3) and photoinduced deprotection reaction to polymeric carboxylic acid; (b) schematic device fabrication of PEDOT:PSS/pentacene bottom-contact OTFT; and optical image of the OTFT (Reprinted with the permission from Reference [96]).

Although the good resolutions, the typical dissolution mechanism of the previously reported photoresist may include most of the time harsh developing solvents, which could be particularly undesired for applications in biological field.

Different approaches were developed in order to use mild buffer solutions for the photoresist's developing step [72,73,97–99]. The basic idea was the following: being carboxylic acids one of the reaction products of the isomerization reaction of o-NBE (Figure 1.2), they could be negatively charged after deprotonation at neutral or basic pH. Then, the electrostatic charge repulsions could be conveniently exploited in order to dissolve the UV irradiated area in mild aqueous solution at certain pH values. In order to exploit successfully this polyelectrolyte property in aqueous media, the polymer network should be hydrophilic enough to ensure water penetration into the matrix.

The possibility to fabricate photoresist with high resolution and in mild reaction conditions were widely explored for the fabrication of protein microarrays. Different works on this topic were conducted by Doh and co-workers [97]. They synthetized a terpolymer (o-NBEMA-MMA-PEGMA) containing an o-nitrobenzyl methacrylate (o-NBEMA), methyl methacrylate (MMA), and poly(ethylene glycol)methacrylate (PEGMA) for preparing thin photo-responsive films. The patterns were accomplished after UV illumination, by dissolving the irradiated polymer area in a phosphate buffer solution with a pH above 6.6. Further conjugation of biotin to the hydroxyl end groups of PEGMA units allowed selective immobilization of streptavidin on the surface, enabling a multicomponent protein patterning (Figure 2.2).

The same group fabricated micropatterns for protein adhesion and cells culture, with microscope projection photolithography [98]. In a first step, they coated a biotinylated substrate (for proteins adhesion), on the top of which they deposited a photo-responsive terpolymer (42 wt% DMNBMA (4,5-dimethoxy-2-nitrobenzyl

methacrylate), 24 wt% MMA, and 34 wt% PEGMA) by spin casting. The photoresist design was then inscribed through microscope UV light projection, dissolving the irradiated terpolymer coating.

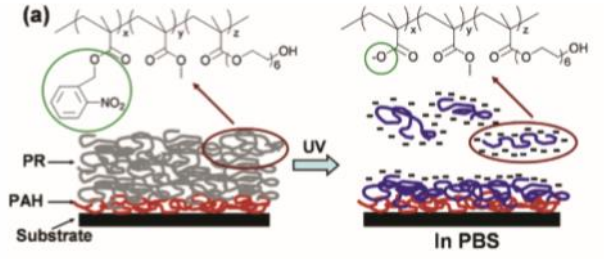

Figure 2.2 Chemical structure of Photoresist and its mechanism for in situ polyelectrolyte bilayer formation (Reprinted with the permission from reference [97] Copyright 2004 American Chemical Society).

The exposed underlying biotin groups were subsequently exploited for a selective immobilization of streptavidin proteins. By repeating the previous procedure, the authors were able to immobilize different type of proteins in a selective manner, and in micro-arrays with high-resolution capability (1 μm). In a further step they successfully extended the procedure to the fabrication of micro-scaffolds for immune cells (Figure 2.3a).

In a further work [99], they extended the concept to the fabrication of a multi-topographical structures, combining two different lithographic techniques: capillary force lithography and microscope projection photolithography (Figure 2.3b).

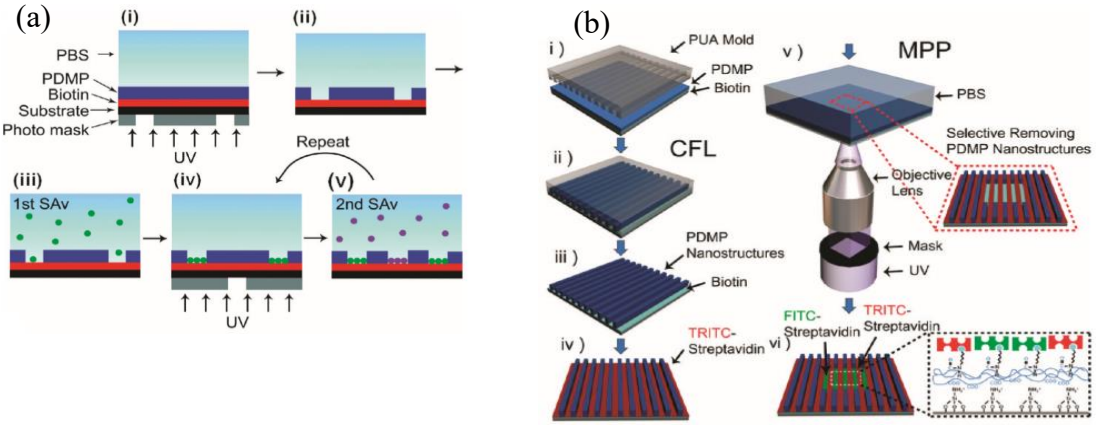

Figure 2.3 (a) Schematic of multiple streptavidin (SAv) patterning (Reprinted with the permission from reference [98] Copyright 2010 American Chemical Society). (b) Schematic diagram of the sequential fabrication of multiscale, multicomponent protein-patterned surfaces by combining CFL and MPP (Reprinted with the permission from reference [99] Copyright 2011 American Chemical Society).

In a double step procedure, they coated a first pattern of the previously synthetized terpolymer on a biotinylated substrate using capillary force lithography, and they immobilized a first type of streptavidin protein on the uncovered biotinylated area. In a subsequent step, they projected a second pattern with UV light projection, and immobilised a second type of protein on the exposed area. Combining these techniques, they were able to design more complex topographical structures for protein microarrays, which were used as a scaffold for studying cells behavior in a multi-topographical domain. This study reported that for a colon cancer cells culture (SW480) the nanoscale topographical cues, as compared to microscale topographical cues, had an ability to elicit the selective adhesion of the cells.

Because of their polyelectrolytes nature, o-NBE groups were also used for the fabrication of PEMs (polyelectrolyte multilayers) [72,73]. PEMs are multi-layered films in which layers of polycations and layers of polyanions are alternated [100,101]. The electrostatic attraction between oppositely charged macromolecules provides the enthalpic driving force for the layers assembly [102].

In a responsive PEM network, an external trigger (such as pH, light or temperature) could selectively change the charge interaction force among the layers, thus promoting a de-assembly mechanism in proper solvents [103]. As regard to this concept, Thomas and co-workers employed an o-NBE methacrylate monomer for the fabrication of photo-responsive PEMs networks. In a first work [72], photo-responsive PEMs networks were fabricated overlapping two domains with different wavelength responsiveness (Figure 2.4).

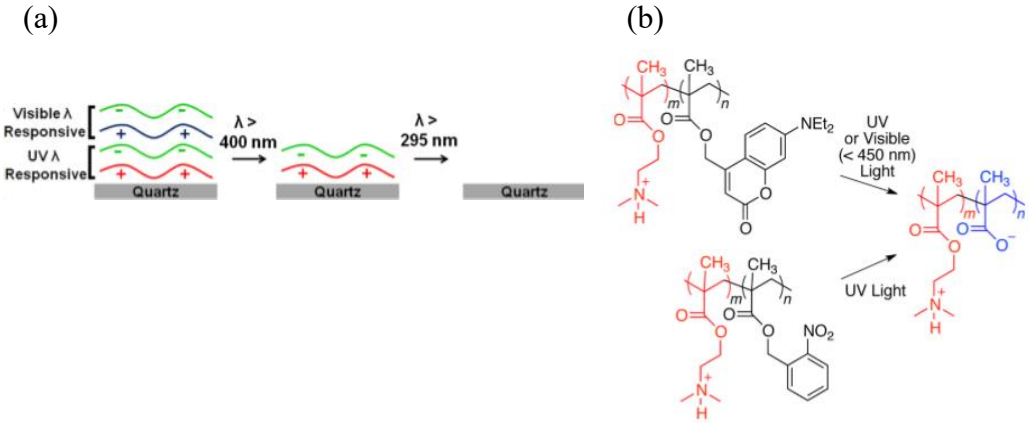

Figure 2.4 (a) Schematic illustration of the de-assembly process through different wavelength irradiations. (b) Design of photosensitive polycations that reduced net charge upon irradiation with either visible (coumarinyl groups) or UV (coumarinyl or nitrobenzyl groups) light (Reprinted with the permission from reference [72] Copyright 2014 American Chemical Society).

Their idea was to selectively de-assembly the two PEMs domains using light sources operating at different wavelengths. In order to meet this challenge, they included two photolabile groups; a dialkylamino-coumarin ester molecule, which

is responsive to visible light, and o-nitrobenzyl molecules, which are excited with UV light. In particular, the first domain alternates layers of poly(styrene sulfonate) (PSS), which contain polyanions ($\boldsymbol{SO_3^-}$), with layers of 2-(N,N dimethylamino)ethyl methacrylate-o-NBE-methacrylates), which contain polycations. A second domain alternates between PSS and co-2-(N,N dimethylamino)ethyl methacrylate-dialkylaminocoumarin methacrylate, as shown in Figure 2.4.

The layers electrostatic interaction was then selectively disrupted by irradiating in series the two domains with two distinct wavelength sources: $\lambda > 400$ nm for the photolysis of the coumarin ester and $\lambda < 400$ nm for the photocleavage of the o-NBE groups, taking advantage from the photo-release of ionizable carboxylic acid species. The layers de-assembly was promoted in a buffer solution since polyanions are formed by the de-protonation of the carboxylic acid groups in neutral and basic environment.

By including two different classes of pendant dyes in the two distinct domains, they demonstrated high wavelength selectivity in the de-assembly process through fluorescent measurements.

In a follow-up work [73] the authors increased the level of selectivity by adding two other classes of chromophores. Following the same procedure, four different domains were fabricated containing: dialkylamino coumarin (DEACM) groups ($\lambda < 450$ nm), two ortho-nitrobenzyl ester groups ($\lambda < 400$ nm), and para-methoxyphenacyl (PMP) groups ($\lambda < 320$ nm).

In order to enhance the level of selectivity, they employed two different types of o-nitrobenzyl molecules, which have similar absorbance spectra but different photolysis quantum yields: a 2-nitrobenzyl ester (NBE) unsubstituted at the benzylic position, and an α-methyl-2-nitrobenzyl ester (MNBE). The MNBE has a methyl group at the benzylic position, and a quantum yield of photolysis approximately five times higher than the unsubstituted NBE group. In this way, they were able to design complex patterns by varying both wavelength and intensity of the light source.

The previously mentioned procedures are mainly based on the idea to use o-nitrobenzyl links, in order to spatially control the solubility of thin polymer films in organic solvents or in aqueous solutions. Although good resolutions are achieved, there are some disadvantages, which include the impossibility to inscribe 2.5D or 3D profiles, because of the limitations of the photo-lithography techniques [104].

In a recent and very interesting work, Batchelor et al. [105] adopted the idea of combing a 3D printing process with a subsequent network erasing, only changing the wavelength emission of a 2 photons laser source. They synthetized a diacrylate crosslinker with o-NBE groups. In the first step, they 3D printed micrometric structures using a two photons emission laser source (900 nm). In a second step, they selectively erased the structure by tuning the laser wavelength emission (700 nm). In particular, the authors fabricated a cubic structure of length 15 μm using wavelength of 900 nm, and in a second step they inscribed submicrometric tunnels, which crosses inside the 3D structure, with a laser irradiation of 700 nm, owing to the two photons photocleavage of o-NBE groups (Figure 2.5).

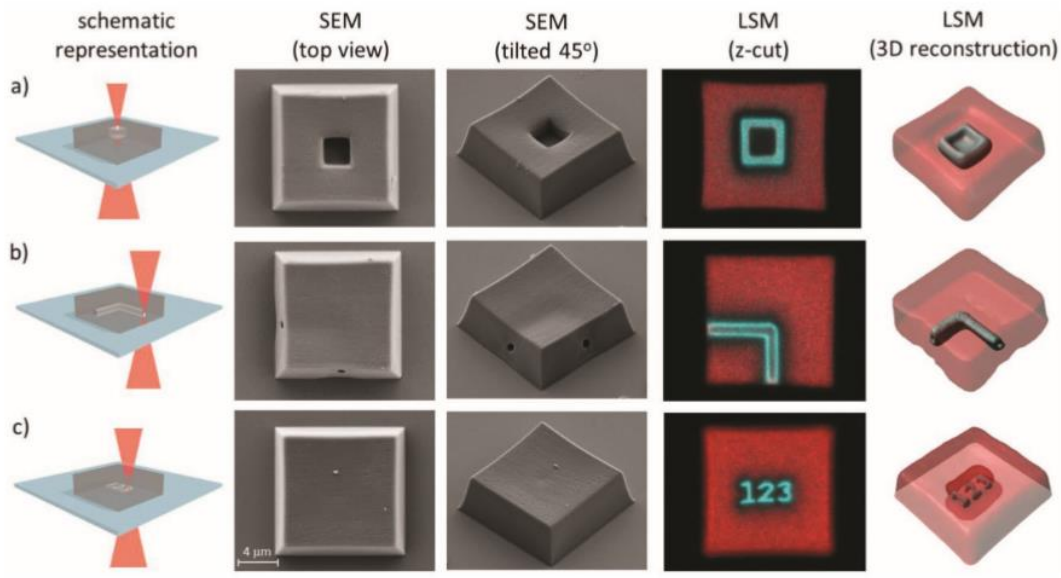

Figure 2.5 Laser erasing schematic procedure and SEM pictures of the printed micrometric (15 × 15 × 5 µm^3) blocks using a 700 nm femtosecond laser. (a) 3 ×3 × 3 µm3 block, (b) 90° 1 µm diameter tunnel, and (c) simple text "123" (Reprinted with the permission from reference [105]).

o-Nitrobenzyl chemistry was also widely explored as an efficient tool for tuning polymer surface properties in terms of both physical-chemical properties and morphology. Properties such as adhesion, cohesion, optical refraction, surface wettability, or morphology on a micro and nanoscale can be selectively tuned upon UV irradiations, because of the light-responsive nature of nitro-benzyl ester moieties, and their reaction products [67–69,76,77,106,107]. An interesting work in this sense is reported by Minkyu Kima and Hoyong Chung in 2017 [108].

They fabricated a photo-responsive bio-inspired adhesive based on a terpolymer poly(MDOPA-co-SBMA-co-NBEDM), composed by a zwitterionic polymer poly(sulfobetaine methacrylate) (pSBMA); a DOPA (3,4-dihydroxyphenylalanine) for the adhesion properties, and a photo-responsive methacrylate-co-2-nitro 1,3-benzenedimethanol dimethacrylate (NBDM). The photocleavage of the o-NBE groups in the synthetized terpolymer was conveniently exploited in order to decrease the crosslinking density, and hence reducing the adhesion properties of the polymer network. The results showed a decrease of the starting adhesion strength from 341 kPa to 223 kPa after 30 min of UV irradiation (38% reduction), and a further decrease to 150 kPa after 3 h of UV irradiation (56%).

In another work [109], Xue and co-workers reported a photoinduced strategy for regulating the localized growth of swollen microstructures, by coupling photolysis, photopolymerization, and transesterification mechanism together. The material system consisted of a swelled matrix containing the desired solution. The swellable matrix was made by a polymer structure composed of 4-hydroxybutyl acrylate (HBA), for imparting good swelling ability, o-nitrobenzyl acrylate as

photolabile linkers, and 1,6-hexanediol diacrylate (HDDA) for the transesterification reaction.

The swelling solution was instead composed by 4-hydroxybutyl acrylate (monomer), 1,6-hexanediol diacrylate (crosslinker), I-819 (photoinitiator), and benzenesulfonic acid (BZSA) as transesterification catalyst. The basic swelling mechanism was the following: upon light exposure, the solution in the irradiated area photopolymerizes consuming the monomers, and thus creating a concentration gradient of reactive groups in those areas. In this way, the unreacted species diffuse to the irradiated regions, swelling the polymer surface. In addition to this mechanism, the photolysis of the o-NBE groups releases ionizable carboxylic acid groups, which enhance the swelling ability of the irradiated region, by expanding the polymer networks via $-COO^{-}$ $-COO^{-}$ electrostatic repulsions. The combined effect caused a localized swelling of the irradiated network surface, with the formation of micro-pillars (Figure 2.6b). The presence of o-nitrobenzyl ester groups was crucial for enhancing the swelling process.

The authors further showed that the dimensions of the pillars can be properly designed and controlled by tuning the light spot dimensions and intensity. Moreover, multi-pillars growing (one above the others) could be realized by irradiating the surfaces of existing pillars in several steps. In addition, the thermal effect generated by the photopolymerization triggers transesterification reactions, which release any polymerization-induced mechanical tension in the dynamic networks, increasing pillars' mechanical properties. Finally, the authors showed different applications of this dynamic networks, that include surface photo-patterning and healing ability on the millimeter level.

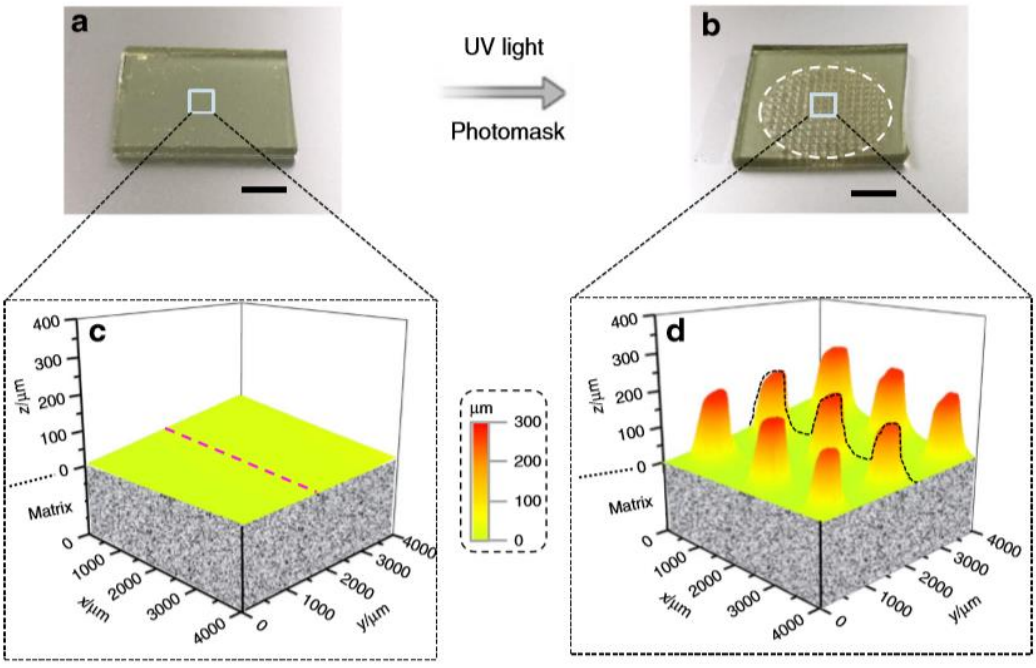

Figure 2.6 Microstructure pattern grown, (a) before UV irradiation, (b) after UV irradiation, (c) 3D profiles before UV irradiation, (d) swollen profile after UV irradiation (Reprinted from reference [109]).

Although several studies report on the use of controlled radical polymerization (CRP) techniques for the polymerization of o-NBE acrylate and methacrylate monomers, there are still some challenges related to the difficulties to synthetize polymers with high molecular weight and low polydispersity [110–113]. These difficulties are due to the intrinsic nature of the nitro-aromatic groups that act as inhibitors in the radical polymer growths, particularly at high temperatures. These inhibition effects were also found in living polymerization of other molecules that contain nitro aromatic groups [112,114]. Below, were reported some works related to CRP polymerization techniques in o-NBE methacrylate and acrylate systems.

A first exhaustive study of o-nitrobenzyl methacrylate and acrylate monomers polymerized by different controlled radical mediated polymerization, was made by Schumers and co-workers in 2011 [112]. The study analyzed different types of controlled-radical polymerization (CRP) techniques, for o-nitrobenzyl methacrylate (NBMA) and o-nitrobenzyl acrylate (NBA) monomers. Particularly, the authors analyzed (i) atom transfer radical polymerization (ATRP), (ii) reversible addition-fragmentation chain transfer polymerization (RAFT), and (iii) nitroxide-mediated polymerization (NMP). Considering RAFT polymerization, the authors could polymerize only methacrylate o-NBE monomers with some degree of control (PDI 1.5) but reaching molar masses up to 11,000 g/mol only after 18 h of reaction.

The study showed that RAFT polymerization of NBA was almost completely inhibited. This behavior was ascribed to the higher reactivity of the acrylate radicals, in comparison to the methacrylate ones, and therefore higher tendency to undergo to side reactions with the o-nitrobenzyl group. Regarding nitroxide-mediated polymerization (NMP), no polymerization was observed under the employed reaction conditions. According to this study, ATRP proved to be the best method for methacrylate monomers, achieving polymers with molar masses between 12,100 and 16,400 g/mol and with low-polydispersity indices ($M_w/M_n < 1.25$). With ATPR, o-nitrobenzyl acrylate with low molar masses and high polydispersity can be polymerized.

In a more recent work Soliman et al. [113] improved these results by single electron transfer–living radical polymerization (SET–LRP). In this study, the authors investigated the influence on the reaction kinetic determined by the presence of ligand, CuBr2 (used for preventing the formation of high molecular weight contaminant), and Cu(0) wire length used as a catalyst for starting the reaction.

In this study, the authors polymerized o-nitrobenzyl acrylate monomers through SET–LRP method, showing the effect on the polymerization kinetics due by the ligand and $CuBr_2$ concentration, as well as Cu(0) wire length used as a catalyzer for starting the reaction.

Optimizing these parameters, they were able to synthetize polymers with a molecular weight up to 28,600 g/mol and a narrow distribution ($M_w/M_n < 1.2$).

o-NBE moieties were also employed as photocleavable junctions in copolymer blocks, in order to make micelles, or well-defined nano-porous structure in thin coating applications [43,55,65,115]. Block co-polymers comprise two or more

chemically distinct homo-polymer units, linked by covalent bonds [116]. They have attracted much interest in polymer chemistry because, in thin polymer coatings, they are able to self-assembly into arrays of microscopic or nanoscopic domains [117,118]. The self-assembly behavior is a consequence of the intrinsic immiscibility between the two polymer blocks, together with the presence of covalent bonds among the monomer units [119].

Under annealing treatment in vapor solvent, the intrinsic block immiscibility promotes a self-assembling process of the co-polymer networks in well-defined and distinct domains. Photocleavable junctions among the two polymer blocks were successfully exploited as powerful tool, in order to selectively photocleave only one domain of the co-polymer structure, thus realizing porous-ordered domains or spatial-controlled surface post-modifications treatments [110,120].

In an interesting work, Schumers and co-workers [110] synthetized a copolymer block (P(NBA-r-AA)-b-PS), based on a photo-responsive poly(2-nitrobenzyl acrylate-random-acrylic acid) unit, and a polystyrene block, PS. After showing a convenient synthesis technique for the block copolymers, they employed the (P(NBA-r-AA)-b-PS) for micelles preparation, by UV irradiating the co-polymer block in a chloroform solution. Because of the UV-induced photo-deprotection mechanism, insoluble acrylic acid functions were released, which promoted co-polymer self-assembling with the formation of micelles with PAA core and a PS corona structure (Figure 2.7a).

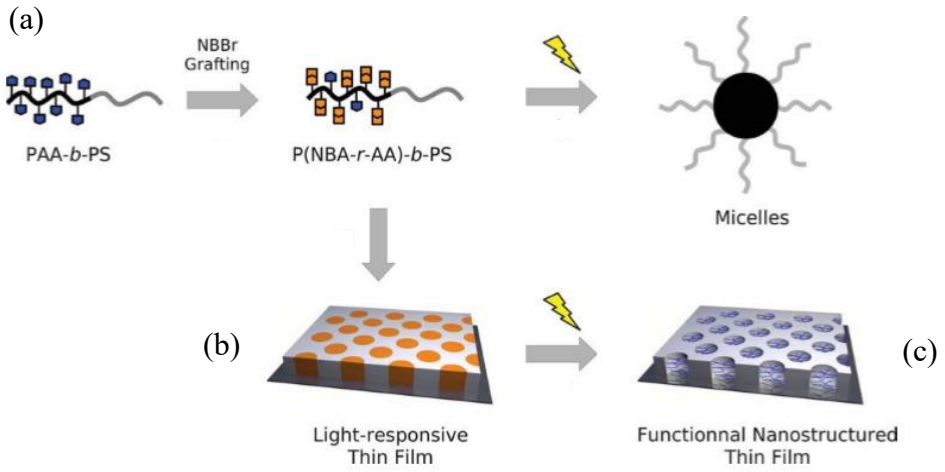

Figure 2.7 Schematic representation of light-responsive behavior of P(NBA-r-AA)-b-PS photocleavable block copolymers (a) light-induced micellization in a selective solvent of PS, (b) self-assembly in thin film with a cylindrical morphology, and (c) light exposure leading to functional and nanostructured thin films (Reprinted with permission from reference [110]).

TEM characterization showed the formation of 13 nm radius micelles, after 5 h of irradiation at 300 nm and 38.5 mW/cm^2 of light intensity. The authors were also able to encapsulate, and then photo-release, coumarin 343 as a fluorescent dye. In a further step, thin coatings with a cylindrical morphology were accomplished

by self-assembling the P(NBA-r-AA) 74-b-PS581 block copolymers onto silicon substrates (Figure 2.7b). The authors also studied the influence, in the annealing process, that different solvents had on the co-polymers self-assembling. After UV irradiation, they were able to selectively photo-cleave and extract the o-NBE domains, therefore obtaining well-ordered hollow structures (Figure 2.7c).

The control of the self-assembly process of the copolymer blocks, and domains orientation, still represents an ambitious challenge in coating applications. Several works have shown the influence of the substrate on the orientation of the structure domains of a coated block co-polymer [121,122]. In a recent work, Sol and co-workers [123] proposed an interesting approach in order to control the domains' orientation of a coated co-polymer blocks, by photo-controlling the substrate wettability. They fabricated a substrate with photo-responsive wettability based on a block copolymer of poly(styrene-r-2-nitrobenzyl methacrylate-r-glycidyl methacrylate). Because of the release of hydrophilic carboxylic acids under UV light, they were able to change the substrate's surface polarity. In a subsequent step, by coating block copolymers of poly(styrene-b-methyl methacrylate), they demonstrated that the different substrate wettability was a crucial factor in the self-assemble process of the coated block co-polymer, co-(PS-b-MM), into lamellar or cylinder-forming domains. Particularly, they were able to control the domains' orientation, from perpendicular to parallel orientation, changing the surface polarity by appropriate UV exposure dose.

In order to enhance the stimuli-responsiveness and the level of selectivity in changing polymer properties, some researches have focused on the design of polymer networks with multi-responsive properties [61,124,125].

Adopting a very original approach, Ionov and Diez [126] fabricated a polymer network that combines thermo- and photo-responsive properties by incorporating o-NBE acrylate photocleavable monomers into thermo-responsive poly(N-isopropylacrylamide) (PNIPAM) chains. The photocleavage of the o-NBE groups, upon UV irradiation, was conveniently exploited in order to tune the thermo-responsive behavior of the o-NBE-PNIPAM networks. In this regard, the o-NBE photocleavage reaction influenced the low critical solution temperature (LCST), defined as the temperature below which the network is soluble in aqueous solutions.

The results showed a decrease of the LCST in aqueous solutions of 50 °C after UV irradiation, because of the formation of hydrophilic carboxylic acid species.

This temperature-responsive behavior was used in order to sequentially remove irradiated and non-irradiated areas of a photo-patterned surface by carrying out developing steps at different temperatures. In a subsequent step, they were able to selectively immobilize proteins on the patterned surfaces.

2.2 Photo-Responsive "Thiol-Click" Networks

Introduced in 2001 by Kolb and co-workers, click chemistry refers to a group of reactions in organic chemistry, that are characterized by fast reaction rates,

regioselectivity and stereospecificity, high yields and mild reaction conditions [127]. The term "thiol-click" refers to a large subcategory of click reactions, in which monomers with thiol functionalities react with different type of co-monomers via radical or catalyzed reactions [128]. The reason why they have attracted particular interest in polymer chemistry, is related to their fast reaction rate and the high final monomers conversion. In addition, thiol-click reactions do not suffer from oxygen or water inhibition [128–131]. The step-growth polymerization mechanism further leads to homogeneous polymer matrix with low shrinkage stresses and narrow glass transition regions [128,130–133].

Taking advantage of the unique properties of thiol-click reactions and the versatile nature of o-NBE chemistry, various photocleavable "thiol-click" networks containing photosensitive o-nitrobenzyl ester moieties are reported in literature [106,107,134]. The basic idea which inspired these works was to synthetize of o-nitrobenzyl ester monomers with different terminal functionalities such as alkene, acrylate, epoxy, and alkyne, whose can further polymerize with different thiol crosslinker via thiol-click reactions (Figure 2.8).

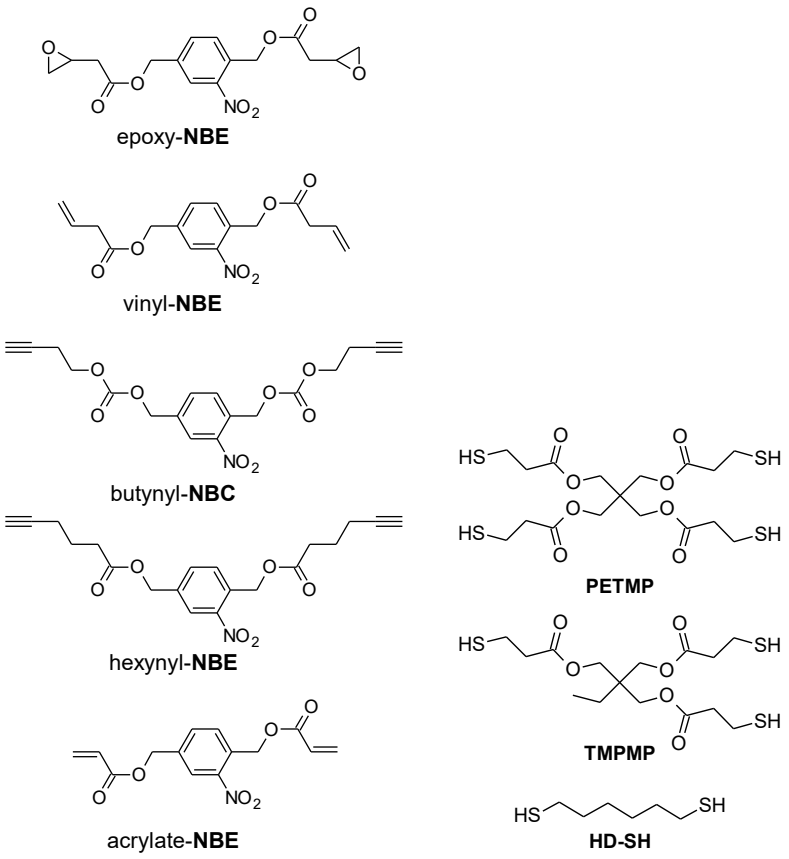

Figure 2.8 Monomers used for the preparation of the different photo-responsive thiol-click formulations.

The design of photocleavable "thiol-click" photopolymers by introducing o-NBE chromophores was reported by Radl and co-workers in 2017 [134]. Radical-

mediated thiol-ene photopolymerization of a photo-sensitive alkene(2-nitro-1,4-phenylene)bis(methylene) acetate with multi-functional thiols yielded polymer networks with photosensitive covalent links. The curing of the monomers was carried out by visible light exposure using phenyl bis(2,4,6-trimethylbenzoyl)-phosphine oxide as long wavelength absorbing photoinitiator (λ = 360–440 nm). The absorbance of the initiating system did not interfere with the absorbance of the o-NBE links, as vinyl-NBE absorbs below 380 nm. Thus, efficient photoinitiation of the thiol-ene reaction was accomplished without electronically excite the photosensitive vinyl-NBE. Going beyond the fabrication of positive tone patterns, the spatial and temporal control of the photocuring process enabled the fabrication of complex two-dimensional polymer patterns with photo-responsive properties. Microstructures with a resolution of 4 μm were accomplished by dissolving the cleaved networks in organic solvents (Figure 2.9).

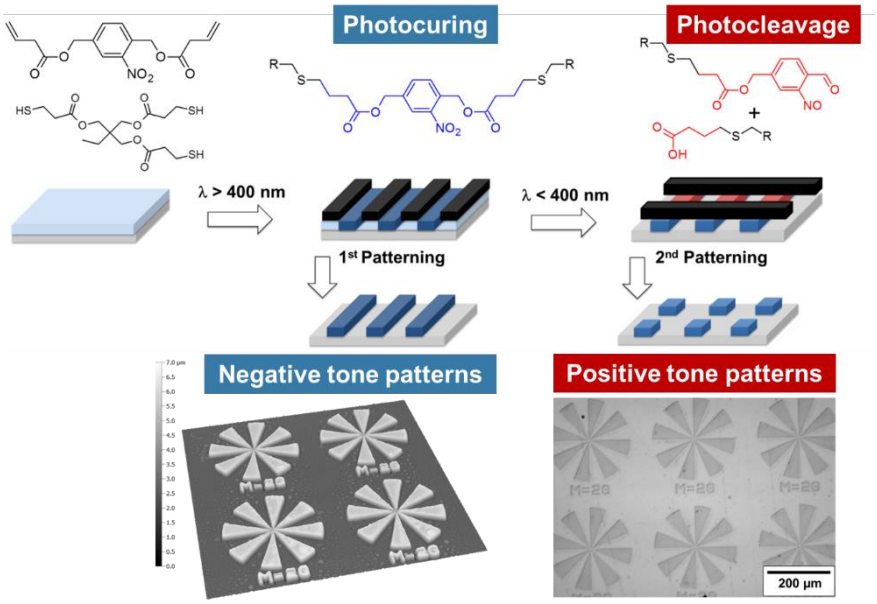

Figure 2.9 Photo-induced formation and light triggered cleavage of thiol-ene networks for the design of switchable polymer patterns. (Adapted from reference [134] published by the Royal Society of Chemistry).

Rossegger and co-workers [106] exploited the significant change in surface wettability to photo-tune the surface properties of thiol-click networks. In this purpose, they demonstrated the possibility to drive water droplets across the surfaces through a photo-inscribed wettability gradient. They synthetized o-nitrobenzyl alcohol derivatives with terminal alkyne groups, which were then crosslinked across multi-functional thiols, by a photo-induced thiol-yne reaction. In order to maintain orthogonality between the crosslinking and the cleavage step, the curing reaction was initiated by visible light exposure, using phenyl bis(2,4,6-trimethylbenzoyl)-phosphine oxide as photoinitiator. They showed that the surface wettability can be controlled over a broad range, with water contact angles ranging

from 97° to 27° upon UV irradiation under air, and from 97° to 82° upon UV irradiation in nitrogen atmosphere. The authors demonstrated with XPS measurements that the higher wettability change in air relies on the photo-deprotection of carboxylic acids and also on the photooxidation of the unreacted thiol groups yielding sulfonic acid moieties. The high wettability gradient generated upon gradual UV exposure together with a Laplace pressure gradient were used to move water droplets on the sample's surface. For the preparation of this multi-gradient surfaces, a V-shaped pattern geometry with a lengthwise wettability gradient was inscribed into the thin films by photolithography (Figure 2.10). Because of this design, they were able to move a 2 µL water droplet over a distance of 10 mm; not only on a planar polymer surface but also on surface, which were tilted (20°) or turned upside down.

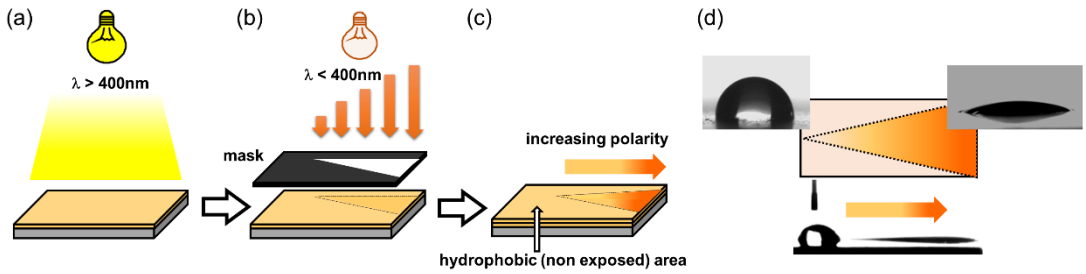

Figure 2.10 Schematic illustration of (a) photopolymerization of the thiol-yne network at long wavelength. (b) Patterned and asymmetrical UV exposure to realize (c) a wedge-shaped surface area with a lengthwise wettability gradient, which is surrounded by the hydrophobic (not exposed and thus, not-cleaved) thiol-yne network. (d) Water contact angle and droplet movement on the irradiated surface (Adapted from reference [106] published by the Royal Society of Chemistry).

The wettability of solid surfaces mainly depends on the chemical surface composition and on the microstructure morphology [135]. It is well-known, through the Wenzel equations and other physical models, that surface roughness influences the wettability properties compared to an ideal planar surface with the same chemical composition [135,136]. In this regard, Rosario et al. reported that an appropriate surface roughness amplifies the light-induced change in water contact angle of a photo-responsive silica surface [137].

Taking advantages of this effect, in a further work, Rossegger and co-workers [107] increased the wettability gradient by introducing a needle-like micropatterns on the sample surface, with visible light-assisted nanoimprint lithography (NIL). In order to increase the mechanical properties of the coating, for the light-assisted NIL procedure, they prepared a thiol-acrylate photopolymer with a higher T_g. For the sample preparation, an o-nitrobenzyl alcohol derivative with terminal acrylate groups (acrylate-NBE) was synthetized and cured upon visible light exposure in the presence of multi-functional thiols, isobornyl acrylate, and a fluorinated methacrylate. The combined effect of the needle-like microstructures and the fluorine groups increased the surface hydrophobicity, with static water contact

angle of 140°. Under UV light irradiation, not only the chemical surface composition but also a photoablation of the microstructures was observed (Figure 2.11, c and d). With this combined effect, they were able to increase the surface hydrophilicity in a controlled manner and obtained photopolymer surfaces with a water contact angle of 7°. The higher wettability gradient, in combination with a Laplace pressure gradient (V-shaped pattern), was exploited in order to move a water droplet over a distance of 22 mm, double than the distance reported in the previous work (Figure 2.11).

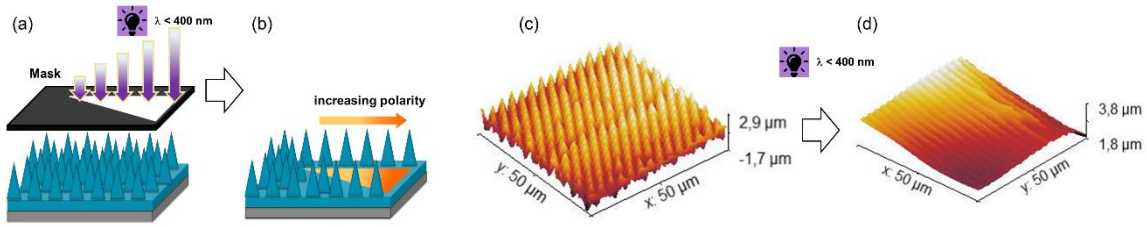

Figure 2.11 Schematic illustration of (a,b) Patterned and asymmetrical UV exposure on NIL thiol-acrylate structure. (c) SEM micrographs of the topography of needle-like micropatterns inscribed by visible light assisted NIL (d) Surface structures of the photocured photopolymer after 1500 s of UV exposure (269 mW/cm^2) under air (Adapted from reference [107] published by the Royal Society of Chemistry).

According to the cited literature [106,107,134], general considerations of the o-NBE cleavage reaction in thiol-click networks can be at this point derived. Particularly, it is possible to observe that the isomerization reaction proceeds with fast rate and high reaction yields as consequence of the typical low Tg, and thus high network flexibility due to the thioether bonds present in thiol-click networks.

The correlation between network flexibility and o-nitrobenzyl ester isomerization reaction was also reported in the work of Schwalm, in which a high network mobility allows large free volume for the photoisomerization of the o-NBE groups, thus ensuring high reaction yields [90]. Despite these advantages, a typical drawback of o-NBE groups applied in polymer networks regards the formation of secondary photoproducts, that act as intrinsic UV absorbers reducing light penetration in coatings. Moreover, the formation of secondary photoproducts can lead to a re-crosslinking of the polymer chains at prolonged UV exposure. This behavior was confirmed also in other polymer structures containing o-NBE chromophores, limiting the performance of these groups in photoresist applications.

Thiol-click reactions have been also widely explored as facile and efficient coupling procedures in surface modifications [138]. As regard to this, Li and co-workers [139] accomplished photolabile network containing both o-NBE and "clickable" groups, in order to realize photoresists with "click" modifiable surfaces (Figure 2.12). They synthetized three different monomers containing o-NBE links and with three different functionalities; allyl (M1), propargyl (M2), and epoxy (M3). In a second step, polymer chains were accomplished through Passerini MCP

reactions, containing the synthetized monomers (M1, M2, and M3), 1,6-hexanedioic acid, and 1,6-diisocyanohexane. The synthetized polymer chains were then crosslinked through amine-epoxy reactions, coupling the epoxy groups (M3) of the polymer chains and diethylenetriamine monomers. The o-NBE groups of the amine-epoxy networks were then exploited as decrosslinking points for fabricating positive tone photoresists. In a further step, the allyl and propargyl groups on the photoresist surface were used as "clickable" points, for anchoring fluorescent molecules with copper(I)-catalyzed azide alkyne cycloaddition (CuAAC), and thiol−ene reactions (Figure 2.12).

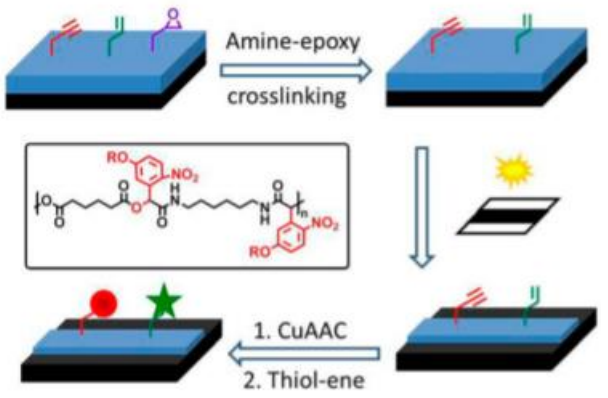

Figure 2.12 Schematic representation of the process for generation of multifunctional pattern on silicon wafer (Reprinted with the permission from reference [139] Copyright 2014 American Chemical Society).

Another route to match the cited advantages of photo-responsive of o-NB chromophores together with the thiol click chemistry, could be in the adoption of o-nitrobenzyl molecules as protection groups for thiols species. In a similar light deprotection mechanism, the o-nitrobenzyl thioether leads to a release of free thiol groups that, considering their wide possibility to react with different organic and inorganic species, can be further post-functionalized in multiple manners.

A first and exhaustive work in this context was reported by Pauloehrl and co-workers [129] that showed the potentiality of this photo-deprotection route in thiol click chemistry. In this aim, a 2-((3-((2-nitrobenzyl)thio)propanoyl)oxy)ethyl methacrylate monomer was synthetized and polymerized through ATRP technique (Figure 2.13). The so obtained polymers exhibited similar properties in terms of average molecular weight (13000 g mol^{-1}), and polydispersity (1.3) compared to a methacrylate o-nitrobenzyl ester monomer (see literature [112]), revealing that o-nitrobenzyl thioether moieties didn't differ in terms of monomers reactivity in the ATRP studied conditions. The deprotonation upon UV irradiation, followed a similar mechanism of the studied o-nitrobenzyl ester moieties but leading the formation of o-nitrosobenzaldehyde species and free PEG-based thiol terminal groups. The authors also observed high stability of the free deprotected thiol groups, that formed disulphide bonds only in low amount, hence confirming the potentiality

of this method for post modification treatments. The attempt in conducting the o-nitrobenzyl deprotecting together with thiols post functionalization didn't exhibit satisfying results because of the high by-products formation. By contrast, polymer backbone modification towards a first UV deprotection and a further thiol-maleimide reaction, revealed high reaction yields (>90%), confirming the potentiality of the novel approach in the thiol-click chemistry.

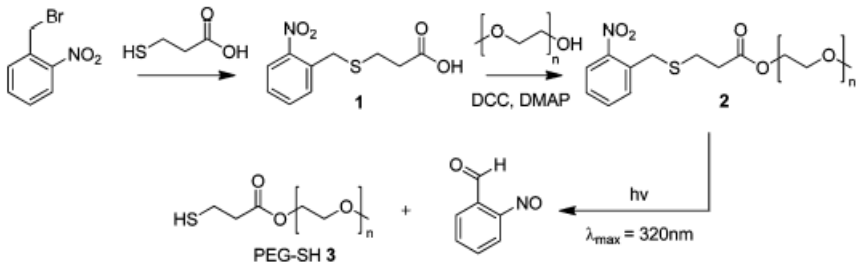

Figure 2.13 Schematic representation of the methacrylate o-nitrobenzyl thioether synthesis and subsequent UV deprotection process (Reprinted with the permission of The Royal Society of Chemistry from reference [129])

2.3 Photo-Responsive Epoxy Networks

Although there are several studies reporting the use of o-nitrobenzyl ester chromophores in acrylate and methacrylate coatings, there are few works in literature which report their use in epoxy-based networks [140–142].

Because of their salient properties, such as low shrinkage upon polymerization, insensitivity to oxygen inhibition, good mechanical strength and adhesions to various substrates, epoxy resins have become popular materials in numerous fields of applications ranging from lightweight composites, functional coatings, electronics, and adhesives [143]. The curing of epoxy monomers either proceeds in the presence of hardeners (e.g., amines, amides, anhydrides, phenols, thiols, and imidazoles) or through anionic or cationic homo-polymerization [144]. In the last years, cationic curing of epoxy resins has gained increased attention since the initiator are usually inert in the presence of epoxy monomers, and could be activated on demand by external stimuli such as temperature or light [144]. In this regard, the remarkable work of James Crivello on diarylsulfonium and triarylsulfonium salts, which can be used as cationic photoinitiators for the homo-polymerization of epoxy monomers, has become the starting point for studying photo-triggered curing reactions of epoxy networks [143,145].

A first work on photo-responsive epoxy networks containing o-NBE moieties was made by Radl and co-workers in 2015 [141]. In this study, a di-functional epoxy monomer containing o-NBE groups (epoxy-NBE) was synthesized and thermally cured with an anhydride hardener. In a further step, positive tone

photoresists with pattern resolution in the range of 8 µm were inscribed, taking advantages of the photo-cleavage of o-NBE groups. In order to study the applicability also in recycling concepts, the o-NBE photo-cleavage reaction was also exploited in order to promote network degradability in thicker coatings (1 mm), and for reducing the matrix-fiber adhesions in polymer-based composites.

Mechanical tests showed a good degradation behavior of the UV irradiated coatings, with a depletion of the storage modulus and glass transition temperature with increasing UV exposure dose (see Figure 2.14). Additionally, single fiber pull-out tests revealed a significant decrease of the interfacial adhesion at the fiber-matrix interface due to the photo-triggered cleavage reaction.

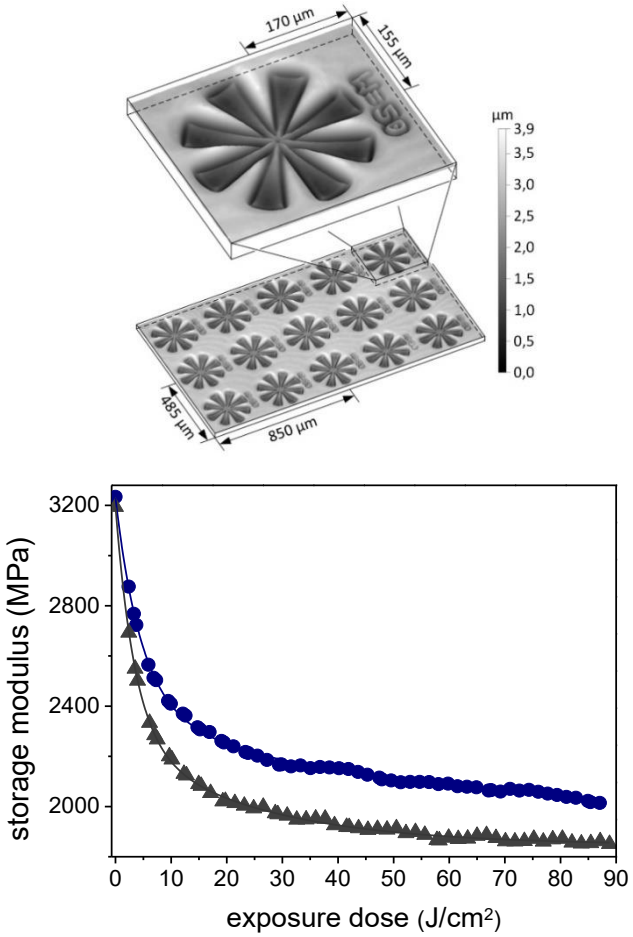

Figure 2.14 Positive-type photoresists and storage modulus variation of epoxy-NBE network upon UV exposure (Reprinted from reference [141] with the permission of Elsevier).

In a follow-up study, the same working group [142] highlighted the possibility to cure epoxy-NBE through a cationic ring opening mechanism using an appropriate photoacid generator as initiator. Two different approaches were explored to activate the photoacid generator without premature cleavage of the o-NBE links, which absorb between 300 and 365 nm. The first approach included the use of a radical promoted sensitization mechanism of the photoacid generator, enabling an excitation upon visible light exposure ($\lambda > 400$ nm). The second approach involved a photo-initiation mechanism by sulfonic acids, formed by a

direct photolysis of N-hydroxynaphthalimide triflate upon deep UV exposure. In both concepts, the cationic ring opening reaction progressed very slowly and a thermal post-treatment was necessary in order to obtain high final monomer conversions. These results could be related to the low reactivity of the epoxy monomers because of the presence of the o-NBE groups. A possible explanation can be found in a previous work of Crivello and Sangermano [146], which demonstrated that the presence of nucleophilic ester groups decreases the reactivity of epoxy monomers in cationic ring opening reactions. However, after thermal post-treatment, epoxy networks with stimuli-responsive properties were successfully obtained, and positive tone photoresists with pattern definition of 20 μm were inscribed onto the polymer surface.

Regarding the photo-cleavage reaction of the o-NBE groups in epoxy networks, the trends and kinetics are comparable to the previously cited thiol-click networks.

In order to better understand how the photocleavage reaction is influenced by the network properties, Giebler and co-workers [140] recently studied different epoxy-anhydride networks containing o-NBE groups. In this purpose, they thermally cured epoxy-NBE with different types of cycloaliphatic anhydrides in order to obtain networks with varying thermo-mechanical properties. Their results demonstrated that the networks with glass transition temperature (T_g) below room temperature exhibited a higher cleavage reaction rate, but were more prone to undergo secondary photoreactions, and therefore, leading to a re-crosslinking of the cleaved polymer chains. This result is easily explained considering that, higher network flexibility allows large free volume space for the photolysis, but at the same time, higher probability for the photocleaved chains to couple and to re-crosslink. At the same time, networks with a T_g above room temperature showed lower cleavage reaction rate, but at the same time lower tendency to go through secondary photoreactions. Networks with a higher T_g also exhibited superior performance as resists, with a contrast of 1.17 and a resolution of 8 μm. These results are in good agreement with other studies cited in this manuscript and evidence how the polymer network properties are crucial for the photo-cleavage kinetics of the o-NBE groups and in general for the photoresist performance.

2.4 Photo-Responsive PDMS Networks

Polydimethylsiloxane (PDMS), also known as dimethylpolysiloxane or dimethicone, is by far the most widely used siloxane (“silicone”) elastomer in technical application [147]. Its fame in polymer chemistry stems from the special rheological properties and other remarkable material properties such as nontoxicity, biocompatibility, blood compatibility, elasticity, transparency, and durability [147–149].

Because of these unique properties, PDMS-based polymer networks are widely used in numerous applications ranging from electrical insulations to contact lenses. PDMS is also often employed in soft lithography and in 3D printing, for the

fabrication of micro-scaffold and microfluidic devices [150]. Despite the widespread use of PDMS, there are almost no studies on the design of photo-responsive PDMS coatings with photolabile o-NBE groups.

The first study on PDMS polymer networks with o-NBE junctions was conducted by Giebler and co-workers [151] in 2018. In this work, polydimethylsiloxane (PDMS) oligomers with terminal anhydride groups were thermally crosslinked with epoxy-NBE. The introduction of o-NBE groups enabled the introduction of a dual-responsive behavior in the PDMS network, which were degraded either upon UV light exposure or in alkaline environment. In addition to the well-known UV degradation mechanism, the hydrolysis-sensitive ester groups of the epoxy-NBE crosslinker undergo hydrolytic degradation in alkaline environments. As regard to this, the results demonstrated a complete hydrolytic network degradation within few hours or some days, as a function of the NaOH molar content in the alkaline solution. In order to show the dual-responsiveness, the o-NBE groups were also employed for a selective photo-degradation, and positive tone photoresist with a resolution of 50 µm were inscribed into the PDMS surface.

However, re-crosslinking reactions because of the side reactions were observed at high UV energy dose. Taking advantages from the reformed crosslinks that showed less sensitivity to hydrolytic degradation, the authors were able to inscribe also negative tone photoresist microstructures, in which the not irradiated area were dissolved in alkaline environment (Figure 2.15).

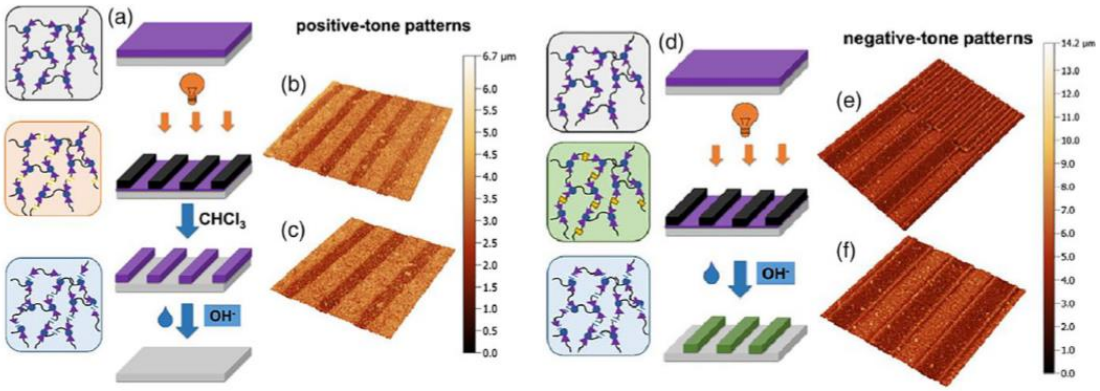

Figure 2.15 Schematic representation of the formation of a positive-tone resist and (a) subsequent removal of the resist by hydrolytic degradation of the PDMS network. (b and c) Confocal micrographs of positive-tone relief structures (100 µm lines and spaces) inscribed into PDMS-1 by photolithography after the development in chloroform. (d) Schematic representation of the formation of a negative-tone resist. (e and f) Confocal micrographs of negative-tone relief structures (50 and 100 µm lines and spaces) inscribed into polymer network by photolithography after the development in 1 M aqueous NaOH (Reprinted with permission from reference [151]).

2.5 Photo-responsive micro and nanoparticles

Stimuli-responsive micro and nanoparticles have gained a lot of interest in many fields of material chemistry including nanocomposites [152], control of the surface properties [153] and nanomedicine areas [154].

In surface treatment and nanocomposites, nano and microparticles are widely employed for imparting different features, such as antifouling activity [155], bactericidal and fungicidal properties [156] and hydrophilicity or hydrophobicity characteristics [153]. Especially regarding surface treatment, light stimulus seems to be the best candidate because of its spatial and time control, and the total absence of any other drawbacks such as light absorbance in thick coatings.

In their work, Lin and Zhou synthetized photo-responsive nanoparticles in the aim to change surface properties from super hydrophobicity to super hydrophilicity, upon UV stimulus [153]. The synthetic procedure included a first synthesis of a silane agent through the reaction between 5-propargylether-2-nitrobenzyl alcohol (PONB) and 3-(Triethoxysilyl) propyl isocyanate (IPTES), followed by a further condensation on silica nanoparticles. Eventually, the super hydrophobicity feature was achieved coupling a 6-Azido-1,1,1,2,2,3,3,4,4-nonafluorohexane (F-N3) molecules to the alkyne groups of the silane agent via "azido-yne" click reaction (Figure 2.16). The functionalized nanoparticles were then placed on a glass surface and UV irradiated. Their results showed a decreased of water contact angle from 143.5 ° to 10.1 ° upon 35 min of UV light irradiation (365nm), due to the o-nitrobenzyl cleavage and the subsequent formation of carboxylic acid together with the elimination of the hydrophobic fluorine groups. Finally, they showed the potentiality of the photo-responsive nanoparticles in fluorocarbon coatings measuring a shifting in water contact angles from 106.4° to 33.3°, at a particle content of 5 wt%. The wettability values of the fluorocarbon composite obtained with low nanoparticles weight percentage, suggested a particles migration mechanism on the coating surface.

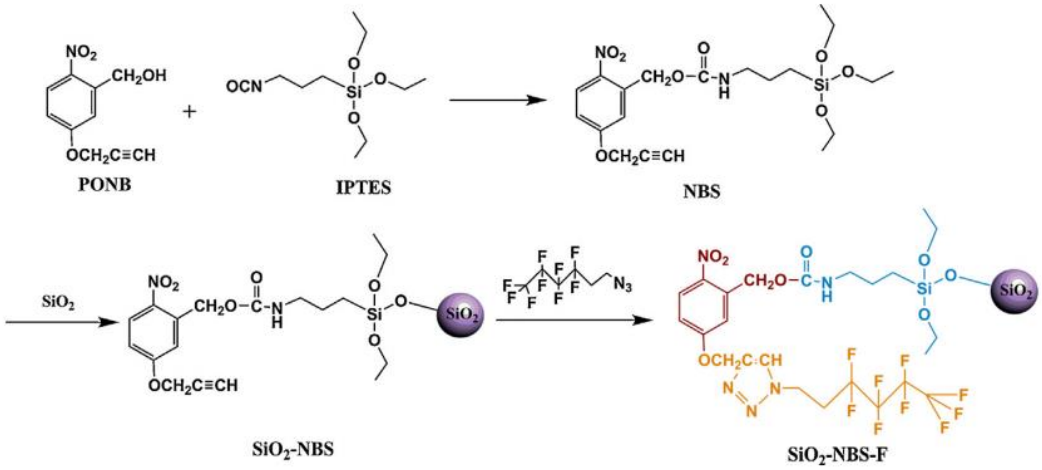

Figure 2.16 Synthetic route of light-responsive silica nanoparticles (Reprinted with permission of Elsevier from reference [153]).

As already introduced in the previous paragraphs, o-nitrobenzyl alcohol derivatives were successfully employed in co-polymer block mainly in the aim to fabricate photo-patterned coatings and to control surface morphologies. In this context, Lee and co-workers proposed a very interesting application of o-NBE and coumarin groups as photo-responsive surfactants for the fabrication of co-polymer blocks with photo switchable color and shape [157]. In particular, they first synthetized a co-polymer block of Polystyrene-b-poly(2-vinylpyridine) PS_{102k}-b-$P2VP_{97k}$, and two photo-responsive surfactants based on o-NBE and coumarin groups respectively; 5-hexyloxy-2-nitrobenzyl-16-N,N,N-trimethylhexadecan-1-ammonium bromide (N-CTAB) and 7-(diethylamino)-4-(N,N,N-trimethylhexadecan-1-ammonium bromide)coumarin (C-CTAB). In a further step, the particles were prepared emulsifying the PS_{102k}-b-$P2VP_{97k}$ co-polymer blocks (0.5 mg) and chloroform (50 µL) in an aqueous solution containing the photo-responsive surfactants as surface stabilizer. Once the emulsion was formed, the procedure followed a slowly evaporation of the chloroform contained in the block co-polymer, in order to obtain solid onion-shaped particles with the outer layer of Polystyrene (PS) (Figure 2.17).

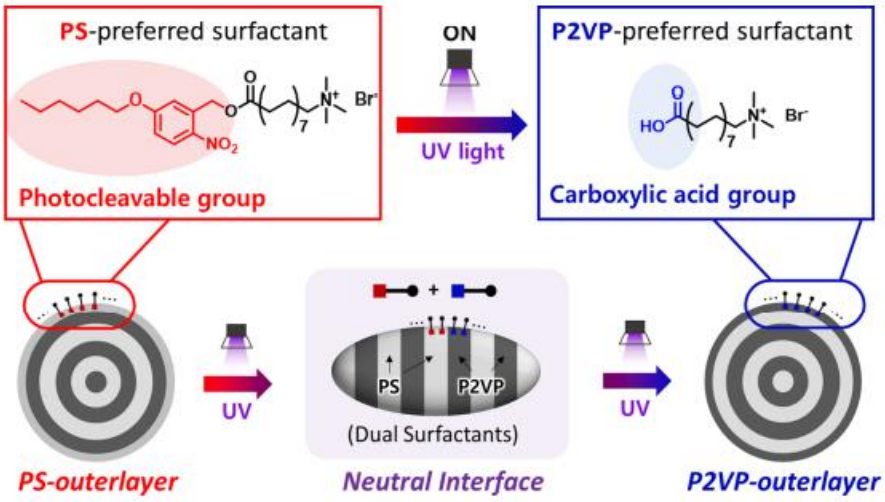

Figure 2.17 Schematic Illustration of the Photo-Induced Shape Transformation of PS-b-P2VP Particles Enabled by Light-Active 5-Hexyloxy-2-nitrobenzyl-16-N,N,N-trimethylhexadecan-1-ammonium Bromide (N-CTAB) Surfactants (Reprinted with permission from reference [157] Copyright 2019 American Chemical Society).

The authors attributed this shape orientation as a consequence of the favored hydrophobic interaction between PS and N-CTAB and/or C-CTAB surfactants at the polymer/water interface. It is then reasonable that the hydrophilic switching of the N-CTAB and/or C-CTAB surfactants, caused by the formation of carboxylic acids upon UV stimulus, can promote different rearrangement of the particles in the surrounding media (Figure 2.17). Exploiting this mechanism, the authors demonstrated that upon 30 min of UV irradiation, the particles undergo to a first tulip-bulb shapes, in which the surface alternates PS and P2VP regions as a

consequence of the -COOH formation in the surfactant species, and their consequent affinity to both PS and P2VP domains. Eventually, irradiating the system until full o-NBE conversion provoked an irreversible particles transformation to a reverse onion shape with the outer layer of poly(2-vinylpyridine) species. This behavior is due to the ability of the pyridine groups in P2VP to form hydrogen bonds with carboxylic acids and thus causing a preferential interaction between the cleaved surfactants and the P2VP domains (Figure 2.17). Another interesting feature of this light-induced particles "rearrangement" was the possibility of a color monitoring over the shape transformation, due to the tunable optical properties of the coumarin ester of C-CTAB surfactant upon UV irradiation. Taking advantages from this property, the shape-color tunable particles were embedded in hydrogel coating allowing an irreversible photo-patterning in microscale resolution.

In previous paragraphs, were presented many works in which o-NBE links were used as photo labile crosslinkers in the aim to selectively degrade the polymer networks and therefore changing bulk and surface properties [57,89,90,93]. With an original approach, Picchetti and co-workers transferred this idea to silica nanoparticles in the aim to induce particles degradation upon light stimulus [158].

Particularly, they synthetized a bis-alkoxysilane molecule with o-nitrobenzyl moieties linker (Figure 2.18), with the idea to exploit the photocleavable linkers for obtaining particle structural breakdown. The synthesis of the mesoporous particles followed a modified Stöber process in which the photolabile alkoxysilane linker was co-condensed to tetraethyl orthosilicate (TEOS), by using a molar ratio TEOS/linkers of 2.25:1. The obtained particles exhibited an average size of 303 ± 34 nm within narrow distribution and a porosity volume and BET specific surface area of respectively; 0.26 cm^3/g and 318 m^2 /g. In a further step, they UV irradiated the silica particles demonstrating a degradation mechanism which was correlated to the o-nitrobenzyl isomerization, and characterized by the loss of the initial morphology and a decrease of porosity volume and BET specific surface area to respectively; 0.03 cm^3/g and 57 m^2/g. Moreover, "in vitro" drug release test of the synthetized carrier on HeLa cell, exhibited low cytotoxicity together with selective drug release upon light trigger.

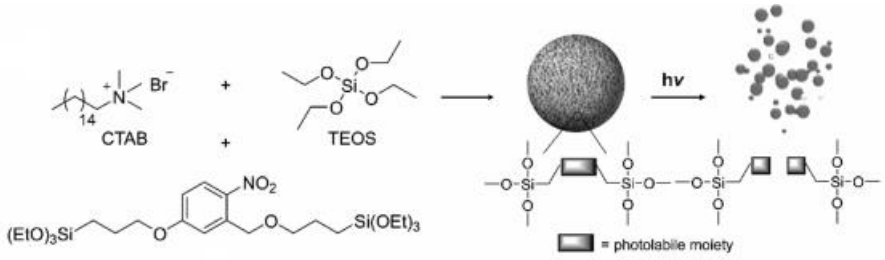

Figure 2.18 Schematic representation of the preparation and light-induced degradation of silica nanoparticles. (Reprinted with permission from reference [158] Copyright 2020 American Chemical Society).

Nanomaterials such as liposomes, metallic nanoparticles (NPs), and nanogels, are currently under development and used in various biomedical applications; those can play an important role in sensing, biomedical imaging, diagnosis as well as in drug delivery [154,159]. These smart carrier have been widely developed as responsive systems to exogenous (e.g., pH, temperature, light, and ultrasound) and endogenous (e.g., redox potential and enzyme presence) stimuli [160].

This attained special interest in the cancer cell treatment, where the use of toxic molecules has promoted the adoption of silenced drug delivery units, which can selectively release, on demand, once reached the selected target [161]. In the last years, smart carriers were widely explored and different activation mechanism were proposed. For instance, magnetic field has been exploited as an interesting tool for this purpose [162,163]; other approach relies on the use of electric current for turning "on-off" the drug release mechanism [164]. In this frame, the capability of light to be localized with precision gained a lot of interest for the drug release process [165].

To this aim, o-nitrobenzyl alcohol derivatives received special attention, being a prominent and well-known class of light responsive molecules [43]. Despite the advantages of o-nitrobenzyl alcohol derivatives and generally light responsive systems, the use of UV light is still a limit for biomedical applications due to the low penetration in tissues and, most of all, its harmfulness for living cells [166].

A possible solution to this limitation is to use NIR light, which could be employed as drug release stimuli in a double manner [166]. A first mechanism may exploit plasmonic nanoparticles, which absorbing the radiation may induce a local temperature increase and, accordingly to the design of the Nanoparticles, a subsequent drug release [167]. A second modality, which is interesting for UV stimuli responsive molecules, consists in exploiting an upconverting nanocarrier whereby the penetrating NIR light is locally absorbed and transduced in shorter wavelength which therefore activate the drug release mechanism [168].

Taking advantage from this second mechanism, Cristobal and co-workers [168] synthetized nanoparticles based on an upconverting core of NaYF4:Yb,Tm covered by silica shell, which was further functionalized by APTES (3-Aminopropyl)triethoxysilane) groups (Figure 2.19). The amine groups, on the nanoparticles surface, were further coupled with the carboxylic acids of an acrylate o-nitrobenzyl ester monomer, (4-(3-(acryloyloxymethyl)-4- nitrophenoxy) butanoic acid), through EDC-NHS protocol. Finally, in the aim to prove the potentiality as smart carrier, thiolate doxorubicin molecules (dox), were linked to the o-NBE molecules acrylate chains following a thiol-acrylate Michael addition. (Figure 2.19)

In a further step, dox release was achieved by employing a NIR laser beam at 908 nm, which leads to core particles absorption and photon emission in UV-vis regions; the results reported in this work exhibited a release cumulative curve proportional to the NIR irradiation time, demonstrating the successful control of the drug release mechanism by laser beam triggering. "In vitro" experiments of the synthetized nanoparticles in HeLa cells culture, exhibited low toxicity effect on

cells viability in absence of the NIR stimulus, thus proving high selectivity in the release mechanism.

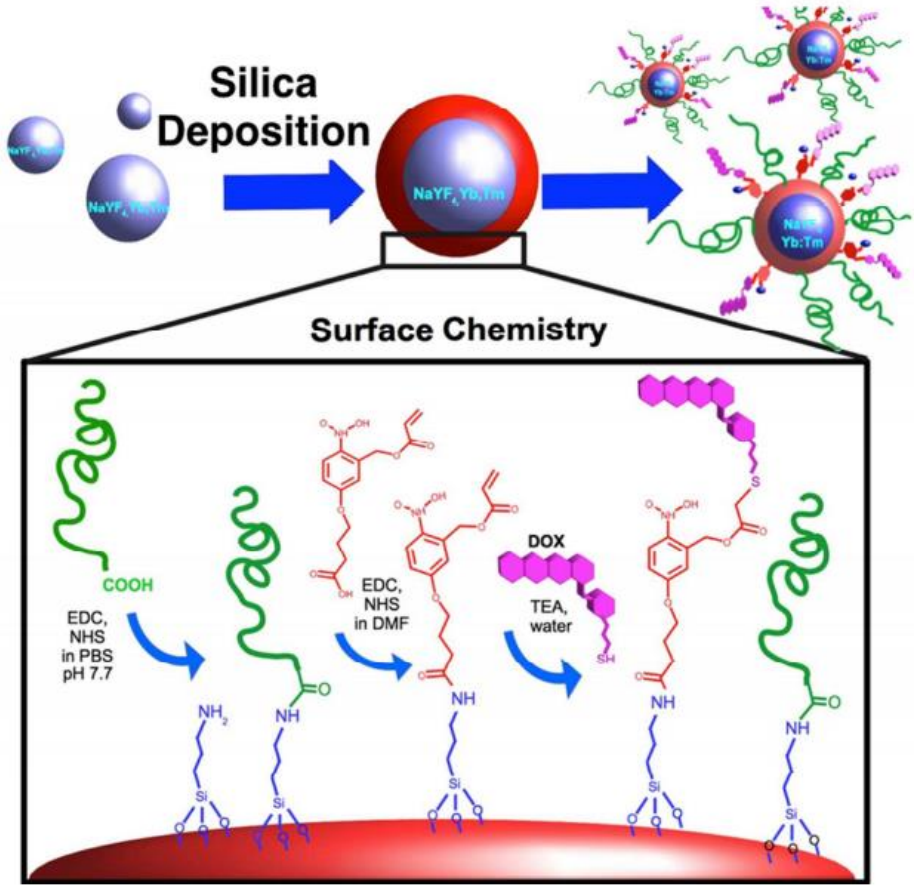

Figure 2.19 Synthetic pathway used in the preparation of the NIR light responsive drug delivery system. (Reprinted with permission from reference [168], Copyright 2015 American Chemical Society).

In the crowded area of smart carriers, stimuli responsive nanogels were also explored as responsive drug carriers [165]. Xin and co-workers designed a nanogel based on a methoxy polyethylene glycol methacrylate (MPEGMA) and UV-light responsive cross-linker 5-(acryloyloxy)-2-nitrobenzyl acrylate (ONB) [169]. In particular, the authors were interested in controlling the nanogels degradation and thus drug release through the synthesis of different polymeric structures. In this aim, they choose tree different MPEGMA monomers, with molecular weight of 300, 500 and 950 Mw. The further crosslinking with o-NBE monomers followed two different routes, a classical free radical mechanism and a RAFT technique. The photodegradation mechanism was then studied through the release of coumarin 102 molecules upon the UV stimuli. Their results showed a more effective coumarin encapsulation and subsequent release in nanogels synthesized with shorter MPEGMA monomers and thus smaller particles size. This behavior was mainly attributed to the MPEGMA hydrophilic ether chains that hinder the encapsulation and release of hydrophobic coumarin; at the same time the results confirmed that the o-NBE isomerization is influenced by particles size and hence coating thickness. In the same work it was reported that the nanogels synthetized by RAFT technique showed narrower size distribution than the ones synthesized by radical

polymerization, exhibiting better results (almost double) in terms of cumulative coumarin release. The “in vitro” tests conducted on HeLa cells following MTT essay protocol suggested low cytotoxicity property of the photo-responsive nanogels (cells viability of 91%).

Dual stimuli responsive smart carriers are of particular interest because of their higher level of selectivity, compared to classical ones [170]. This interest relies on the consideration that cancer cells exhibits abnormally low pH [171,172], or for instance inflamed tissues measure higher concentration of oxidative species, such as hydrogen peroxide and nitrogen derivatives compounds [173]. In the design of a smart carrier, this peculiar characteristic could be successfully exploited by synthetizing materials which could be activated only in particular conditions and hence only in specific tissues [172]. In particular, the local change in the redox environment of a cell due to oxidative stress can be an important indicator of many diseases including cancer [174], atherosclerosis [172], neurodegenerative diseases such as Parkinson’s disease and Alzheimer’s disease [175], or heart failure [176]. For this reason, the design of smart carriers which can respond to a double level of stimuli would be particularly attractive in order to delimit drug treatment in a specific area, without damaging the surrounding tissues.

Following this idea, Sokolovskaya and co-workers proposed an interesting route in the fabrication of dual stimuli responsive carriers [177]. The proposed material consisted in a poly(ethylene glycol) (PEG) polymer functionalized with both redox-responsive thioether moieties and light-sensitive NB groups (Figure 2.20).

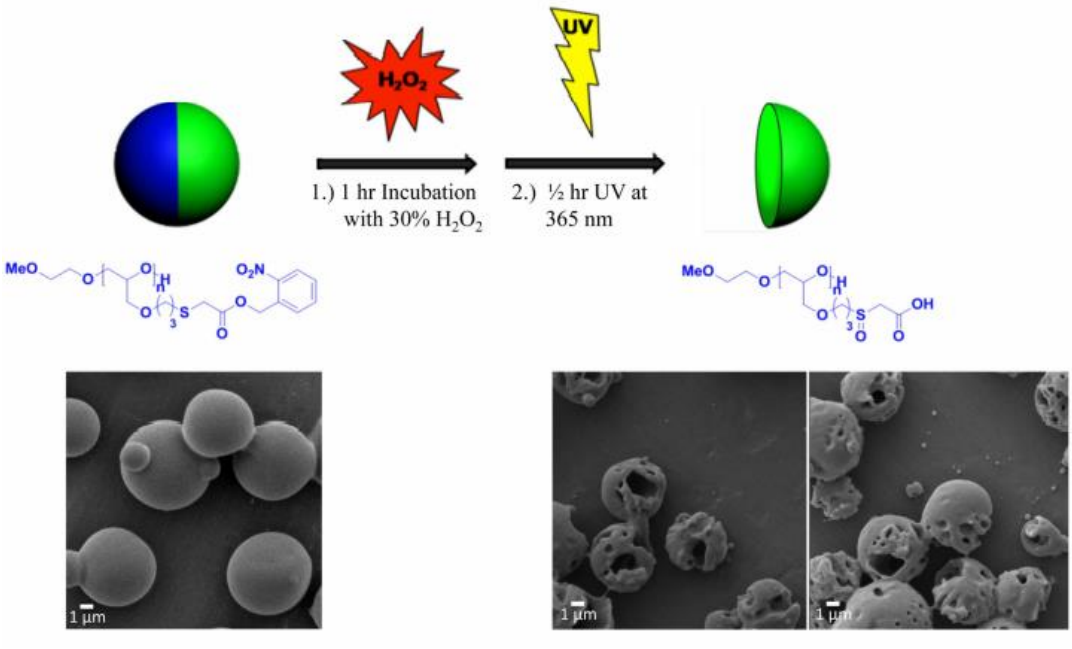

Figure 2.20 Degradation mechanism through oxidation and UV-illumination of bicompartmental microparticles. The particles were incubated in 30% v/v hydrogen peroxide for 1 hour, followed by UV illumination at 365 nm for 30 min. The SEM images on the right visualize the degradation of the particles (Reprinted with permission from reference [177],Copyright 2015 American Chemical Society).

The double stimuli mechanism relies on the oxidation of the thioether into sulfoxide groups under oxidative stress (endogenous stimulus), and photocleavage of NB groups (exogenous stimulus) that can act cooperatively, increasing the polymer hydrophilicity and therefore its solubility in aqueous solution. In the aim, to prove the dual responsive behavior, the authors fabricated Janus microparticles and microfibers, characterized by an unfunctionalized-PEG compartment (green side in Figure 2.20) and a PEG-functionalized one which contains both the thioether and o-NBE groups (blue one in Figure 2.20). They were then able to selective degraded the PEG-functionalized area only after the dual stimulus trigger; oxidative and UV, confirming the double level of selectivity of the synthetized polymer. "In vitro" studied conducted on Raw264.7 cells, that are able to phagocytize microparticles, confirmed the potentiality of this approach in functional imaging or cell tracking experiments.

Li and co-workers proposed a different cytotoxic mechanism exploiting PEG based light responsive particles containing o-nitrobenzyl crosslinkers [178]. The cytotoxic mechanism is based onto the observation that o-nitrobenzyl cleavage reaction in cells provoke PEG swelling, due to the major water up-taking driven by the unprotected carboxylic acids. For PEG particles of a certain dimension, this mechanism could induce irremediable cells damage and eventually death.

In the area of metamaterials, the ability to control molecular self-assembly via non-covalent interactions is an emerging strategy in order to obtain controllable and reversable colloidal aggregates systems [179]. In this aim, molecular recognition, which refers to noncovalent bonding interaction such as dipole-dipole[180], metal coordination [181], hydrophobic forces [182], and/or hydrogen bonding (H-bonding) [183], could be employed as a powerful tool to direct the assembly of micron-sized colloids [184] or even macroscopic objects [185] and create larger aggregated structures with emergent optical [186], mechanical [187] or catalytic properties [188]. Furthermore, an external stimulus which could selective trigger molecular interaction mechanisms promoting molecular self-assembly into complex structures, could be a powerful tool for tailoring the properties of the colloidal dispersions [180,188,189].

In this perspective, Vilanova and co-workers [189] designed two different photo-responsive molecules based on o-nitrobenzyl protected benzene-1,3,5-tricarboxiamide (BTA) derivatives and o-nitrobenzyl protected 2-ureido-4 [1H]-pyrimidinone (UPy) derivatives (Figure 2.21; a, b). Upon UV irradiation and in low polar media, the BTA and UPy molecules self-assemble via H-bonds preferentially into single component clusters and homodimers, following a phenomenon called as "narcissistic aggregation" [190]. Taking advantage of this orthogonal assemble behavior at the molecular level, the authors prepared a dispersion of BTA and UPy functionalized silica microparticles, which spontaneously self-sort into single-specie clusters upon UV-illumination (Figure 2.21; c, d, e, f). The results of this work are of great interest because show that the intrinsic light responsiveness of small molecules can be effectively harnessed to

program the mesoscale assembly of silica microparticles, whose properties can be dynamically modulated. This may allow the manufacturing of complex colloidal metamaterials in aqueous and organic milieu.

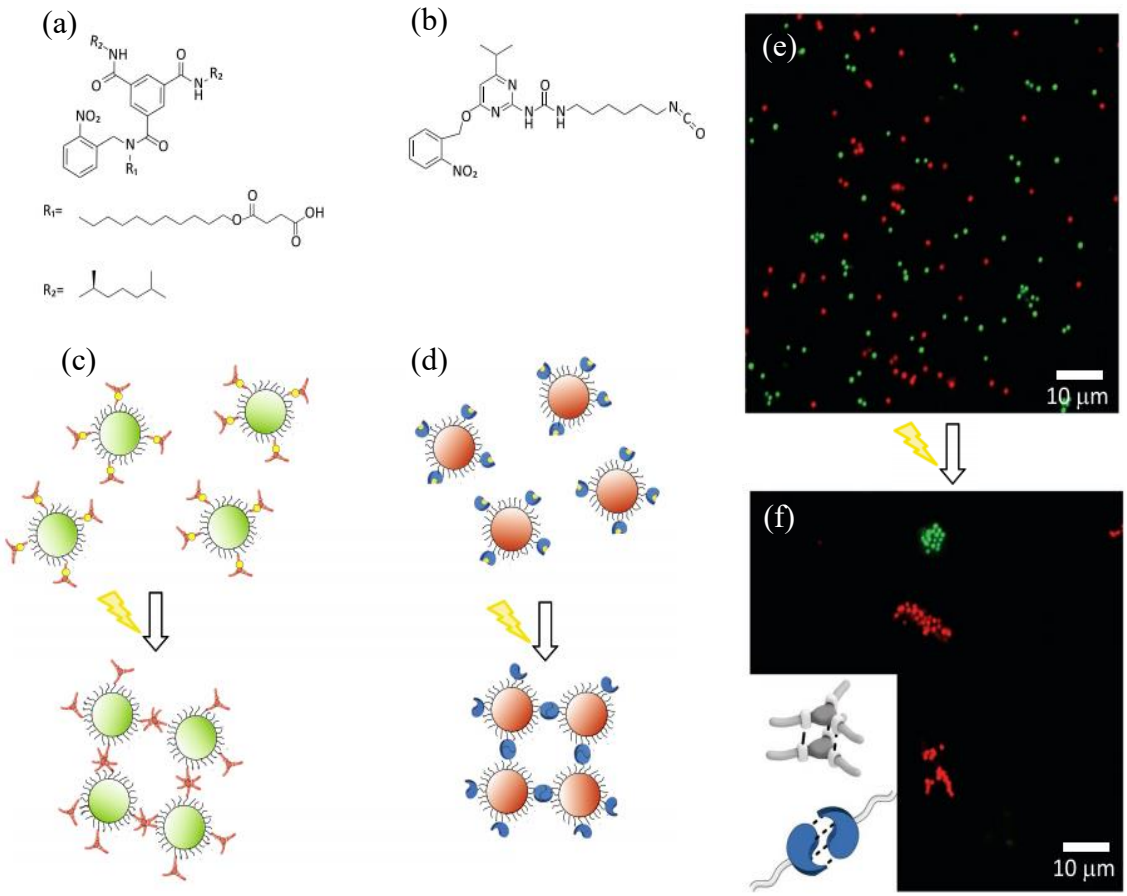

Figure 2.21 Chemical structures of the (a) BTA- and (b) UPy- derivatives. Schematic representation of the behavior of (c) BTA- and (d) UPy-colloids. Upon UV-irradiation, the labile o-nitrobenzyl group is cleaved of and the H-bonds become active, triggering colloidal clustering. Confocal images of an equal mixture of BTA-colloids (green) and UPy-colloids (red) (e) before and (f) afer 30min of irradiation (λmax=354mm). (Reprinted with permission from reference [189]).

Chapter 3

Epoxy-thiol network with bulk and surface photo-triggered properties

The work described in this chapter was published in [38]: "Romano, A.; Roppolo, I.; Giebler, M.; Dietliker, K.; Možina; Šket, P.; Mühlbacher, I.; Schlögl, S.; Sangermano, M. Stimuli-Responsive Thiol-Epoxy Networks with Photo-Switchable Bulk and Surface Properties. *RSC Adv.*, **2018**, *8*, 41904–41914".

3.1 Introduction

As already introduced in chapter 2.2 "click chemistry" has become an attractive route for the synthesis of well-defined macromolecular structures [127]. Along with radical-mediated thiol-ene or thiol-yne chemistry, nucleophilic ring-opening reactions of strained heterocyclic electrophiles carry the salient features of a click reaction. Thiol–epoxy, thiol–isocyanate, and thiol-Michael addition are typical thiol-click reactions that proceed through a nucleophilic attack by either thiols or thiolate anions [128].

These reactions are initiated by strong bases which are added separately, as catalyst, or released in situ by the means of a thermal or photo stimuli. Several examples of photo-latent bases mechanism are shown by Dietliker et al. [191].

Among these reactions, the ring opening of epoxides with thiols yielding β-hydroxythio-ethers, is characterized by a quantitative conversion of the reactants and the absence of any by-products. In a detailed review, Fringuelli, Vacarro and co-workers, showed the intrinsic potentials of thiolysis of 1,2-epoxides, which is involved in many biomedical and biosynthetic applications such as the metabolic detoxification of olefinic xenobiotics and, also as an adjuvant mechanism for cancer chemotherapy [192]. Following the click paradigm, epoxy-thiol proceeds in water and in solvent-free conditions with high yield.

In fact, in the presence of a sufficiently strong base catalyst the reaction occurs at low temperature and with short reaction time (see Figure 3.1) [193,194].

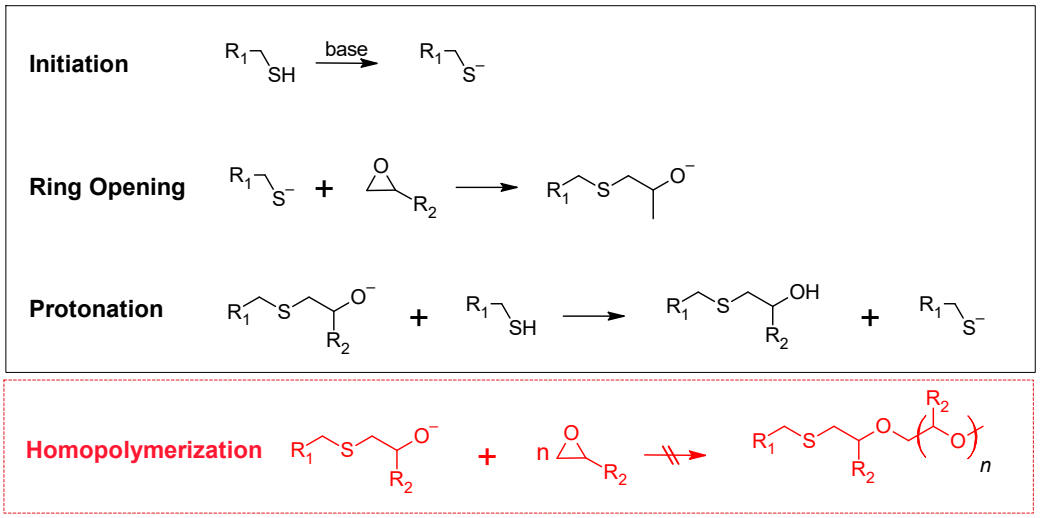

Figure 3.1 Reaction mechanism of the base-catalyzed nucleophilic addition reaction between thiol and epoxy groups. Homopolymerization of the epoxy groups does not occur due to the thermodynamically favored protonation step [194].

In the initial step of the catalyzed thiol-epoxy click reaction, the thiol group is deprotonated by a base catalyst. A thiolate anion is formed, which undergoes a nucleophilic addition (SN2) reaction across the less hindered site of the epoxy moiety. The generated alkoxide anion is then quenched by the thiols or by the presence of protic compounds in the system, leading to the formation of a β-hydroxythio-ether bond. The protonation step is thermodynamically driven and crucial for the click reaction as it prevents the homo-polymerization of the epoxy groups. In addition, it should be noted that the thiol-epoxy addition reaction is autocatalytic, since the formed secondary hydroxyl groups accelerate the ring-opening of the epoxy moieties [128].

Thiol-epoxy reactions have gained increased attention in the preparation of functional polymers and polymer networks as a large number of low molecular weight epoxides and thiol compounds are commercially available [195–197]. The variety of polymeric architectures ranges from the synthesis of linear polymers [198] and dendrimers [199], to the growth of polymer brushes onto various substrates [200–202]. The formed secondary hydroxyl groups are often exploited as reactive anchor groups for post-modification or post-polymerization reactions, which typically involve esterification reactions with activated carboxylic acids or the formation of carbamates with isocyanate derivatives [203–205].

Along with polymer synthesis and surface modification, thiol-epoxy chemistry is also used for the preparation of polymer networks and hydrogels [206,207]. In particular, the interest of thiol-epoxy networks for application in adhesives, coatings or composites is steadily growing, since the materials are characterized by a high optical transparency and flexibility [194,208,209]. However, thiol-epoxy formulations suffer of poor storage stability as the nucleophilic attack of commonly applied base catalysts (e.g. tertiary amines) cannot be controlled temporally [210]. One approach to overcome this drawback is the use of nucleophilic tertiary amine catalysts with poor basicity. Due to a slow activation, the resin formulations can be prepared and processed within a reasonable time whilst the strong auto-accelerating effect ensures a complete curing at low temperature [195,211].

Another promising strategy towards an increased shelf life of thiol-epoxy resins involves the use of latent catalysts that are activated by an external stimulus such as temperature and/or UV-light [193,212]. With respect to photolatent bases, catalysts such as tertiary amines, 1,5-diazabicyclo-[4.3.0]non-5-ene (DBN), tetramethylguanidine or 1,8-diazabicyclo-[5.4.0]undec-5-ene (DBU) are released upon UV exposure [213,214]. Sangermano and co-workers demonstrated the optically triggered curing of thiol-epoxy formulations and the formation of hybrid coatings due to the photo-release of DBN [215]. Other promising classes of photolatent bases involve quaternary ammonium salts of phenylglycoxylic acid or thioxanthone acetic acid [216].

Advancing from both the “click properties” of thiol-epoxy networks and the photo-responsive features of o-NBE chemistry, we designed a stimuli-responsive

thiol-epoxy systems that change both their bulk and surface properties upon UV exposure exploiting the photo-responsive nature of the o-NBE chromophores.

Following the idea of a photolatent thiol-epoxy system with photo-responsive properties, a formulation (see Fig. 3.2) was designed containing a multi-functional thiol monomer (TMPMP), a bi-functional epoxy crosslinker (epoxy-NBE) with photosensitive o-nitrobenzyl ester (o-NBE) group and a photolatent base PLB.

Moreover, a photosensitizer (ITX) was added to the formulation to shift the absorption window of the photolatent base to the visible light region. Thus, the base-catalyzed curing reaction was triggered upon visible light exposure ($\lambda > 400$ nm) without inducing the cleavage of the photolabile o-NBE groups, which proceeds upon exposure with light in the UV-A spectral region. Once formed, the thiol-epoxy networks were cleaved across the o-NBE links upon UV exposure, by the photoisomerization reaction that yields a free carboxylic acid and an o-nitro benzaldehyde derivative [34] as described in the previous chapters.

In this work, the photocleavage of o-nitrobenzyl (o-NB) alcohol derivatives was pursued in order to impart spatially and temporally controllable material properties into the epoxy-thiol network. The UV induced changes in polarity and solubility of polymer networks are of particular interest for the design of functional polymers applied in drug delivery, tissue engineering, photoresists and coatings [217–220]. In chapter 2 it was shown how polymer networks containing o-NBE functionalities were conveniently adopted for the fabrication of positive tone photoresists by controlled degradation upon UV exposure. [106,107,134,141,142,151,221]

It should be point out, that cationic ring opening of epoxy monomer containing o-NBE moieties show a low reactivity and thus, an additional post-curing step at elevated temperature is required for efficient chain propagation and full conversion of the monomers [142].

In the following work, we extended the concept of photocleavable networks to thiol-epoxy click systems. Whilst epoxy monomers with o-NBE groups suffer from low reactivity in cationic ring opening reactions, the base-catalyzed nucleophilic ring opening with thiols is reasonably efficient. The optically triggered change in the bulk properties involving the formation of soluble products due to network degradation was studied in detail and exploited for inscribing positive tone relief structures into the cured thiol-epoxy films by photolithography. The photocleavage of the o-NBE group was further applied to facilitate irreversible changes in the surface wettability of thiol-epoxy networks.

As already mentioned, several studies report the controlled switching of surface properties by the photocleavage of o-NBE chromophores [222]. In the majority of the concepts o-NBE groups are cleaved off from polymer chains leading to an increase of the surface's hydrophilicity due to the formation of polar cleavage products. Encouraged by these studies, we exploited the photosensitivity of the o-NBE links to spatially control surface wettability in thiol-epoxy networks. A distinctive increase of the surface polarity was observed due to the photo-induced formation of hydrophilic cleavage products, which enables a switching of the wettability over a broad range.

3.2 Materials and chemicals

The following materials were employed in the photocurable formulations (Fig. 3.2):

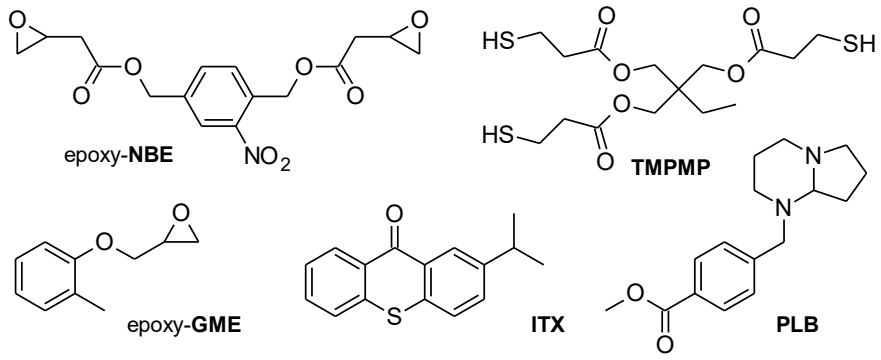

Figure 3.2 Components used in photo-responsive thiol-epoxy resin formulations.

(2-Nitro-1,4-phenylene) bis(methylene) bis(2-(oxiran-2-yl)acetate) (epoxy-NBE) as photosensitive monomer was synthesized as reported in ref.[141]. Glycidyl 2-methylphenyl ether (epoxy-GME), 2-isopropyl thioxanthone (ITX) as photo-sensitizer and all other chemicals were purchased from Sigma-Aldrich (St. Louis, US) and were used without further purification. The photolatent base 4-(hexahydro-pyrrolo[1,2-a]pyrimidin-1-ylmethyl)-benzoic acid methyl ester (PLB) was kindly provided by BASF (Switzerland). In the formulations, PLB and ITX were introduced at different amounts (2, 3, 4 and 5 wt% with respect to the amount of resin), keeping constant the weight ratio of 1:1 between them. The structures of the monomers, crosslinker and photo-initiating system are displayed in Fig. 3.2.

3.3 Experimental procedure and characterization techniques

3.3.1 Preparation of thiol-epoxy formulations

Photocurable formulations were prepared by mixing the trifunctional thiol (TMPMP) with an equal molar epoxy bond concentration of epoxy-NBE and epoxy-GME (0, 5%, 7%). PLB and ITX were also added to the formulations. The resin mixture was stirred at 50°C for 45 min to dissolve the PLB and the ITX. The composition of the different thiol-epoxy resin formulations is summarized in Table 3.1.

Table 3.1 Composition of photocurable thiol-epoxy resin formulations comprising a stoichiometric concentration of epoxy and thiol groups.

sample	epoxy-**NBE** / mol% [1]	epoxy-**GME** / mol% [1]	molar ratio epoxy/thiol groups	ITX / wt. %	PLB / wt. %
PI2	100	0	1:1	2	2
PI3	100	0	1:1	3	3
PI4	100	0	1:1	4	4
PI5	100	0	1:1	5	5
PI4-G5	95	5	1:1	4	4
PI4-G7	93	7	1:1	4	4

[1] mol% related to the total epoxy resin

3.3.2 Curing and cleavage kinetics of thiol-epoxy formulations

In order to study the curing and cleavage kinetics of the thiol-epoxy networks, the prepared formulations (see table 3.1) were photocured by the use of visible light, and then photocleaved by the use of UV light.

Formulations were coated on a silicon wafer and spread with a wire wound bar (coated film thickness, 4 μm). The thin films were illuminated with a Hamamatsu LC8 lamp with visible bulb and a cut-off filter below 400 nm in air for 460 s. The light intensity was 4 mW/cm^2 (λ> 400 nm). For the subsequent cleavage studies the cured samples were irradiated in nitrogen atmosphere with a medium pressure mercury lamp: Hamamatsu LC30, equipped with an optical waveguide, and with a light intensity on the surface of the sample of about 75mW/cm^2 (λ = 250 - 470 nm).

The photocuring of the monomers and the photocleavage of the networks were monitored by FTIR spectroscopy employing a Nicolet iS50 FT-IR spectrometer (Thermo Scientific, Milano, IT) in transmission mode, with a resolution of 4 cm^{-1} and 16 scans. The spectra were recorded in a wavenumber range between 450 and 4000 cm^{-1} and the absorption peak areas were calculated with OMNIC software.

In this regard, the photocuring reaction was studied following the depletion of thiol peak at 2580 cm^{-1}. The photoisomerization of the o-NBE groups, was instead followed through the depletion of NO_2 signals which give two distinct and clear peaks in the FTIR spectrum, 1537 cm^{-1} (asym. stretching) and 1348 cm^{-1} (sym. stretching).

A better description of the theoretical working principle of FTIR is given in appendix A1.

3.3.3 Sol-gel analysis of the cured epoxy-thiol formulations

In the aim to analyse the efficiency of the o-NBE photo-cleavage upon UV light irradiation, a sol-gel extraction analysis was made on the cured thin films of the formulations PI4, PI4-G5 and PI4-G7 (see table 3.1).

The formulations were coated on Si wafer and photocured as described in the previous section. The cured sample were then UV irradiated for inducing the o-NBE photoisomerization using the Hamamatsu LC30 and with a light intensity on the surface of the sample of about 75 mW/cm^2 (λ = 250 - 470 nm).

The soluble species were then extracted by immersing the sample in tetrahydrofuran (THF) for 10 min. The gel fraction was quantitatively evaluated by FT-IR spectroscopy (Thermo Scientific in transmission mode) comparing the area of the ester peak (1752 cm^{-1}), using the equation: gel fraction $\mathbf{gf = A_g/A_o*100}$ where A_0 and A_g equals to the area of ester prior to and after the developing of soluble species. The amount of the soluble species that were extracted gives an idea on the efficiency of the o-NBE links cleavage reaction in changing the bulk properties of the thiol-epoxy polymer coatings.

3.3.4 Photo-Patterning of the cured epoxy-thiol formulations

The photolithographic patterning was manufactured with a quartz-chromium mask in contact mode. For the sample preparation of positive tone patterns, the resin of the PI4-G5 formulation (see Table 3.1) was spin cast on silicon wafer and cured as described in the previous chapter. The subsequent patterning of the polymer networks was performed with the quartz chromium mask in contact mode using UV light with the medium pressure mercury lamp (Hamamatsu LC30, 75 mW/cm^2 ; λ = 250 - 470 nm; atmosphere N_2).

The exposure dose amounted to 7.5 J/cm^2 and after UV illumination the polymer films were developed by dipping the samples for few seconds in tetrahydrofuran.

The patterned films were examined by confocal microscopy (MicroProf®, Fries Research and Technology, Germany). In our specific procedure the adopted measuring frequency, defined as the number of images taken per second, was 2000 Hz and the measuring speed amounted to 607 $\mu m\ s^{-1}$. The resolution in height was 10 nm and a lateral resolution <2.5 μm was accomplished. In addition, the resolution of the patterned film was evaluated by scanning electron microscopy (Auriga 60, Zeiss, Germany) operating at 20 kV after gold sputtering using an Agar Sputter Coater (Agar Scientific, United Kingdom).

A better description of the theoretical working principle of confocal microscopy is given in appendix A3.

3.3.5 Solid state NMR

In our work, solid-state NMR experiment were performed in the aim to determine the formed cleavage products and carried out on an Agilent Technologies NMR System 600 MHz NMR spectrometer equipped with 3.2 mm NB Double Resonance HX MAS Solids Probe. Larmor frequencies of carbon and proton nuclei were 150.75 MHz and 599.46 MHz. Samples were packed into zirconia rotors. The cross polarisation (CP) and magic-angle spinning (MAS) solid-state NMR were used in ^{13}C experiments. Acquisition time and relaxation delay for ^{13}C experiments were 0.025 and 3 s, respectively. Spectra were recorded at spinning rates of 10 and 16 kHz. ^{13}C chemical shifts were externally referenced to the adamantane peak (δ 38.3 ppm relative to tetramethylsilane). For the sample preparation, PI4-G5 was cast on glass slides with a coating knife (120 μm film thickness) and photo-cured as described in the previous paragraph. Subsequently, UV cleavage of the samples

was carried out as described in the previous paragraph in either air or nitrogen atmosphere. For the solid-state NMR measurements, the cured material was peeled off from the glass slide.

A better description of the theoretical working principle of NMR-solid state is given in appendix A.2.

3.3.6 Surface characterization

The switching of wettability was analysed with contact angle measurements performed by using a drop shape analysis system, DSA 100, from Krüss GmbH, (Hamburg, Germany). Thin film of PI4-G5 formulation were spin-coated on Si wafer in order to obtain a flat and homogeneous layer and to avoid that the surface energy measurement was influenced by surface roughness. The cured samples were UV irradiated with a medium pressure mercury lamp: Hamamatsu LC30 (138 mW/cm^2; λ =250 - 470 nm; N_2 and air) in order to facilitate the formation of hydrophilic cleaved species. The wettability of the irradiated sample was calculated with contact angle measurements (water was used as test liquid) few minutes after the irradiation in order to let cool down the surface.

In the aim to have a better comprehension of the surface properties of the UV irradiated and not UV irradiated samples, zeta potential measurements were performed with an Electrokinetic Analyser (EKA, Anton Paar, Graz, Austria) to determine the isoelectric point.

In our measurement set up, a streaming potential method was applied to obtain the zeta potential of the thiol-epoxy surfaces prior to and after UV exposure in 1 mM KCl. The zeta potential was measured starting from natural pH to lower acidic values by adding 50 mM HCl using an autotitrating unit (RTU, Anton Paar, Graz, Austria).

A better description of the theoretical working principle of zeta potential is given in appendix A.4.

3.3.7 Mechanical characterization

Nanoindentation measurements were performed in order to study the mechanical properties of the fabricated polymer coatings. Nanoindentation technique gives information related to the stiffness of a sample and the experiment is carried out by pressing a hard tip, with known properties (such as diamond) into a specimen with un-known mechanical properties [223]. The carried load at the indenter tip increases as the tip penetrates the specimen, and reaches a user-defined value, after which the load may be held constant for a period or may be removed. The hardness is then evaluated by the following formula: $H = \frac{P_{max}}{A_t}$ where P_{max} is the maximum load and A_t is the indentation area [223]. The indentation area is measured with advanced microscopic technique (such as AFM) or adopting special tip geometry, such as Berkovich tip [223,224].

Differently from other characterization techniques employed for studying mechanical properties such as DMA, that gives average properties without variability across the sample, nanoindentation gives more punctual information of

a specimen determining film properties for which conventional testing are not feasible.

The nanoindentation experiments were performed with the Ultra Nanoindentation Tester from Anton Paar (Graz, Austria) using a pyramidal-shaped Berkovich tip. The contact force amounted to 50 µN whilst the maximum indentation force was set to 1000 µN, with a loading rate of 6000 µN/min and an unloading rate of 6000 µN/min. A 30 s hold segment was applied at the maximum load to obtain reliable stress-strain curves. The distance between two measurements was 150 µm and 15 indents were performed over an area of 300 x 600 µm to record the mechanical properties over a larger length scale and to get reliable results. For the determination of the indentation hardness (HIT) the Oliver-Pharr method was used.

3.4 Results and discussion

3.4.1 Curing of photo-responsive thiol-epoxy networks

For the preparation of photo-responsive thiol-epoxy networks, epoxy-NBE was mixed with a stoichiometric concentration of the tri-functional thiol. A photolatent DBN derivative (PLB, see Fig. 3.2) was added as base photolatent catalyst, since amidine structures are well-known for their high nucleophilicity and basicity. Compared to tertiary amines, their basicity is three to four orders of magnitudes higher, which makes them interesting candidates for base-catalyzed crosslinking reactions. In the present study, a latent DBN structure was obtained by protecting the nitrogen with a photoremovable unit, yielding an N-benzylated photolatent amine. By possessing isolated secondary and tertiary amine groups, the photolatent amine comprises a low basicity with a pKa of 8.96 [213]. Upon UV exposure the protecting group is removed by a photoinitiated oxidation reaction and DBN is released. Owed to the conjugative interaction of the two nitrogen atoms across the carbon-nitrogen double bond, DBN is a much stronger base (pKa = 13.41) than the non-illuminated photolatent amidine precursor, and efficiently catalyses the nucleophilic ring opening of the epoxy groups [213].

It should be noted that the spectral sensitivity of PLB is in the UV-B region and thus, interferes with the absorbance of the o-NBE groups [213]. To avoid a premature cleavage of the photosensitive o-NBE links during the photocuring process, the photosensitivity of the photolatent base has to be extended towards longer wavelengths. Previous work has shown that the absorption characteristics of photolatent DBN derivatives can be adjusted over a wide range, either by introducing selected substituents onto the aromatic ring, or by adding various sensitizers (e.g. aromatic ketones or thioxanthone derivatives) [215]. To enable the curing of the photo-responsive thiol-epoxy resin formulation upon visible light exposure, ITX was added as a photosensitizer in the present study. Thus, curing and cleavage of the networks are orthogonal processes that proceeded at different

wavelengths, which is crucial for the successful light-triggered modulation of network properties (see Fig. 3.3).

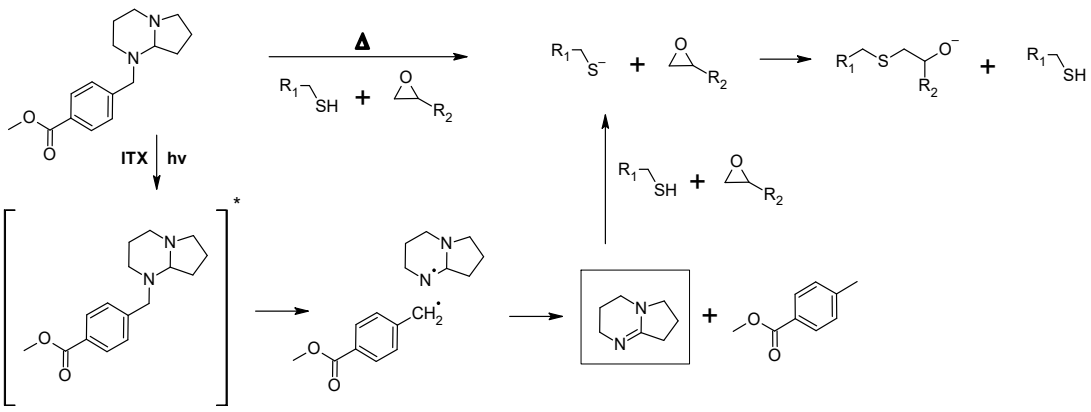

Figure 3.3 Thermally and photochemically triggered base-catalyzed curing of photo-responsive thiol-epoxy networks in the presence of a photolatent base and ITX as photosensitizer, which shifts the spectral sensitivity of the photolatent base towards the visible light region [215].

Fig. 3.4a provides the FT-IR spectra of formulation PI4 (for the exact composition of the formulations used, see Table 3.1 in the Experimental Part) comprising a 1:1 stoichiometric ratio of thiol and epoxy functionalities at a photolatent base and ITX concentration of 4 wt%, prior to and after visible light exposure. The successful network formation by the photo-induced nucleophilic ring-opening reaction is confirmed by the depletion of the characteristic thiol absorption band at 2580 cm-1 (see insert II in Fig. 3.4a) and the epoxy signal at 906 cm^{-1} (see insert III in Fig. 3.4a). The decrease of the functional groups is accompanied by the appearance of the OH absorption band between 3200 and 3600 cm^{-1} (see insert I in Fig. 3.4a) giving rise to the formation of β-hydroxythio-ether links.

The curing kinetics of the ring opening reaction was studied by following the depletion of the functional thiol and epoxy groups upon prolonged visible light exposure. However, the conversion of the epoxy groups could not be calculated accurately due to peak overlapping (see insert III in Fig. 3.4a). Consequently, the curing reaction was monitored by the depletion of the thiol peak at 2580 cm^{-1}. [193,225]. The influence of the photolatent base content (2 -5 wt%) on the curing kinetics was studied by keeping the weight ratio between photolatent base and ITX constant at 1:1 (see Fig. 3.4b). As expected, the results revealed that both reaction rate as well as final monomer conversion increased with rising base concentration, since a higher content of DBN is released deprotonating a larger number of thiol groups. In particular, at a photolatent base content of 2 wt% a final thiol conversion of 83% is obtained upon 50 min visible light exposure. In contrast, nearly full thiol conversion (98%) is accomplished within 8 min at a base concentration of 5 wt%.

It should be noted that dark reactions proceed within the illuminated resins and full monomer conversion is observed in each resin formulation independent of the base concentration after storing the films at room temperature overnight (see Fig. 3.4b).

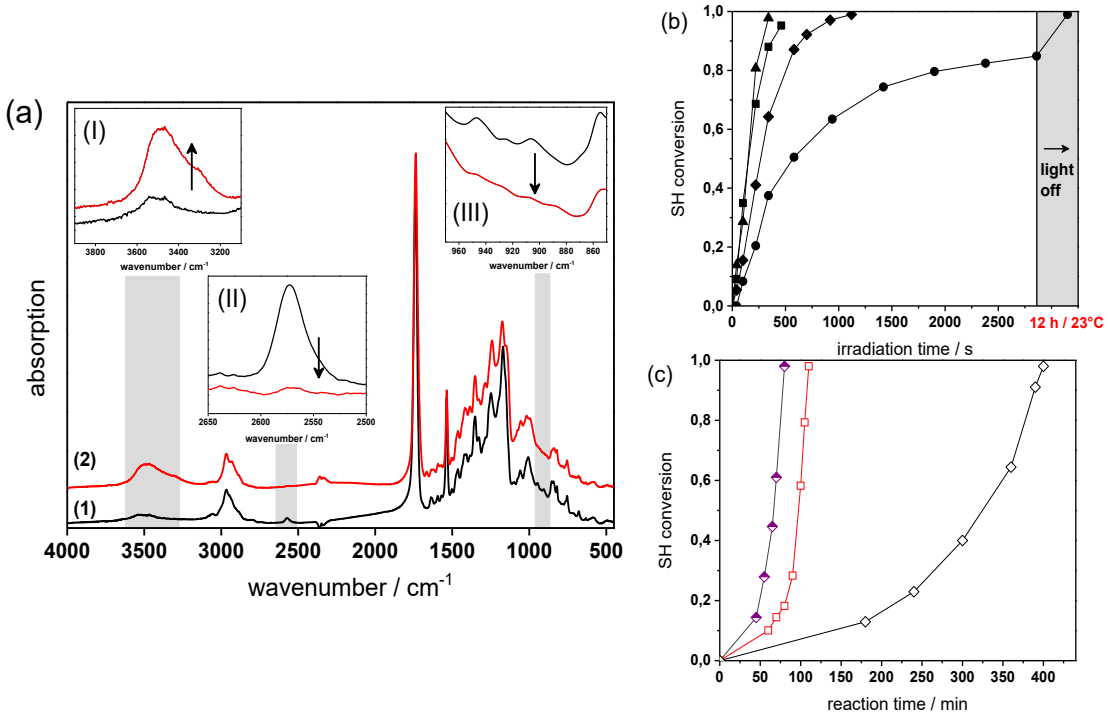

Figure 3.4 (a) FT-IR spectra of PI4 (1) prior to and (2) after photo-curing (1.8 J/cm^2, λ > 400 nm, air). Inserts show the IR bands of the characteristic (I) OH, (II) SH and (III) epoxy groups magnified out of the FT-IR spectra. Normalized depletion of (b) the thiol absorption band (2580 cm^{-1}) versus illumination time (1.8 J/cm^2, λ > 400 nm, air). Resin formulations contained varying amounts of photolatent base and ITX: Pl2 (solid circles); Pl3 (solid diamonds); Pl4 (solid squares) and Pl5 (solid triangles). (c) Normalized depletion of the thiol absorption band (2580 cm^{-1}) of non-illuminated resin formulation PI4 versus reaction time. The reaction temperature amounted to 23 (open diamonds), 50 (open squares) and 70 °C (half open diamonds).

Since the pKa of the N-benzylated photolatent base is in the range of some tertiary amines it might be also capable to catalyse the thiol-epoxy reaction under dark storage conditions [213]. Fig. 3.4c shows the thiol conversion of the non-illuminated resin formulation PI4 as a function of the reaction temperature (23, 50 and 70 °C) and the reaction time. At room temperature the thiol conversion of the non-illuminated resin formulation remains below 15% within 3 hours.

However, upon prolonged storage time the curing reaction is also catalyzed by the less reactive N-benzylated photolatent base and once initiated, the reaction proceeds rather quickly due to the autocatalytic nature of the nucleophilic ring opening reaction. This auto-acceleration effect is nicely demonstrated by the fact that after 240 min in the dark the thiol conversion is <15%, while it reaches nearly full conversion (97%) after 400 min (at 23°C). At 70 °C, the base-catalyzed reaction

of the N-benzylated photolatent base is significantly accelerated and 96% conversion of the thiol moieties is obtained after 80 min only.

From the results of the FT-IR studies it can be concluded that the pKa difference between the N-benzylated photolatent base and the photo-released DBN is large enough to ensure fast reaction rates upon visible light illumination whilst ensuring a sufficient storage stability of the resin formulation at room temperature of over three hours.

Regarding the light induced modification of the cured material, previous studies demonstrated that the efficiency of the cleavage is higher in networks with lower cross-linking density since less crosslinks must be cleaved for the formation of soluble cleavage products [134,142]. To decrease the network density of the thiol-epoxy systems, the photocuring was also carried out in the presence of a mono-functional epoxy monomer (epoxy-GME). In particular, 5 and 7 mol% of epoxy-GME (see Fig. 3.2) was added to the resin formulation while keeping the stoichiometric ratio between thiol and epoxy groups at 1:1. The FT-IR results revealed that the low amount of mono-functional epoxy monomers within the thiol-epoxy resins did not influenced reaction rate or final monomer conversion of the nucleophilic ring opening reaction (see Fig. 3.5).

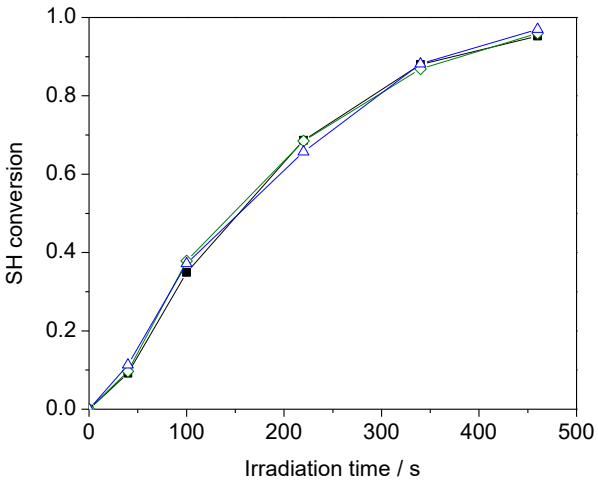

Figure 3.5 Normalized depletion of the thiol absorption band (2580 cm^{-1}) versus illumination time (4 J/cm^2, $\lambda > 400$ nm, air). Resin formulations contained varying amounts of epoxy-GME at a given PLB and ITX level of 4 wt%: Pl4 (solid squares); PI4-G5 (open diamonds) and PI4-G7 (open triangles).

3.4.2 Cleavage of photo-responsive thiol-epoxy networks

The photocleavage of photo-responsive thiol-epoxy networks was followed in thin films, which were drop-cast on Si wafers. The cured samples were illuminated with UV-light at wavelengths below 400 nm to induce the cleavage reaction of the o-NBE links, which proceeds via biradical intermediates formed by β-hydrogen abstraction by the excited nitro group analogous to the Norrish-type II reaction (see Fig. 3.6a) [34].

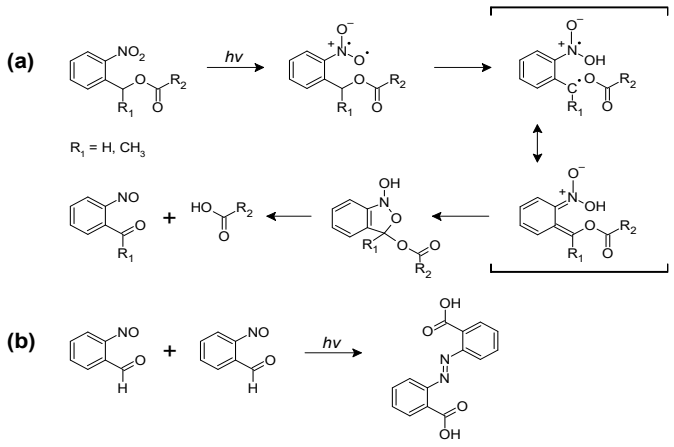

Figure 3.6 (a) Primary and (b) secondary photoreactions during the photoisomerization of *o*-NBE derivatives [36,57,226].

In the triplet state, a proton abstraction from the methylene or methine carbon in γ-position takes place by one oxygen atom from the nitro group, which is followed by the generation of an aci-nitro tautomer in the ground state. The latter can undergo cyclization to form a benzoisoxaline derivative. The resonance stabilized five-membered ring is subsequently cleaved yielding a carboxylic acid and an o-nitrosobenzaldehyde as primary photoproducts. In secondary photoreactions the formed o-nitrosobenzaldehyde dimerizes and is able to form azobenzene groups (see Fig. 3.6b) [36,57,226].

In Fig. 3.7a, FT-IR spectra of formulation PI4 are compared prior to and after UV exposure. The UV induced conversion of nitro moieties to nitroso groups is indicated by the decrease of the two characteristic NO_2 signals at 1537 cm^{-1} (asym. stretching) and 1348 cm^{-1} (sym. stretching). Moreover, the C=O absorption band (1635 - 1802 cm^{-1}) is broadening, which is related to the formation of the characteristic cleavage products such as carboxylic acids.

For cured thiol-epoxy resin formulations with varying amount of epoxy-GME, the photoisomerization kinetics was determined by following the depletion of the NO_2 signal at 1537 cm^{-1} upon prolonged UV exposure (see Fig. 3.7b). From the FT-IR studies it can be obtained that the photocleavage proceeds rapidly in thiol-epoxy click networks and nearly full conversion of the nitro groups is observed upon 16 min UV exposure. As demonstrated in previous work the photocleavage kinetics of o-NBE links are strongly governed by film thickness (i.e. penetration depth of the incident light) and mobility of the chromophore [134]. Owed to the thioether link, thiol-epoxy networks are typically characterized by a high flexibility and low glass transition temperature, which ensures a high mobility of the o-NBE groups leading to a fast photoisomerization reaction.

Comparing thiol-epoxy networks with varying content of epoxy-GME (0, 5 and 7 mol%), it is obvious that the addition of the mono-functional epoxy monomer does not affect the photocleavage rates within the applied concentration.

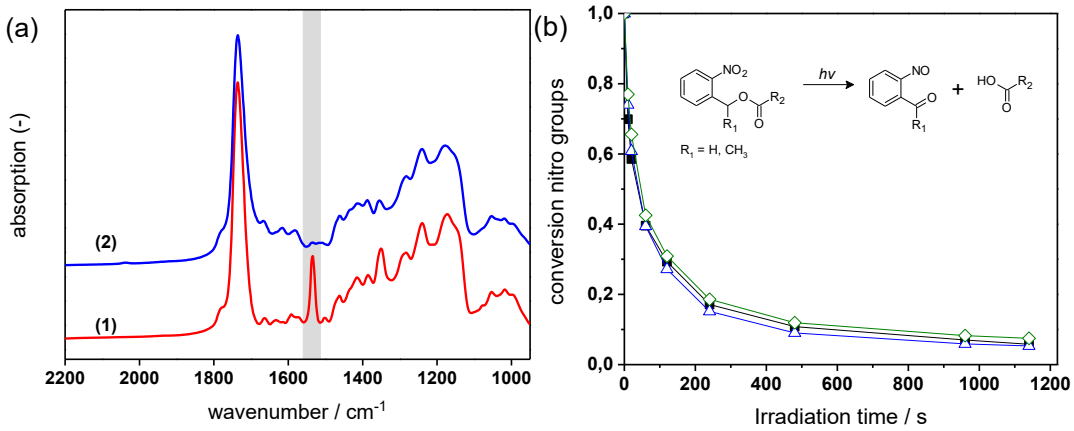

Figure 3.7 (a) FT-IR spectra of cured **PI4** (1) prior to and (2) after photo-induced cleavage of the *o*-NBE links (85 J/cm^2, $\lambda < 400$ nm, N_2). (b) Following the photocleavage kinetics of the *o*-NBE links by FT-IR spectroscopy upon prolonged UV exposure: Decrease of the normalized intensity of the nitro band at 1537 cm^{-1} in **PI4** (*solid squares*), **PI4-G5** (*open diamonds*) and **PI4-G7** (*open triangles*).

To study the change in solubility properties sol-gel analysis of thiol-epoxy formulations with varying amount of epoxy-GME was carried out (see Fig. 3.8a). As mono-functional epoxy monomer, epoxy-GME can act as chain extender, since it increases the molecular weight between two crosslink points [151]. In the absence of the mono-functional epoxy monomer (PI4), the gel fraction of the cured thiol-epoxy networks amounted to 98%. By adding 5 or 7 mol% epoxy-GME (PI4-G5, PI4-G7), the gel content decreased to 95 and 89%, respectively. The results indicate that epoxy-GME does not only affect the network structure but also the gel fraction, as a higher content of soluble species (e.g. oligomers) is formed in the presence of the mono-functional epoxy monomer.

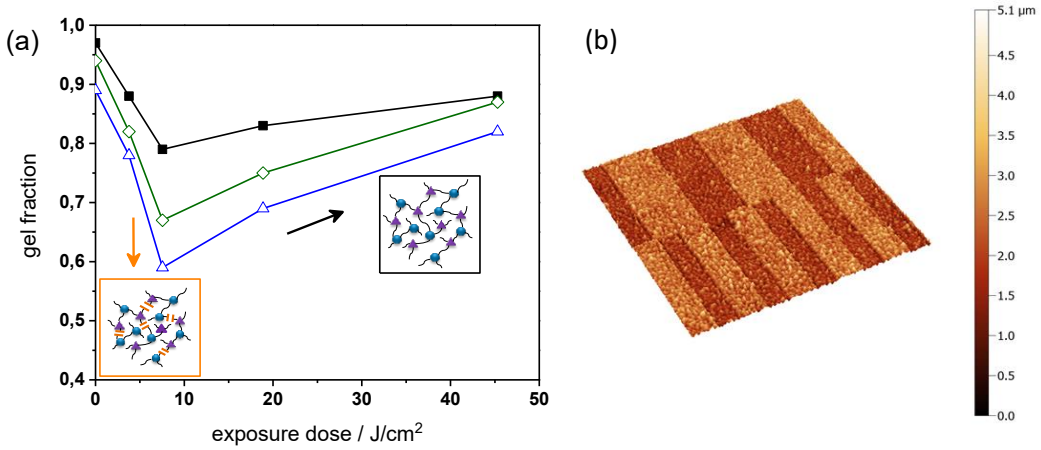

Figure 3.8 (a) Gel fraction of **PI4**, **PI4-G5** and **PI4-G7** versus exposure dose (75 mW/cm^2, $\lambda < 400$ nm, N_2) as obtained from FT-IR measurements. (b) Confocal micrograph of positive-tone relief structures (100 and 50 µm lines and spaces) inscribed into **PI4-G5** by photolithography after the development in tetrahydrofuran.

In a subsequent step, the cured films were UV irradiated and the gel fraction was monitored upon prolonged UV exposure. Independent on the epoxy-GME concentration the gel fraction of the photo-responsive thiol-epoxy networks followed the same trend. Upon a UV exposure of 7.5 J/cm^2, the gel content steadily decreased corresponding to the photo-induced formation of soluble species.

However, if the exposure dose exceeded 7.5 J/cm^2, the gel content increased and ranged between 82 and 88% after a UV exposure with 45 J/cm^2 indicating a reformation of covalent links, which may be attributed to the photoinduced crosslinking via azobenzene group formation as shown in reaction (b) in Fig. 3.6. This phenomenon was also observed in photocleavable polyether and thiol-ene networks [134,142].

To get an insight into the structure of the cleavage products formed in photo-responsive thiol-epoxy click networks, solid state NMR experiments were performed. In particular, the influence of the exposure dose and the atmosphere, in which the UV irradiation had been carried out (air versus nitrogen), was studied. ^{13}C solid state NMR analysis of cured but not illuminated networks did not reveal any cleavage products (see Fig. 3.9).

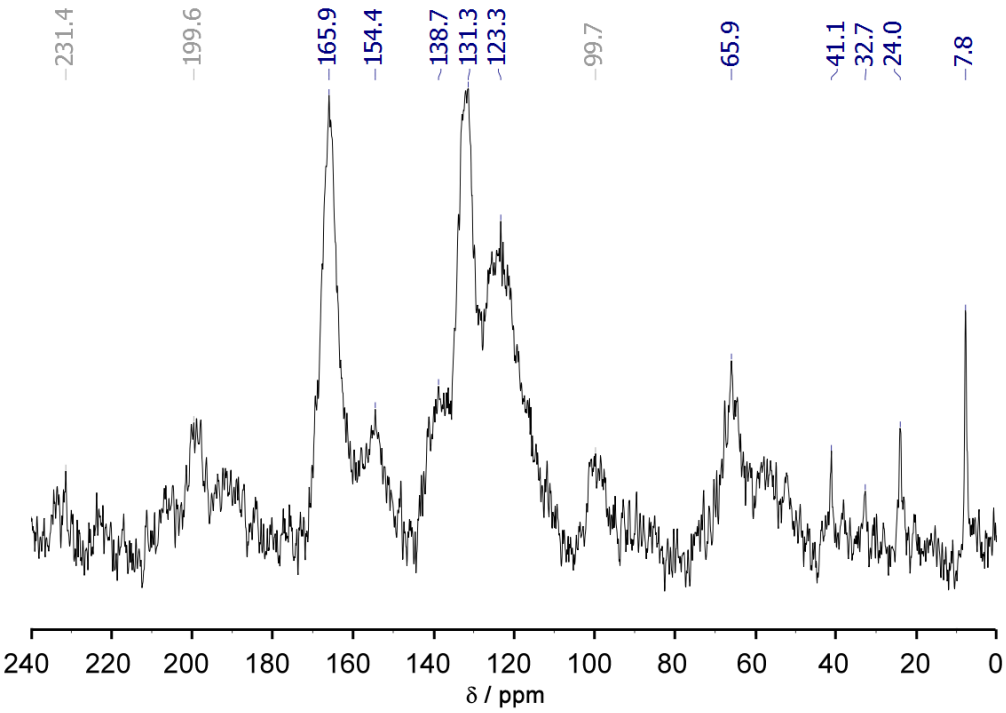

Figure 3.9 ^{13}C CP/MAS solid state NMR of crosslinked PI4-G5 acquired on 600 MHz solid state NMR. Sample was spun at 10 kHz. Chemical shift of signals belonging to the formulation components are marked in blue, spinning side bands are marked in grey.

By UV illuminating the network with an exposure dose of 100 J/cm^2 (compared to sol-gel analysis higher exposure doses were chosen since the film thickness of the samples was one order of magnitude larger) signals at δ 166 and 157 ppm, belonging to carbon atoms of a carbonyl ester and to carbon atoms linked with a nitro group, respectively, decreased (cf. Figure 3.10a and 3.10b). Simultaneously, new signals emerged at δ 172 and 147 ppm, which are related to

carboxylic acids and carbon atoms linked with an azo group. Moreover, the formation of the azobenzene side products is independent on the atmosphere, since the signal was found in spectra of thiol-epoxy networks, which were either illuminated under air (see Figure 3.10a) or nitrogen (see Figure 3.10b). However, the intensity of the signal at δ 172 ppm (carboxylic acid) was slightly higher if the irradiation was performed under air. This increase is attributed to additional photo-oxidation reactions, since the kinetics of the cleavage reaction is not significantly affected by the presence of oxygen. At a higher exposure dose (300 J/cm^2) this behaviour is even more pronounced (see Figure 3.11a and 3.11b). However, in none of the spectra a signal related to an aldehyde group was observed around δ 190 ppm. This result confirms that the aldehyde as primary photocleavage product rapidly undergoes secondary reactions involving the formation of azobenzene (dimerization) and carboxylic acid (oxidation).

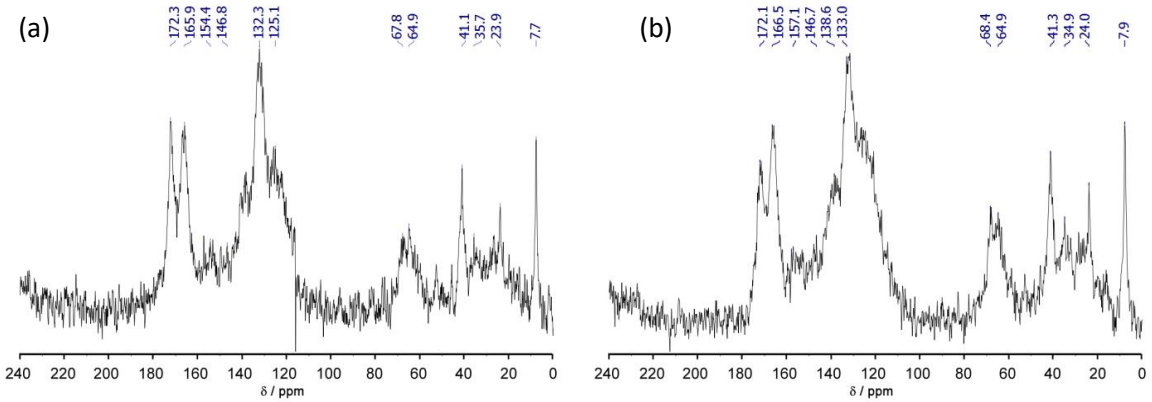

Figure 3.10 ^{13}C CP/MAS solid state NMR of crosslinked Pl4-G5 illuminated with a low UV exposure dose (100 J/cm^2) acquired on 600 MHz solid state NMR. Sample was spun at 16 kHz. UV irradiation were carried under (a) air or (b) nitrogen.

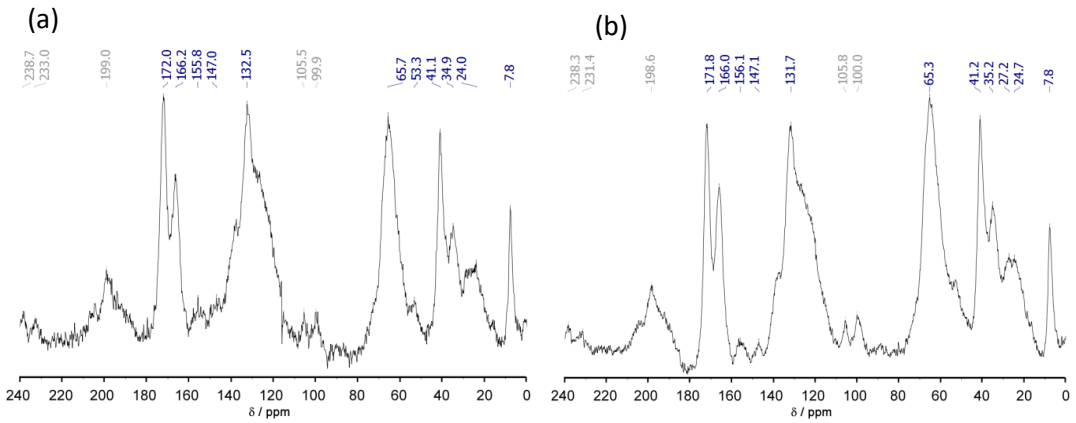

Figure 3.11 ^{13}C CP/MAS solid state NMR of crosslinked Pl4-G5 illuminated with a high UV exposure dose (300 J/cm^2) acquired on 600 MHz solid state NMR. Sample was spun at 16 kHz. UV irradiation were carried under (a) air or (b) nitrogen. Chemical shift of signals belonging to the network and cleavage products are marked in blue, spinning side bands are marked in grey.

The results of the sol-gel analysis further revealed that the relative decrease of the gel content is more pronounced in thiol-epoxy networks containing a higher amount of epoxy-GME. In particular, in the formulation containing no epoxy-GME (PI4) the relative decrease of the gel content was 24%, whilst it is up to 29 and 34% in the presence of 5 and 7 mol% epoxy-GME, respectively (Figure 3.8a). This behavior is expected since an increasing epoxy-GME concentration corresponds to a decreasing crosslink density and in lower crosslinked networks fewer crosslinks have be cleaved before soluble products are formed.

Since the photodegradation was reasonably efficient in PI4-G5, the spatial control of solubility properties was exploited to inscribe micro-sized patterns within cured thiol-epoxy networks by using photolithography. For sample preparation, thin films of resin PI4-G5 were spin cast onto Si wafers. Once the resin formulation was photo-cured, positive-tone relief structures were obtained by UV exposure through a quartz-chromium mask, followed by a development step, washing off the photodecomposition products. The non-exposed areas remained insoluble during the development in tetrahydrofuran, whilst the illuminated areas became partly soluble due to the photolysis of the o-NBE links. Relief patterns with a structure size of 50 and 100 µm were obtained, which were visualized by confocal microscopy (see Fig. 3.8b).

The photocleavage of covalent crosslinks was further demonstrated by nanoindentation measurements. The data were analyzed according to the "Oliver & Pharr Method", in which mechanical properties are derived from the unloading-part of the load-displacement curve [227]. In the present work, the indentation hardness (HIT) was determined by taking an average of 15 individual indents over a 300 x 600 µm area. For sample preparation, the formulation PI4-G5 was cast on glass slides and the change in the hardness was measured in the cured and photocleaved state (UV exposure with 7.5 J/cm^2). The results revealed that HIT distinctively decreases from 33.02 ± 1.05 MPa to 19.21 ± 2.42 MPa due to the photo-induced network degradation.

3.4.3 Light-triggered modulation of surface wettability

In addition to an irreversible transformation of bulk properties, the photo-responsive nature of the o-NBE links in thiol-epoxy click networks was used for altering the surface wettability. Since polar species such as carboxylic acids are formed upon photocleavage, the surface polarity of thin polymer films is expected to be switched conveniently.

For sample preparation, thin films from resin PI4-G5 on silicon wafer were obtained by a spin-cast process. After curing, the films comprised a water contact angle of 77 ± 3°, which is in the range of typical amine-cured epoxy resins [228]. In a subsequent step, the cured thiol-epoxy films were UV illuminated to induce the isomerization reaction of the o-NBE links. The illumination was carried out either under nitrogen or air to study the influence of the atmosphere on the photo-switchable wettability. The change of the contact angle as a function of the exposure time and atmosphere is displayed in Fig. 3.12a. In nitrogen atmosphere the water contact angle steadily decreases with rising exposure dose and reaches a plateau (62

± 4°) if the UV exposure dose exceeds 41 J/cm^2. This behavior is explained by the photo-induced cleavage of the o-NBE links yielding polar groups, as shown by solid state NMR experiments. At a certain exposure dose the o-NBE groups on the surface of the thiol-epoxy network are fully cleaved and thus, no further change of the contact angle is observed. Since the irradiation is carried out under inert conditions, the surface is also not prone to photo-oxidation reactions, which would affect the surface polarity.

In contrast, the UV irradiation under air enables a distinctive shift of surface wettability due to the combined processes of photocleavage of the o-NBE groups and photo-oxidation. From the kinetics of the contact angle over exposure time three different regimes can be distinguished. In the first stage, a sharp decrease of the contact angle from 77 to 60 ± 4° is observed at low exposure doses. This behavior was also detected in the experiments carried out in inert atmosphere, but the decrease of the water contact angle is more pronounced under air due to the additional photo-oxidation of the surface. By irradiating with an exposure dose between 41 and 207 J/cm^2, the decrease of the contact angle slows down but does not reach a stable plateau due to the ongoing photo-oxidation. If the exposure dose exceeds 260 J/cm^2, the decrease of the water contact angle is accelerated until the surface becomes fully wettable and it is no longer possible to record the static contact angle anymore. Comparing the kinetics of both experiments (air versus nitrogen atmosphere) the results suggest that the third regime is mainly controlled by photo-oxidation.

In addition to contact angle measurements, zeta potential experiments were performed to study the changes in surface polarity in dependence on the applied UV irradiation step in more detail (see Fig. 3.12b). The isoelectric point (IEP) of the cured thiol-epoxy network amounts to 4.35, which is in the range of uncharged polymer surfaces such as polyolefins (IEP ~ 4).

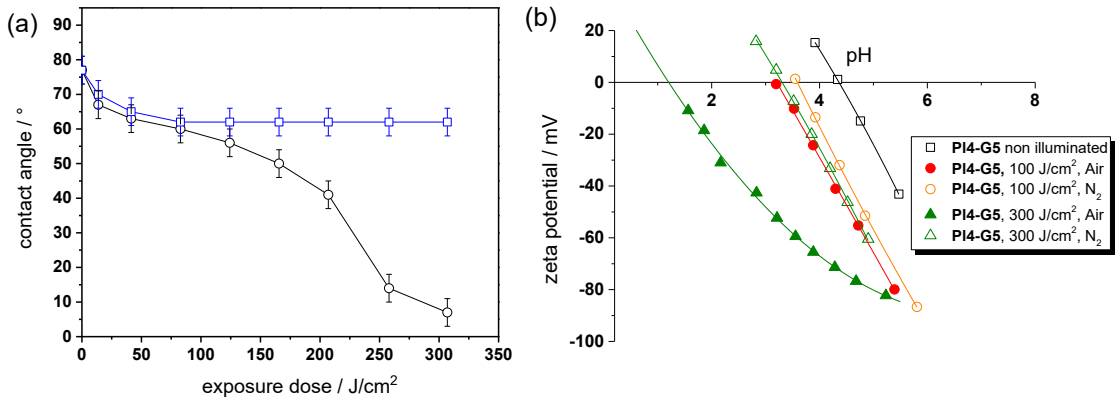

Figure 3.12 (a) Water contact angle of cured **PI4-G5** versus exposure dose (138 mW/cm^2, λ < 400 nm). UV exposure was carried out either in air (*open circles*) or nitrogen (*open squares*). (b) Zeta potential as a function of the pH value of cured **PI4-G5** versus exposure dose (138 mW/cm^2, λ < 400 nm) and atmosphere (nitrogen *versus* air).

The results further indicate the absence of unreacted thiol moieties on the surface of the cured thiol-epoxy formulation since the IEP of surfaces bearing –SH groups is in the range of 3 [229,230]. Upon UV exposure in inert atmosphere, the IEP shifts to lower values, which confirms the formation of acidic groups. It is interesting to note, that a gradual decrease of the IEP is detectable with zeta-potential measurements at prolonged UV irradiation, whilst a plateau of the contact angle data is observed. This can be mainly related to the high sensitivity of the zeta-potential to small changes of the chemical surface composition in comparison to the less sensitive static contact angle.

However, the shift of the IEP is far more pronounced if the UV irradiation is carried out under air, which correlates well with the contact angle data. In particular, at high exposure doses (under air), the IEP drops to 1.25. This gives rise to an acidic surface due to photo-oxidation reactions, which are expected to become the dominating reaction pathway at higher exposure doses. From the results it can be concluded that the versatility of o-NBE chemistry in combination with classic photo-oxidation enables a convenient switching of surface wettability as a function of the exposure dose and atmosphere.

Conclusions

Photocleavable thiol-epoxy networks were prepared by base catalyzed ring opening reaction of multi-functional thiols across bi-functional epoxy monomers bearing photo-sensitive o-NBE links. Photo-triggered curing of the UV sensitive epoxy monomer was accomplished with a photolatent base and ITX as sensitizer, which shifted the initiating window to the visible light region. Photocuring proceeded rapidly due to the highly nucleophilic and basic nature of the photo-released base (DBN) and nearly full conversion of the thiol groups was observed after 8 min of visible light exposure. At room temperature the non-illuminated resin formulation is stable over three hours but at elevated temperature (70 °C), the base-catalyzed reaction of the N-benzylated photolatent base is highly efficient and it turned out that 96% of the thiol moieties are consumed after 80 min.

The subsequent photo-induced network degradation upon UV exposure was confirmed by sol-gel analysis and nanoindentation experiments. The formation of soluble species is compromised by side reactions leading to a regeneration of covalent crosslinks upon prolonged UV exposure. In particular, the formation of azobenzene side products was confirmed by solid state NMR experiments. The addition of 5 and 7 mol% mono-functional epoxides improves the yield of soluble species from 24 to 29 and 34%, respectively. The photocleavage is reasonable efficient to inscribe positive-tone relief patterns within the cured thiol-epoxy networks by photolithography.

Besides the wavelength dependent change in network properties, the photosensitive nature of the thiol-epoxy networks was used to alter their surface wettability. In particular, contact angle and zeta-potential measurements revealed that the photo-induced formation of polar cleavage products such as carboxylic acids leads to a significant enhancement of the surface polarity and wettability. The results further showed that the decrease of the water contact angle is influenced by both exposure dose as well as the atmosphere in which the UV illumination is carried out. Whilst under nitrogen the change in the contact angel does not exceed 15°, the surface of the thiol-epoxy networks becomes fully wettable if the UV irradiation is performed under air due to additional photo-oxidation of the surface.

Chapter 4

Laser triggered writing and bio-functionalization of thiol ene network

The work described in this chapter was published in [231]: "Romano, A.; Angelini, A.; Rossegger, E.; Palmara, G.; Castellino, M.; Frascella, F.; Chiappone, A.; Chiadò, A.; Sangermano, M.; Schlögl, S.; Roppolo, I. Laser-Triggered Writing and Biofunctionalization of Thiol-Ene Networks. **2020**, *2000084*, 1–7".

4.1 Introduction

As reported in previous chapters and more generally in chapter 2.2, the o-NBE cleavage reaction in thiol-click networks proceeds with fast rate and high reaction yields. This result could be mainly attributed to the typical low T_g and high network flexibility of the thiol-click networks, which is related to the thioether bonds. As also reported in the work of Schwalm [90], high network mobility allows large free volume available for the photoisomerization of the o-NBE groups, thus ensuring high reaction yields. Considering instead the efficiency of the o-NBE isomerization reaction for the formation of soluble polymer chains, the reaction proceeds with hyperbolic trend in which the initial fast reaction rate is followed by a progressively decrease at higher energy dose, as clearly visible in Figure 4.1a.

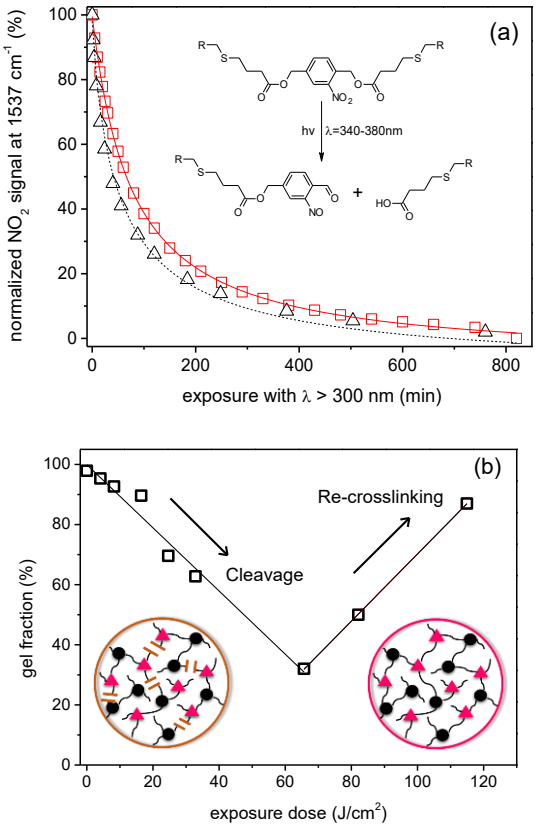

Figure 4.1 (a) Typical ortho-nitrobenzyl cleavage kinetic in thiol-click network. (b) Thiol-ene network's normalized gel fraction after o-NBE photo-cleavage (Adapted from reference [134] published by the Royal Society of Chemistry)

This result, that is common also in other polymer coatings with photolabile o-NBE groups, is related to the formation of secondary photoproducts [221]. On the

one side, they act as intrinsic UV filter and reduce the intensity of the incident light. At last, the formation of secondary photoproducts can lead to a re-crosslinking of the polymer chains at prolonged UV exposure [134,141,151,221].

This behavior was confirmed by sol-gel analysis of thiol-click networks with o-NBE chromophores as function of UV irradiations dose [106,107,134,141,221]. As shown in Figure 4.1b, after a first decrease of the gel content, the network followed a re-crosslinking process, thus decreasing the amount of the extractable soluble species. As shown by solid state NMR experiments on thiol-epoxy network (chapter 3), this mechanism is mainly related to azobenzene side products, which are formed by a dimerization of the nitroso-benzaldehyde. These side reactions limit the performance in photoresist applications.

In order to overcome these limitations, in this research we proposed a new patterning approach based on direct laser writing with a UV-laser. For this purpose, we prepared photocleavable thiol-ene networks by photo-curing a trifunctional thiol with vinyl-NBE (Figure 4.3). In a further step, the network degradation was selectively accomplished through a laser beam source with a wavelength of 375 nm (Figure 4.2). Contrary to conventional photolithography as shown in the previous chapter, in which 2D patterns are inscribed by photomasking techniques and the soluble species are extracted by means of solvents in the development step [107,134,141,142,151,221], in this study a 2.5D profile was simply manufactured by modulating the energy dose of the laser beam in dry conditions, by direct surface ablation of the cleaved network. The direct laser writing offered a further advantage in terms of secondary reaction products. As previously mentioned, prolonged UV exposure significantly limits the amount of extractable soluble species because of the formation of side products and re-crosslinking of the networks [106,107,141,151]. In contrast, with laser irradiation technique, the cleaved off polymer chains are immediately removed by evaporation during the laser writing process, without the possibility for the degraded network to go through secondary photoreactions.

In a further step, we showed the possibility to tailor the presence of carboxylic acids, as primary reaction products of o-nitrobenzyl ester cleavage, on the network surface by tuning the laser energy dose. Along with the realization of dry-developable micropatterns, the chemical surface composition of the exposed areas could be conveniently adjusted since different domains with a tailored content of carboxylic groups were obtained simply by modulating the laser energy dose. Therefore, in a following step, carboxylic acids were activated and exploited as anchor points for attaching an Alexa-546 conjugated Protein A.

The results reported in this work showed as the laser writable thiol-ene networks do not only provide a convenient method for the fabrication of positive tone patterns but also give the possibility to spatially control the surfaces properties with a tailored content of carboxylic groups. Those group could be further employed as grafting point for proteins with a high selectivity and control of the functionalization density.

In Figure 4.2 it is schematized the comparison between photolithography method and direct laser writing for the introduction of micropatterns in photo-sensitive thiol-ene networks.

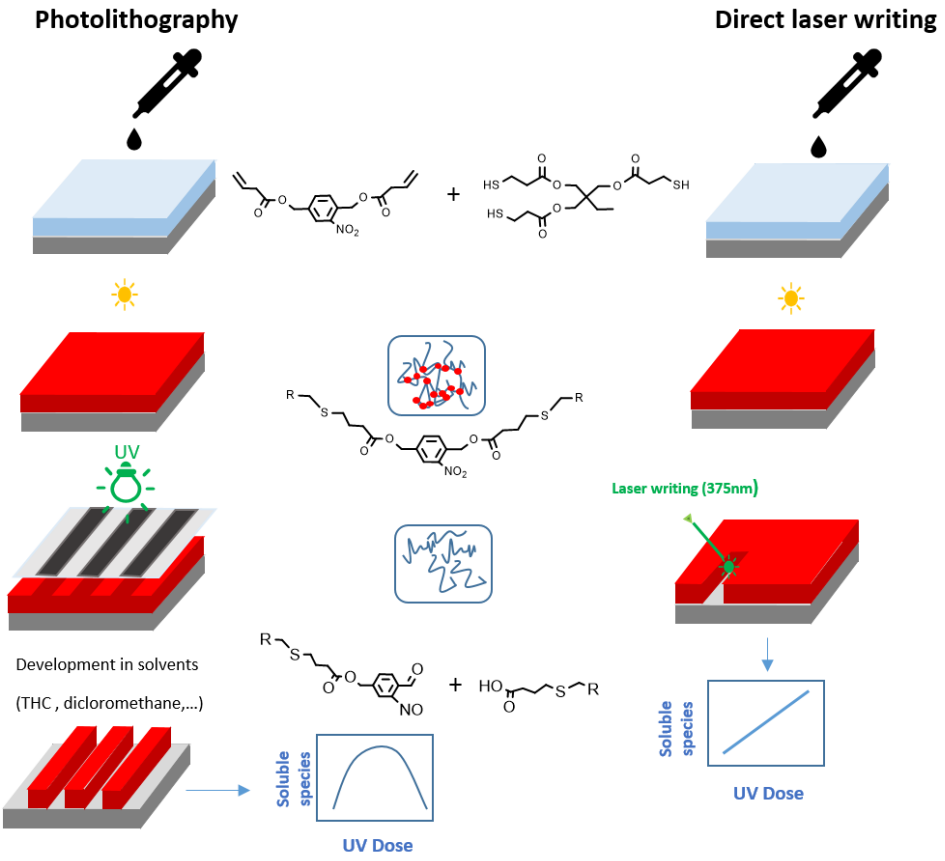

Figure 4.2 Comparison between photolithography and direct laser writing for the introduction of micropatterns in photo-sensitive thiol-ene networks.

4.2 Materials

Trimethylolpropane tris(3mercaptopropionate) (TMPMP) as multi-functional thiol and phenylbis (2,4,6-trimethylbenzoyl)phosphine oxide (BAPO) as photoinitiator were provided from Sigma-Aldrich (Milan, Italy) and were used without further purification. (2-nitro-1,4 phenylene) bis(methylene) acetate (vinyl-NBE) was synthesized as reported in a previous work [134]. Their chemical structures are collected ion Figure 4.3.

For the post functionalization step, 2-(N-morpholino)ethanesulfonic acid (MES, 99.5%), sodium chloride (99.5%), 1-ethyl-3-(3-dimethylaminopropyl)-carbodiimide (EDC, 99%), N-hydroxysulfosuccinimide sodium salt (sulfo-NHS, 98%), Dulbecco's phosphate-buffered saline (PBS) and poly(oxyethylene) glycol sorbitan monolaurate (Tween™ 20) were purchased from Sigma-Aldrich (Milan,

Italy) and used without further purification. Protein A, Alexa Fluor™ 546 conjugated was purchased from Thermo Fischer Scientific (Monza, Italy) and used according to the manufacturer's instructions.

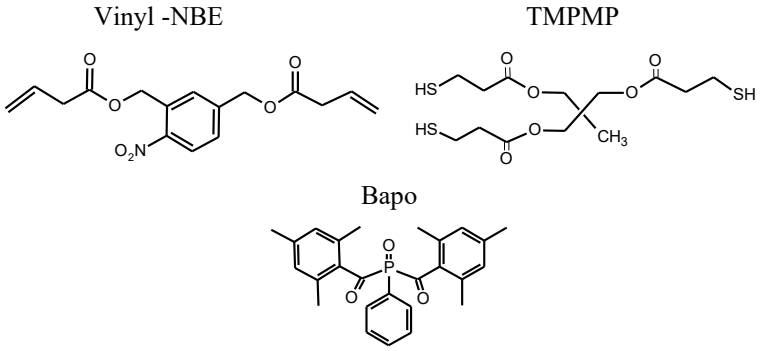

Figure 4.3 Monomers and photoinitiations used for the preparation of thiol-ene photo-responsive network

4.3 Sample preparation procedure and characterization technique

4.3.1 Preparation of the thiol-ene formulation

The photo-curable resin formulation was prepared by mixing vinyl-NBE and TMPMP in stoichiometric amounts (related to monomers' functionality) with 4 wt% of BAPO. The resin mixture was sonicated for 45 min at 50 °C to dissolve the photo-initiator and cured by means of a visible light lamp with a cut off of 480 nm.

4.3.2 Thiol-ene photocuring kinetic

In order to study the thiol-ene curing kinetic, the formulation prepared as described in the previous paragraph, was placed on a silicon wafer and cast with a film applicator bar of 12 μm. The cast film was irradiated using a Hamamatsu LC8 lamp with visible bulb and a cut-off filter below 400 nm with an intensity of 8 mW/cm^2 ($\lambda > 400$ nm) in order to cure the mixture.

FT-IR spectra were recorded on a Nicolet iS50 FT-IR spectrometer (Thermo Scientific, Milano, IT) in transmission mode in the wavenumber range between 450 and 4000 cm^{-1}.The absorption peak areas were calculated with OMNIC software. The kinetics of the light-induced thiol-ene reaction were monitored by the depletion of the IR absorption signals representing the thiol groups (2569 cm^{-1}) and the carbon double bonds (1640 cm^{-1}).

The conversion was further estimated as follows: **conversion = (1-(A_0/A_t))*100**; where A_0 and A_t correspond to the peak area of the IR absorption band at the beginning and after a selected time of light exposure.

4.3.4 Thermomechanical analysis of the cured coating

In order to characterize the thermomechanical properties of the cured polymer network, dynamic-mechanical analysis (DMA) and differential scanning calorimetry (DSC) were carried out. The samples used in DMA and DSC measurements were prepared placing the formulations inside a rectangular mold of 20x15x0.4 mm and curing it with a Hamamatsu LC8 lamp with visible bulb and a cut-off filter below 400 nm with an intensity of 4 mW/cm^2 (λ > 400 nm) for 20 minutes.

DMA measurements were carried out using a Triton Technology TTDMA in the range between -90 and 50 °C at a frequency of 1 Hz and displacement of 20 μm.

DSC measurements were performed with a METTLER DSC-30 (Greifensee, Switzerland) instrument, equipped with a low temperature probe. The samples were heated up in nitrogen atmosphere twice from –90 to 150 °C with a heating rate of 10 K/min, the second scan was analyzed.

4.3.5 Photo-cleavage of o-NBE links with laser ablation

The samples used for the laser ablation were prepared by spin casting 125 μL of the thiol-ene formulation (prepared as described in 4.3.1) on a glass substrate with a SUSS microtec lithography GmbH Delta 6RC BM (500 rpm, 20 s). The spin-cast formulation was irradiated by means of a Hamamatsu LC8 lamp equipped with visible bulb (cut-off filter below 400 nm), with an intensity of 4 mW/cm^2 for 20 minutes in order to produce a photocured film.

Then, selected areas of the cured sample were irradiated with a laser beam using different energy doses (20, 40, 60, 70, 80, 90 and 100 %). The laser source was a 375 nm CW Laser mounted on a μPG101, from Heidelberg. The writing parameters were set as follows: laser spot diameter: 0.6 μm; laser power: 70 mW; energy mode: 4x4 (i.e. 4 passes with a pixel exposure time that is 4 times the standard exposure time). The dose was adjusted by varying the dwell time, given in percentage of the pixel exposure time. These samples were characterized by XPS and laser profilometry and used for subsequent grafting processes.

4.3.6 XPS analysis

XPS analysis were carried out in order to confirm the presence of photo-deprotected carboxylic acids on the sample surface, and thus measuring their amount at different laser UV energy dose. XPS characterization was performed by means of a PHI Versaprobe 5000 instrument, with a mono-chromated X-ray source (Al K-alpha line at 1486.6 eV). A pass energy of 187.85 eV was chosen for survey spectra scans (not reported), while 23.50 eV was used for high resolution (HR) spectra. Data analysis was performed by using a dedicated CasaXPS Version 2.3.13 software. C1s peak maximum at 284.5 eV was chosen as Binding Energy (BE) axis reference. HR spectra background signals were removed by Tougaard functions. A 100 μm spot was used in order to collect the signal only from the inner part of each irradiated rectangle. C1s HR core lines were acquired with at least 50 cycles repeats

each, with an energy step of 0.1 eV and an integration time step of 80 ms. Each peak was deconvoluted with Gaussian-Lorentian functions.

A better description of the theoretical working principle of XPS is given in appendix A5.

4.3.7 Surface profile

The surface profile was analysed in order to measure the laser ablation capability on the photocured thiol-ene surface, and therefore the possibility to fabricate 2.5D positive photo-pattern with z-controllable profiles.

The surface topography has been characterized by an optical profilometer (S Neox 3D Optical Profilometer from Sensofar TM) in Active Illumination Focus Variation Mode with a numerical aperture objective of 20X 0.42NA.

Focus variation is an optical microscopy technique which combines shallow depth of field with a vertical scanning on z-axis, in order to collect different images by variating the focal plane on the sample surface. The collected images are then processed, and the object is rebuilt with all surface areas sharp and in focus.

4.3.8 SEM microscopy

SEM microscopy was used in the aim to record images of the laser fabricated 2.5 D structure. The SEM images were taken with an Inspect F Scanning Electron Microscope from FEI, operating at 30 kV.

A better description of the theoretical working principle of SEM is given in appendix A6.

4.3.9 Post surface modification procedure

Carboxylic acids produced as primary reactions product of o-NBE isomerization, were exploited as anchor points for proteins conjugation. In this aim the carboxylic acids were first “activated”, then conjugated to fluorescent proteins using an EDC/sulfo-NHS protocol.

Carbodiimide compounds are widely used to mediate the formation of amide linkages between carboxylates and amines. Among carbodiimide, EDC (or EDAC; 1-ethyl-3-(3-dimethylaminopropyl) carbodiimide hydrochloride) is the most popular molecule used for conjugating biological substances containing carboxylates and amines. The main advantages are related to its water solubility, also regarding the reaction products [232].

The conjugation process proceeds through a first reaction between the carbodiimide (EDC) and the carboxylic acid, with the formation of O-acylisourea reactive intermediates. O-acylisourea intermediates may then react with a nucleophile amine, through nucleophilic attack, with the formation of an amide bond [233]. The reaction Scheme is reported in Figure 4.4. This reaction procedure counts many potential drawbacks and side reactions, such as the nucleophilic attack of the O-acylisourea intermediates by oxygen atoms, or hydrolysis in water [232]. Especially in aqueous solutions, hydrolysis by water is the major competing

reaction, cleaving off the activated ester intermediate, forming an isourea, and regenerating the carboxylate group [234].

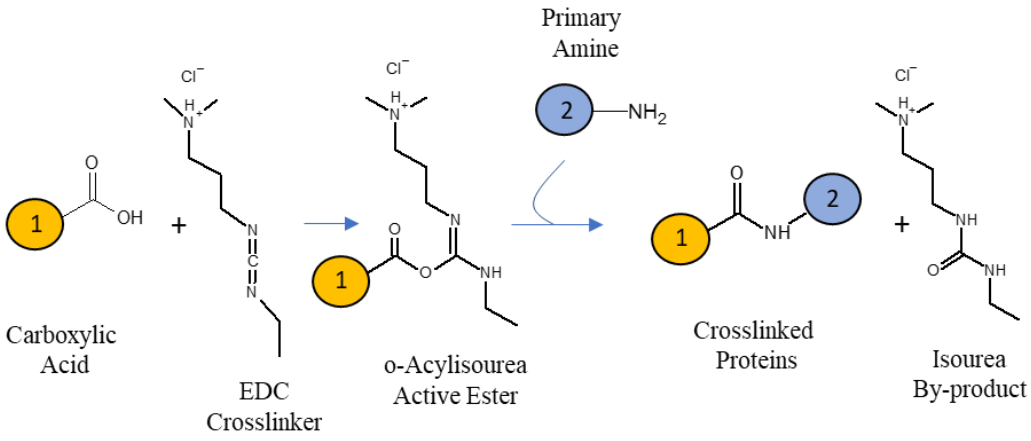

Figure 4.4 EDC (carbodiimide) reactions with carboxylic acid. The conjugation proceeds through a first reaction between the carbodiimide (EDC) and the carboxylic acid, with the formation of O-acylisourea reactive intermediates. O-acylisourea intermediates may then react with a primary amine, through nucleophilic attack, with the formation of an amide bond and isourea by-product.

Other potential side reactions include the formation of anhydride intermediate, as reaction between O-acylisourea and a neighbour carboxylate group, or a rearrangement of the O-acylisourea through the reaction with the neighboring secondary amines in the carbodiimide, with the formation of an inactive N-acylisourea derivative [235].

All these potential side reactions, which may occur in addition to the desired conjugation product, reduce drastically the reaction yields of the desired amide bonds formation.

In order to overcome these limitations, adding a sulfo-NHS to EDC reactions results in a great increase of the solubility and stability of the active intermediate, which ultimately reacts with the attacking amine (Figure 4.5) [232,236]. As visible in the reaction scheme in Figure 4.5, the role of sulfo-NHS is to increase the stability by adding a sulfo-NHS intermediate, which is more stable and less incline to hydrolysis in aqueous solutions compared to the O-acylisourea intermediated [232,237]. Eventually, in the presence of an amine nucleophile, which may attack the carbonyl groups, the sulfo-NHS groups rapidly leave, creating a stable amide linkage with the amine, as also seen with the O-acylisourea intermediate [238].

For the functionalization step of our specimens, an array of three aligned squares, of laser-patterned thiol-ene photopolymer, was incubated in a mixture of EDC/sulfo-NHS (4/10 mM) in MES buffer (0.1 M, pH 4.7) for 15 minutes[239].

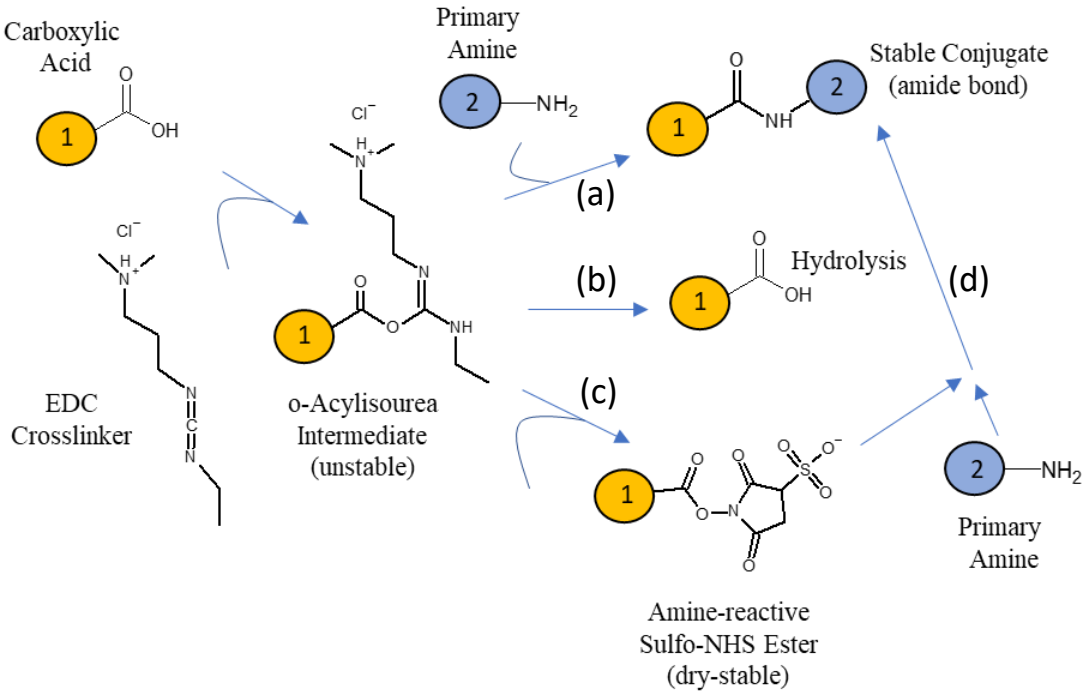

Figure 4.5 EDC/-sulfo NHS reaction scheme. The o-Acylisourea unstable intermediate may undergo through tree different reaction paths (a, b, c). The Sulfo-NHS ester (path c) reacting with a primary amine groups (reaction path d) leads to the formation of amide bonds as final product.

After that, the sample was rinsed twice in PBS for 5 minutes. In this way, the carboxyl groups became more reactive toward primary amines, which are always present in the structure of proteins, with the resulting formation of an amide bond, as clearly seen in scheme in figure 4.5 reaction path c and d. The Alexa-546 conjugated Protein A (50 µg/mL in PBS) was incubated overnight (O/N) by drop casting using a total volume of 50 µL. The activated carboxyl groups were exploited as anchor points for the immobilization of the incubated proteins. Finally, the sample was washed three times in PBS with Tween™ 20 at 0.05% wt.

4.3.10 Fluorescent microscopy

The post modified surface was finally characterized by a fluorescent confocal spinning disk microscopy, in the aim to proof and map the presence of the bio-conjugate proteins.

Fluorescent images were collected using a microscope (Eclipse Ti2 Nikon) coupled with a Crest X-Light spinning disk confocal and a Lumencor SPECTRA X light engine. All images displayed the same scaling and were collected using a Plan Apo 20x 0.75 NA (Nikon).

A better description of the theoretical working principle of confocal spinning disk microscope is given in appendix A7.

4.4 Results and discussion

4.4.1 Photocuring kinetic and thermo-mechanical properties of the thiol-ene network

The network formation occurs upon the radical-mediated thiol-ene click reaction between the double bonds of vinyl-NBE and thiol groups of TMPMP (Figure 4.6). Upon visible light exposure, the photo-initiator (BAPO) undergoes α-bond cleavage mechanism (Norrish type I system) in which free radicals are formed. Those radicals abstract a hydrogen from thiol moieties yielding thiyl radicals (RS*)[128] (Figure 4.6).

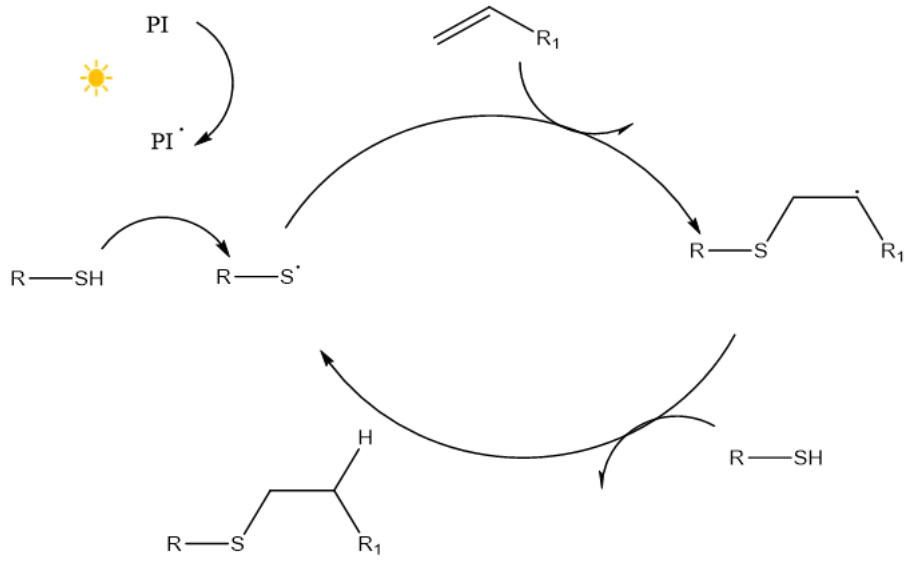

Figure 4.6 Radical mediated mechanism of the thiol-ene click reaction [128].

Once formed, the thiyl radicals initiate the polymerization within two step: first the direct addition of the thiyl radical across the C=C bond, yielding an intermediate carbon-centered radical followed by chain transfer to a second molecule of thiol to give the thiol-ene addition product, with the concomitant generation of a new thiyl radical. Possible termination reactions involve typical radical–radical coupling processes [130].

Regarding the kinetics of the thiol-ene reaction, the molecular properties of both thiol and vinyl monomers influence the reaction rate. At a given thiol moieties, the reaction rate is affected by the structure of carbon-carbon double bonds and particularly by the electron density nearby the double bond functionalities [128,130]. Within few exceptions, the reaction rate increases with rising electron density [131].

The electron deficiency of the vinyl functionality with the electron-withdrawing o-nitrobenzyl group may explain the lower reactivity rate compared to

other thiol-ene formulations [131]. Moreover, as already reported in the previous chapter, -NO_2 moieties seems to reduce the overall reaction speed also in in radical controlled mediated polymerization [112].

IR spectra of the thiol-ene system were collected at different irradiation times. Figure 4.7a shows the comparison between the liquid and the cured formulation while the kinetics is shown in Figure 4.7b.

The kinetics of the vinyl-NBE/TMPMP system (Figure 4.7b) show a fast conversion rate of both thiol and C=C groups in the first 60 seconds of irradiation, reaching a final plateau after 300 seconds at about 88 % of conversion. The studied kinetics are in agreement with a previous work on thiol vinyl-NBE systems [134].

Moreover, the C=C and SH conversions, shown in Figure 4.7b, proceed with a similar reaction rate and final conversion, indicating that co-polymerization is occurring. The high final conversion in this system (88%), compared to other radical mediated reactions such as methacrylic, is a typical key feature of the thiol-ene based system, in which the delay in gel point allows chain mobility inside the network until higher conversions because of the step growth mechanism [128,130,131].

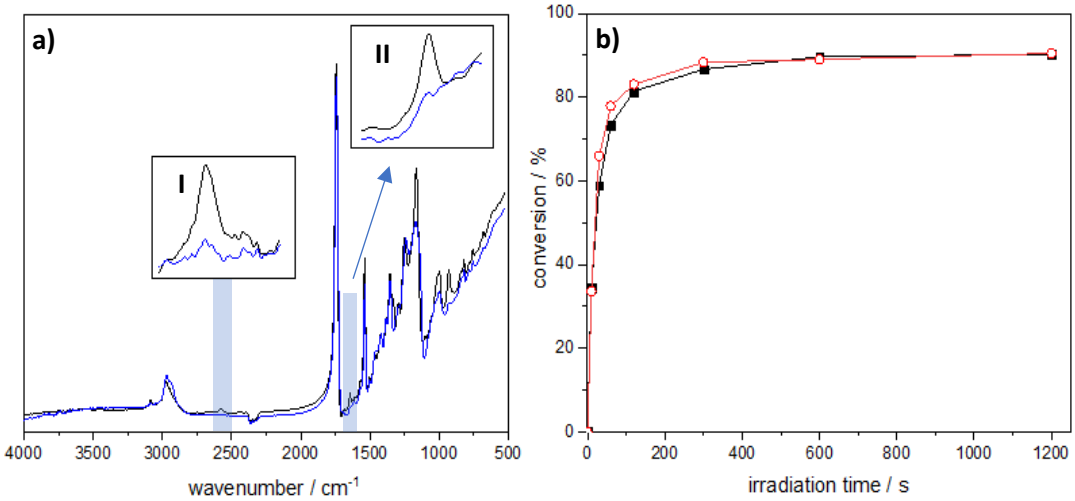

Figure 4.7 a) FT-IR spectra of TMPMP/vinyl-NBE formulation prior (black) to and after (blue) photo-curing (3.6 J/cm^2, λ > 400 nm, air). Inserts show the IR bands of the characteristic (I) SH (2569 cm^{-1}) and (II) C=C (1640 cm^{-1}) groups magnified out of the FT-IR spectra. b) Normalized depletion of the thiol absorption band (2580 cm^{-1}) solid square and double carbon bonds absorption band (1640 cm^{-1}) (open circles) versus illumination time (8 mW/cm^2, λ > 400 nm, air).

In order to characterize the thermomechanical properties of the cured polymer networks, dynamic-mechanical analysis (DMA) and differential scanning calorimetry (DSC) were exploited.

The glass transition temperature (T_g), in DMA measurement, is taken as the temperature corresponding to the maximum of tan δ curve and it is approximately -10 °C. The relatively low glass transition temperature is mainly due to the flexible

thioether bonds throughout the network, and it's a characteristic of thiol-click networks.

Tan δ, defined as the ratio of E″ (loss modulus) to E′ (storage modulus), measures a value of 1,73, thus showing high energy dissipation (damping) of the studied polymer. Moreover, the obtained tan δ curve (figure 4.8, a) revealed the formation of a homogenous polymer network with a single and rather narrow transition phase, and a full width at half maximum (**fwhm**), measured as the width at half of the tan δ peak height, of about 20 °C.

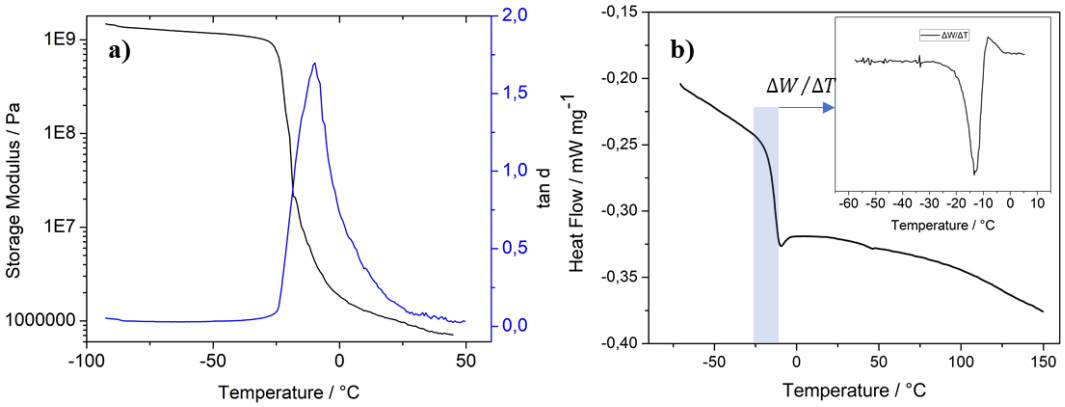

Figure 4.8 a) DMA measurement of TMPMP/vinyl-NBE sample with storage modulus (black) and tanδ (blue) of the crosslinked polymer b) heat flow/temperature curve according to DSC measurement of the TMPMP/vinyl-NBE formulation with insert of first derivate of the heat flow; ΔW/ΔT in the glass transition interval.

The network homogeneity and the narrow glass transition region are in agreement with other thiol-ene polymer structures and represents one of the most salient features of thiol-ene chemistry [128,131,240,241]. This peculiarity depends on the typical polymer step growth mechanism, and the consequent gel point delay compared to others radical mediated polymerizations, such as acrylic and methacrylic [131,242]. The delay in gel point confers many other features such as; reduced mechanical stress upon polymerization process, better adhesion on a given substrate and shrinkage reduction [128,131].

In DSC measurements the transition from glassy to rubbery state is visible in the heat flow versus temperature curve, by the change in the polymer heat capacity value. The DSC measurement (figure 4.8, b) confirms similar mechanical properties as measured in DMA, with a single and narrow transition phase, and a T_g value of -13 °C. The T_g value, which is taken at the peak value of the first order derivate curve (heat flow-versus temperature), is in agreement with the T_g (-10°C) measured with DMA (figure 4.8, b).

4.4.2 Network cleavage and laser ablation

As previously described, the thiol-ene reaction occurs simultaneously by step-growth reaction between the thiol moieties and vinyl double bonds. The final monomer conversions amount to 88% for thiol and C=C bonds, respectively (Figure

4.7). The photocured material results in a transparent soft film, easy to handle, with a glass transition temperature (T_g) about – 10 °C (Figure 4.8).

The insoluble 3D network was then degraded by a UV laser working at 375 nm, which induced the cleavage reaction of the o-NBE links. Compared to classic photolithographic processes, the direct laser writing is characterized by several advantages such as a high time-space control of the reaction, a uniform energy irradiation, and the possibility to control the 2.5D profile simply by modulating the energy dose of the laser beam. The comparison between the two approaches is displayed in Figure 4.2.

Compared to standard lithography, direct laser writing shortens the process steps, and allows a higher degree of freedom in patterning by the use of an electronic control of the light source. It facilitated a direct patterning by following a CAD (computer-aided design) file, without the use of expensive and fix-design quartz masks. Moreover, we observed that in the laser-induced patterning process, the cleaved network is directly abstracted by evaporation: this avoids the use of solvents in the developing step, differently from classical photolithography processes (Figure 4.2).

This last point involves a further advantage, related to the maximum yield of soluble cleavage products formed by the photolysis. In previous works, it was shown that the amount of soluble species in thiol-ene networks with o-NBE groups reaches a maximum at a certain dose if the irradiation is carried out with an UV-lamp. At prolonged UV exposure, a re-crosslinking of the cleaved polymer chains is observed through secondary reactions (e.g. formation of azobenzene groups by dimerization of nitroso-benzaldehyde moieties) that leads to an increase in the gel content [38,142,151,221].

In contrast to the irradiation with the UV-lamp, the cleaved off polymer chains are immediately removed by evaporation during the laser writing process, without the possibility for the degraded network to go through secondary photoreactions. In the laser writing process, we observed that the amount of removed material has a linear dependence to the energy dose of the laser beam if this exceeds 20 % (Figure 4.9b). The results suggest that a minimum of energy is required in order to sufficiently de-crosslink the network and to remove the cleaved off species.

By varying the energy dose of the laser beam, the z-depth of the patterns was conveniently adjusted over a broad range. In particular, the z-depth goes from 130 nm at 20 % of energy dose to almost 10 microns at 100 % laser energy dose (Figure 4.9 a,b).

Moreover, the sharp profiles obtained (Figure 4.9c) indicate that the material was removed by evaporation and not by shape modification (i.e. plastic deformation) suggesting that a precise 3D patterning of the film could be obtained by laser irradiation (Figure 4.9d).

As reference, similar experiments were performed on a classic thiol-ene network: TMPMP was cured with tri(ethylene glycol) divinyl ether (without o-NBE groups) upon visible light exposure, reaching comparable final monomer conversions. In this network, without photolabile compounds, we did not observe

any degradation or change in z-depth, which confirms the active role of the o-NBE groups in the photo-controlled patterning process.

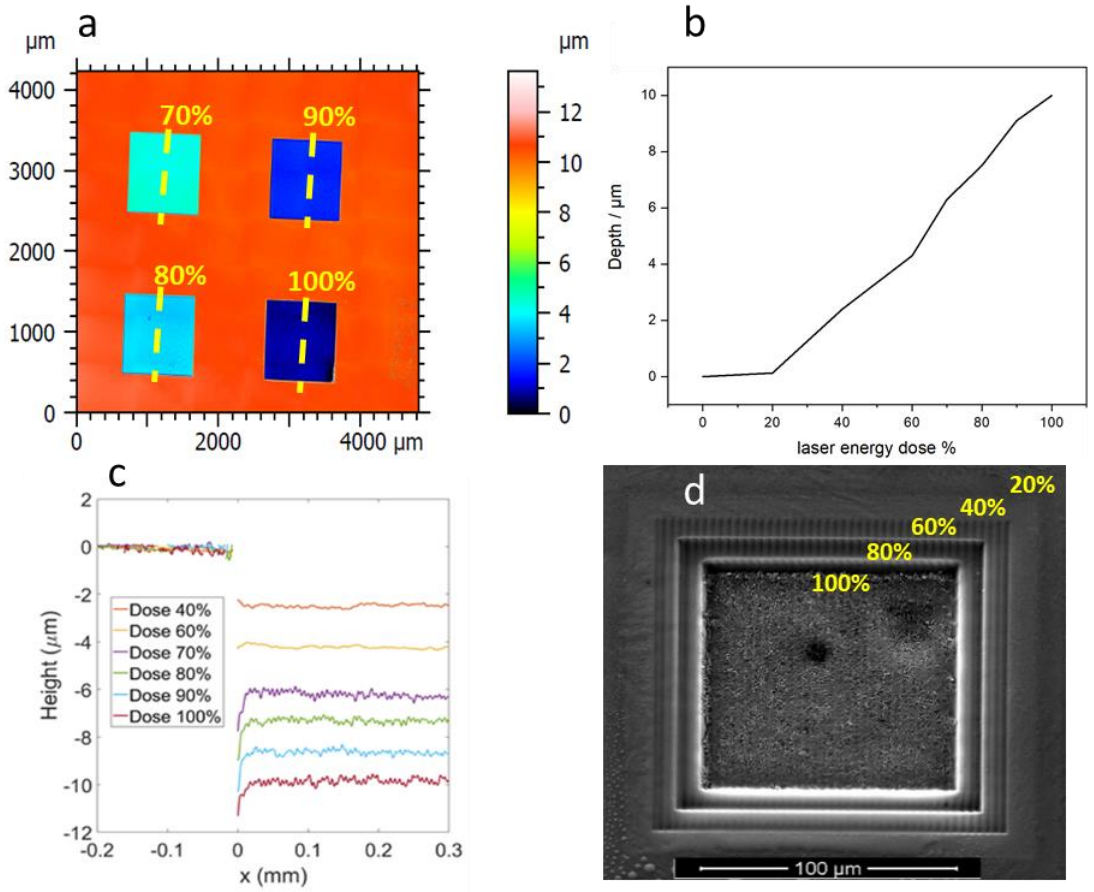

Figure 4.9 a) Profilometer of visible light cured TMPMP/vinyl-NBE samples, cleaved at different energy doses (70%, 80%, 90% and 100%). b) Depth profile/laser energy dose (in %) of visible light cured TMPMP/vinyl-NBE samples, cleaved at different energy doses. c) profilometry of patterns obtained at different laser doses. d) SEM of a 2.5D pattern generated with different energy doses.

4.4.3 Surface post-modification of the photo-deprotected carboxylic acids

In addition, the photo-responsive nature of the o-NBE links in thiol-ene click networks was used for altering the surface properties in a spatially controlled manner. In previous work (chapter 3), we used the presence of polar species such as carboxylic acids, that are formed upon photocleavage, in order to switch the surface polarity of thin polymer film. In this work we modified the sample surface exploiting the carboxylic acids groups generated during photo-decrosslinking (see reaction mechanism described in Figure 4.4 and 4.5) as anchor point for selective protein conjugation. The better time and space control of the photocleavage reaction, and the formed cleavage products achieved upon laser beam irradiation,

enabled a tailoring of the carboxylic acids content in the exposed areas of the surface. Selected sample domains were irradiated with a different laser beam intensity and the presence of carboxylic groups on the surface was characterized by XPS as a function of the energy exposure dose (Figure 4.10).

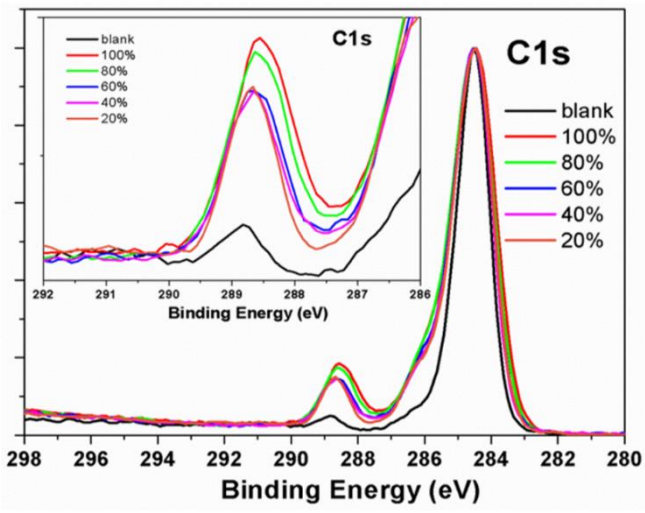

Laser Energy dose	$\frac{[-COOH]}{[C_{TOT}]}$
Blank	1.99%
20%	6.92%
40%	8.12%
60%	8.50%
80%	9.90%
100%	10.73%

Figure 4.10 C1s HR XPS spectra of visible-light cured TMPMP/vinyl-NBE samples, which were then cleaved upon exposure to a laser beam with varying exposure dose. The inset graph shows a magnification of the carboxylic chemical shift, with the peaks located between 288.6 and 288.8 eV. In the Table, UV laser energy dose vs –COOH/CTOT peak area, calculated from HR XPS spectra by a deconvolution procedure applied to C1s peaks, are listed.

As shown in Figure 4.11(blank), the C1s region of the cured thiol-ene sample has been deconvoluted within four components: one for the C-C/H peak at 284.5 eV (peak I), the second one (peak II) at +0.7 eV from peak I, related to C-SH bonds [243,244]; the third one (peak III) at +1.6 eV due to ether bond (C-O) and C-OH and the last one (peak IV) at +4 eV for the ester bond (O-C=O).

The irradiated (i.e. cleaved) samples, instead was deconvoluted with five deconvolution components, in order to overlap completely with the raw signal: the first three already mentioned, peak I, II and III, and two new ones arising for the C=O bond at +2.8 eV and the latter one at +4.2 eV for the -COOH group.

The appearance of these two new components is in good agreement with the photo-cleavage mechanism of o-NBE group, deeply described in previous chapters.

The peak related to carboxylic groups overlaps with the ester at +4.0 eV, representing a sort of offset in the calculation of the peak area ration for the -COOH group towards the total C1s peak area.

The content of -COOH groups was then determined and plotted as a function of the UV irradiation as reported in Figure 4.10, in which for each sample, the -COOH peak area over the total C1s peak area is calculated versus the laser energy dose. It is evident that the -COOH content increases increasing laser irradiation dose. In order to be more rigorous, due to the energy overlapping between ester and carboxylic C, we reported a value (1.99 %) even for the blank sample; however we

expect that this should be only related to the ester O-C=O /C_{TOT} signal. In this regard, the absence of fluorescent signal for the blank specimen in the post modification step (figure 4.12), would make us suppose that is mainly a consequence of the ester (O-C=O) and carboxylic acid (HO-C=O) overlapping in this region. The carboxylic acid formation was also confirmed by the increasing of the area related to C-OH peak (peak III at +1.6 eV, Figure 4.11), at higher laser energy dose.

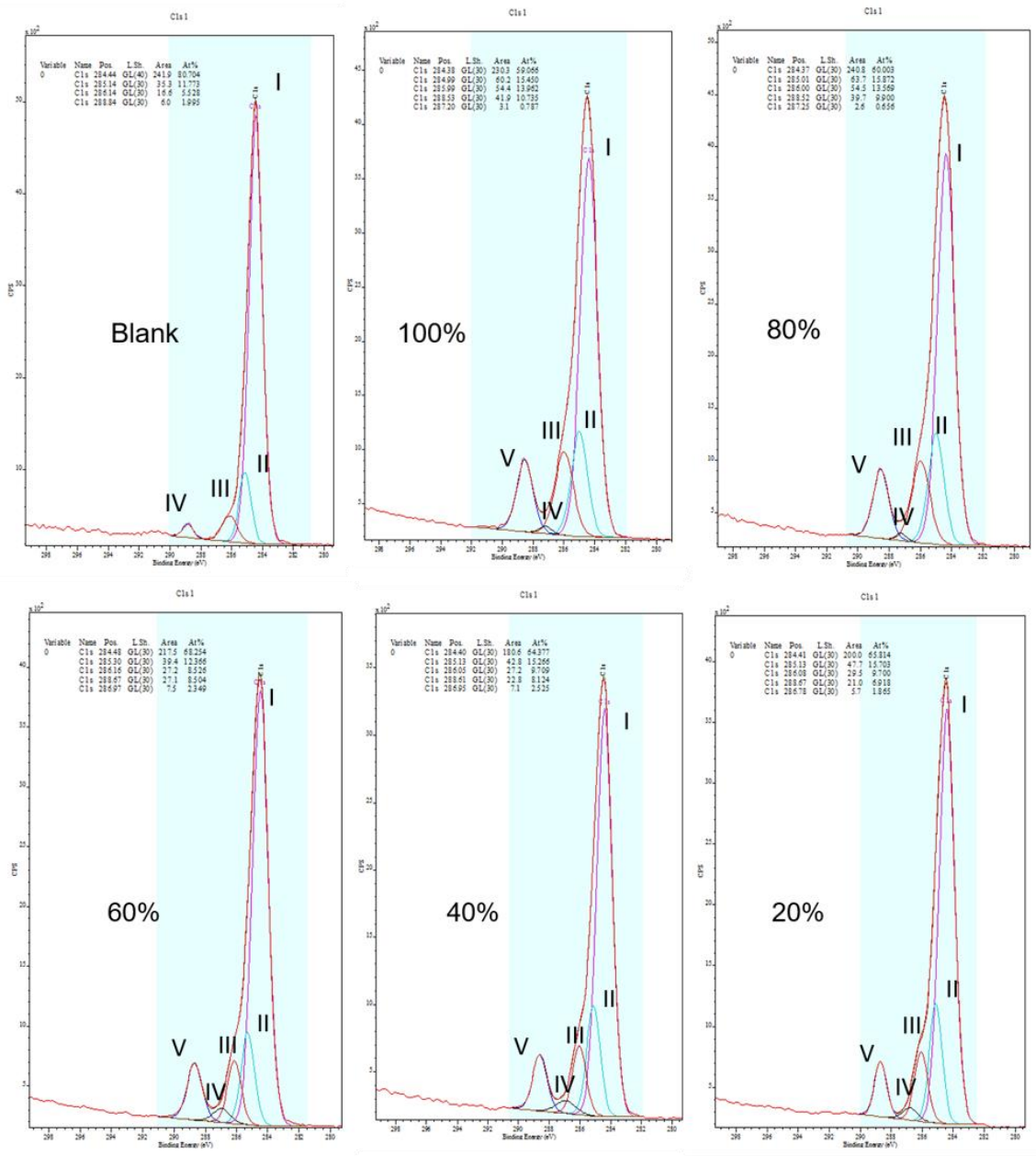

Figure 4.11 High Resolution C1s XPS peaks for the blank sample and the samples irradiated with different laser energy doses.

On the other hand, at maximum laser energy, the content of -COOH groups amounts to 10.73%, indicating an extensive photoisomerization reaction. In order to show clearly the trend, all the C1s graphs were plotted after normalization in the

inset of Figure 4.10. This shows the -COOH group region in more details: the maximum of each peak located between 288.6 and 288.8 eV is clearly visible, with an increasing relatively to laser energy dose.

While it is obvious that we obtained a higher degree of formation of carboxylic groups by increasing the laser irradiation dose, this trend doesn't seem linear as, for instance, for cleavage profiles. One of the possible explanations related to this not linear behavior could be hydrophobic recovery [245].

So, in order to have a better characterization of the correlation between laser irradiation dose and surface modification, the -COOH groups formed by the photo-cleavage reaction were used as anchor points for attaching a fluorescent protein in a spatially controlled manner. In particular, an Alexa-546 conjugated Protein A was used. This allowed us, not only to evaluate the available surface active moieties, but also to demonstrate that these functional groups can be exploited for the immobilization of biomolecules, such as proteins, which is of primary interest in several applications (e.g. biosensors, microarrays, Lab-On-a-Chip) [239,246].

For this purpose, an array of three aligned squares (50x50 μm) for each different laser energy dose (20%, 40%, 60%, 80% and 100%) was prepared in order to create areas with different content of carboxylic acid groups.

The presence of the proteins attached on the surface of the samples was then assessed through a fluorescent characterization (Figure 4.12a). As showed in Figure 4.12a, a large image scan was performed (72 scans with a 20x objective) to provide a wider field-of-view. The wide field fluorescent image clearly states the different emission signal intensity, due to the increasing laser UV irradiation dose for the various squares (in triplicate). The red fluorescence signal, related to the presence of Alexa-546 conjugated protein, was really intense for the higher dose (top of the image) and was barely visible for the lower ones (bottom of the image). This behavior verifies the presence and the availability of -COOH groups at the surface, after the exposure to the UV laser beam. To better highlight these results, the images were further analyzed by using ImageJ 1.50d.

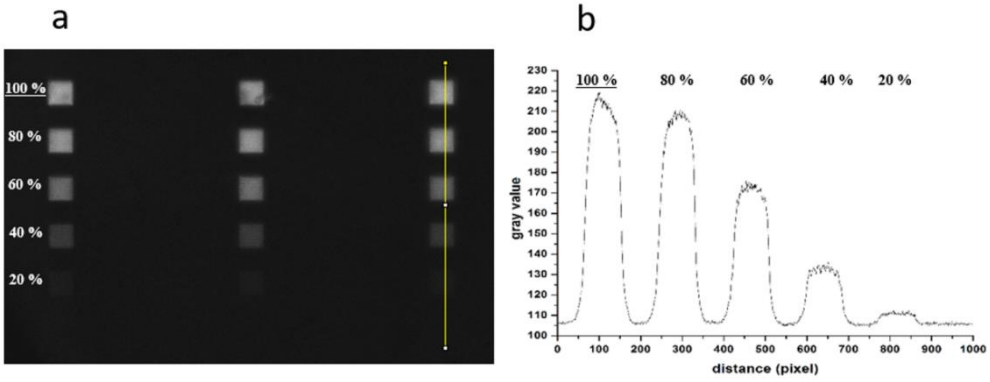

Figure 4.12 (a) Spinning Disk confocal Microscope of the TMPMP/vinyl-NBE sample (each square is 50 x 50 microns) patterned at different laser UV irradiation dose, functionalized with Alexa-546 conjugated Protein A. (b) Plot profile of the average signal (average of 10 profiles) along the yellow line in image (a) for the three replicates of each laser UV irradiation dose.

Figure 4.12b reports the plot profile obtained by taking an average of the signal along the y-axis (yellow line shown in Figure 4.12a). In particular, the image was converted to gray scale and then a line was drawn across all the different squares with different UV laser doses. To be sure that the final plot can be representative of the signal in the image, the profile along this line was acquired ten times in different positions, moving the line on x-direction. This procedure was repeated for all the replicates obtaining an average plot. The grey values in the plot area directly proportional to the amount of signal, enabling a quantification of grafted Alexa-546 conjugated protein A. Therefore, the pattern in Figure 4.12a, clearly shows the possibility to selectively attach a conjugated protein on the laser irradiated areas, with a sharp surface definition. The localized presence of various concentrations of carboxylic acid is also underlined by the linear trend in the plot: the higher the laser dose, the larger the number of available –COOH groups and the higher the amount of immobilized proteins. A similar value was obtained at 80 and 100 % of laser energy dose, confirming the saturation regime reached by this approach, as already reported by the XPS analysis. These results show even a better correlation between the laser energy dose and the presence of carboxylic acid moieties than the data obtained by XPS measurements, especially at low laser energy dose. This apparent mismatch could be explained considering that the typical XPS penetration is 10 nm [247]: it is then reasonable that on this thin surface layer the o-NBE reaction occurs already at low irradiation dose. In contrast to XPS spectra, the amount of immobilized protein correlates with the presence of functional and available carboxylic groups, even below the ~10 nm scanned by XPS. Another possible explanation could be hydrophilic recovery of the surfaces when immersed in water for functionalization [248]. In any case, a higher degree of protein immobilization is related to a higher amount of carboxylic groups generated at higher energy dose.

From these results it can be concluded that this functional test witnesses a more linear correlation with the laser irradiation, demonstrating the potency of the proposed approach for producing 2.5D patterned functional surfaces.

Conclusions

In this work we successfully employed a laser beam source in order to control the patterning and surface properties of a thiol-ene network containing o-NBE groups. A formulation containing a trifunctional thiol and a bifunctional vinyl monomer bearing o-NBE groups was cured using a visible light source. The curing kinetic and mechanical properties match the features of typical thiol-ene polymer networks, within fast and high fields conversion rate and homogeneous cured network. Subsequently, a laser induced degradation of o-NBE moieties with UV light was exploited to create a 2.5D positive pattern with controllable generation of carboxylic acids as photoreaction products. Regarding the patterning, we observed the formation of sharp and defined structures without the necessity of a developing step, enabling a dry-development step. Moreover, SEM analysis on the sample surface showed that it was possible to inscribe a defined pattern with narrow profile, modulating the z-depth by tuning laser energy dose. Regarding the photogeneration of carboxylic groups, we demonstrated by XPS that it was possible to tune the amount of free carboxylic groups as a function of the laser dose. These moieties were exploited for a functional immobilization test, by using Alexa-546 conjugated protein A, showing high linearity between laser energy dose and grafting of proteins. This last result proofs the possibility to use ortho-nitrobenzyl ester chemistry combined with laser technology for developing 2.5D patterned functional structures, which could be fundamental building blocks for a wide range of bio-applications, such as active sensitive layers of biosensors, controlled surfaces for cell growth or Lab-on-Chips.

Chapter 5

Hybrid silica micro-particles with light-triggered surface properties

5.1 Introduction

In the last decades micro and nano particles have increased their range of application in many different fields [249–254]. The particles usually are either inorganic or polymeric [254,255], however an interesting type of those particles are the so-called “hairy” particles. Those have a core, usually inorganic, on which a layer of polymer chains is covalently grafted [256]. These hybrid particles have received tremendous interest due to their chance to design systems with unique and unprecedent properties [254,255,257].

For instance, when the “hairy” surface is comparable in size to the core structure, the particles exhibit interesting features for biomedical applications, because of their possibility to behave as “soft” objects similarly to many biological materials (e.g. blood cells, organs tissues etc..) [258]. Moreover, the “hairy” surface can be exploited in order to change the interface properties of the particles in a surrounding environment, enhancing for example the dispersion in solvents or polymers, or for carrying functional groups and stimuli-responsive moieties on the particles shell [259,260].

Regarding the synthesis strategies, hairy particles are mainly synthetized through two different approaches: (i) grafting-to and (ii) grafting-from procedures [261]. In a grafting-to approach, the polymer chains are directly grafted on the surface via a chemical reaction between surface functionalities of the particles and polymer-end groups [261,262]. This approach is also usually exploited for protein grafting. By properly selecting the molecules to graft, it is possible to achieve a fine control of the surface functionalization. On the other hand, the steric hindrance of the macromolecules as well as the low probability of reaction (only ending groups are used for anchoring) do not allow a densely-packed functionalization. On the contrary, a “grafting-from” strategy, exploits a direct polymer chains growth from the surface in a process known as surface-initiated polymerization. This consists in grafting an initiating species on the surface (i.e. a photoinitiator), and then promote a polymerization starting from those anchoring points. Because in the grafting-from strategy the polymer chains are grown from the surface, it is possible to achieve higher grafting densities and longer polymeric chains grafted [261,262]. Furthermore, in case of employing method as RAFT or ATR, also a good control of the molecular weight polydispersity can be achieved [263–266].

Adding stimuli-responsive features to those hairy particles gives the fascinating possibility to remotely control their properties at a micrometric or nanometric scale [267,268]. Many types of stimuli-responsive micro and nano particles were synthetized and employed in different fields of applications [268]. As already largely discussed in this Thesis, light-responsive systems enhance the level of selectivity allowing a higher control of the stimuli-responsive mechanism. In chapter 2.5, we presented some works in which o-NB alcohol derivatives were grafted on micro and nanoparticles aiming at imparting photo-responsive features.

However, most of the reported literature required long synthesis in harsh conditions such as in temperature and/or using catalyst. On the other hand, other

approaches like photochemical reactions can enable the grafting to or grafting-from processes in milder conditions, furthermore allowing a better control over the process [262,269]. Therefore, photo-grafting from processes are a powerful pathway in environments where heat-sensitive substrates or active-ingredients are employed. Within this frame, in this work we proposed two different procedures in the synthesis of photo-responsive silica particles based on o-NBE chemistry.

In a first synthetic route, an acrylate-NBE photosensitive polymer brush was grown onto silica microparticles through a photochemical grafting-from strategy and at room temperature. The synthetic path, sketched in Figure 5.5, proceeded through a first particles activation conducted by anchoring BAPO silanes derivatives photo-initiators ($TMESI^2$-BAPO), onto the silica surface. In a second step, the BAPO derivatives anchored molecules were exploited as visible light activated radical initiators for the photopolymerization of acrylate monomers containing o-NBE groups; therefore growing photo-responsive polymer brushes on the silica particles. A similar process was already exploited in literature to photoactivate either glass or silica surfaces in subsequent radicals induced photopolymerization process [269,270]. The second proposed strategy instead implies a preliminary silica surface functionalization with 3 aminopropyl trimethoxysilanes, achieving NH_2-surface functionalization. The amino groups were then exploited to induce an epoxy ring-opening polymerization of monofunctional-epoxy-NBE. Even this route allows to obtain silica particles with o-NBE chromophores as pendant groups on the grafted polymeric brushes. Upon UV irradiation, the already described o-NBE photo-isomerization reaction induces the formation of nitroso compounds, which are ideally released in solution, with a consequent formation of -COOH groups on the chains. Eventually, the presence of photo-deprotected carboxylic acids onto silica particles were confirmed by conjugating an Alexa-546 fluorescent Protein. Confocal microscopy images proved the selective anchoring of the fluorescent protein only onto the UV irradiated particles, therefore demonstrating the wide range of potential applications that o-NBE photo-chemistry covers in polymer science.

5.2 Materials and methods

5.2.1 Materials

Silicon dioxide microparticles (1.0 micron, 99.9%) were purchased from Alfa Aesar. Ammonium hydroxide (NH_4OH, 30% solution) and Hydrogen peroxide (H_2O_2, 30% solution) were purchased from Carl Roth GmbH Karlsruhe. Ethanol absolute (EtOH, VWR, 99.9%), ethanol (95%), toluene (99.8%), acetonitrile (99.8%), acetone (ACS reagent), (3-aminopropyl)trimethoxysilane (3-APTMS) were purchased from Sigma Aldrich. 3-(trimethoxysilyl) propyl 3- [bis(2,4,6-trimethyl- benzoyl) phosphinyl]-2-methyl-propionate (TMESI[2] - BAPO) was synthetized as reported elsewhere [271]. (2-nitro-1,4-phenylene) (methylene) acrylate (Acrylate-NBE) and (2-nitro-1,4-phenylene) (methylene) (2-(oxiran-2-yl)acetate) (Epoxy-NBE) were synthetized as reported below. Glass slides were prepared by cutting in pieces of 2cm x 1cm microscopic slides 76x26 mm cut edges purchased by Carl Roth GmbH Karlsruhe.

For the post functionalization step, 2-(N-morpholino)ethanesulfonic acid (MES, 99.5%), sodium chloride (99.5%), 1-ethyl-3-(3-dimethylaminopropyl)-carbodiimide (EDC, 99%), N-hydroxysulfosuccinimide sodium salt (sulfo-NHS, 98%), Dulbecco's phosphate-buffered saline (PBS) and poly(oxyethylene) glycol sorbitan monolaurate (Tween™ 20) were purchased from Sigma-Aldrich (Milan, Italy) and used without further purification. Protein A, Alexa Fluor™ 546 conjugated was purchased from Thermo Fischer Scientific (Monza, Italy) and used according to the manufacturer's instructions.

5.2.2 Synthesis of monofunctional Acrylate-NBE

2-Nitrobenzyl acrylate was synthesized by dispersing acryloyl chloride (4 mL; 49 mmol) with a solution of 2-nitrobenzyl alcohol (5 g; 32mmol) in 50 mL of dry THF. Triethylamine (4.5 mL, 32 mmol) was dissolved in 50 mL dry THF and added dropwise to the reaction mixture over 3 hours. The reaction mixture was stirred for 7 h at room temperature and the progress was monitored by TLC. After evaporation of the solvent, the reaction product, that appeared as a yellowish oil, was dissolved in dichloromethane and extracted with water and saturated Na_2CO_3 solution. The combined organic layers were dried over Na_2SO_4 and the solvent was removed by rotary evaporation. The obtained crude product was further purified by column chromatography (2:1 = cyclohexane:ethyl acetate). Eventually, the solvent was removed by rotary evaporation and the product was collected as yellowish liquid (50 % of the total theoretical yield). In figure 5.1 is plotted the NMR of the synthetized monomer.

^{1}H-NMR:(δ, 400 MHz, 25 °C, $CDCl_3$): δ = 8.1 (d, 1H, -C**H**-^{4}); 7.7 (m, 2H,- C**H**-^{2,3}); 7.5 (t, 1H, -C**H**-^{1}); 6.5 (d, 1H, -CH=C**H₂**^{7}); 6.2 (q, 1H, C**H**^{6}=CH_2); 5.9 (d, 1H, -CH=C**H₂**^{8}) and 5.6 (s, 2H, -C**H₂**-^{5})

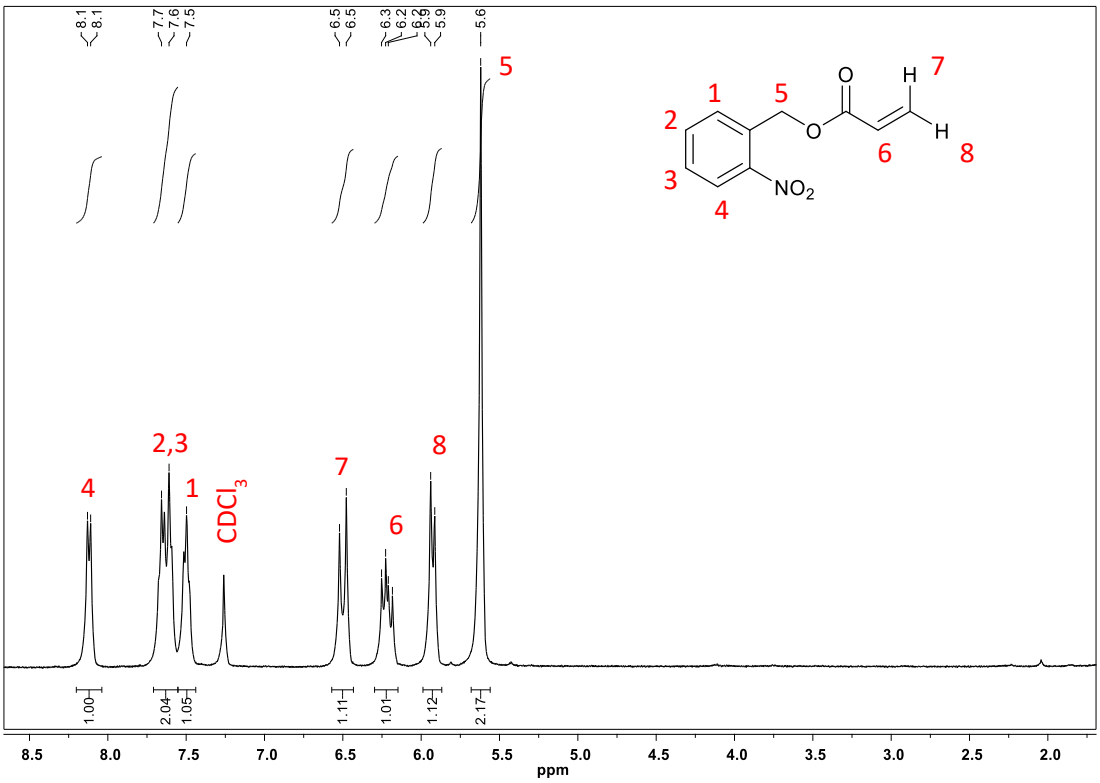

Figure 5.1 H-NMR of the synthetized monofunctional acrylate-NBE

5.2.3 Synthesis of mono-functional Epoxy-NBE

The synthesis of mono-functional epoxy-NBE, (2-nitrophenyl) (methyl) (2-(oxiran-2-yl)acetate), proceeded by two reaction steps. As primary step, 3-butenoic acid (3.5; 41.5 mmol) was added to a stirred solution of (2-nitrobenzyl alcohol) (5.0g; 32.6 mmol) in 40 mL dichloromethane. The reaction mixture was cooled to 0 °C and 4-(N,N-dimethylamino) pyridine (DMAP) (0.8 g; 6.5 mmol) was added.

A solution of N,N'-dicyclohexylcarbodiimide (DCC) (20 g; 96.9 mmol) in 50 mL dichloromethane (DCM) was placed step-wise to the reaction mixture and stirred at room temperature for 2 h. The obtained product of this reaction step was a yellowish precipitate of (2-nitrophenyl) (methyl 3-butenoate). For further purification, the raw product was washed with H_2O and $H_2O/NaHCO_3$, and dried with Na_2SO_4. After further filtration and removing of the DCM under vacuum, a column chromatography (3:1 cyclohexane: ethyl acetate) was carried out. After removal of the solvent, the resulting product amounted at 5g (22.8 mmol). In a subsequent step, an excess of 3-chloroperbenzoic acid (77%) (m-CPBA) (36.0 g; 162 mmol) was added step-wise at room temperature to a solution of the synthetized (2-nitrophenyl) (methyl 3-butenoate) (5 g; 22.8 mmol) in around 100 mL of dichloromethane. The reaction mixture was stirred at room temperature and after a reaction time of 7 days, a yellowish solution with a white-yellowish precipitate was obtained. The product mixture was then dissolved in dichloromethane and the organic layer was extracted with saturated sodium bicarbonate solution and

deionized water. Finally, the solution was dried over sodium sulphate, filtered and the solvent was removed by rotary evaporation at 30°C. For final purification a column chromatography (2:1 = cyclohexane:ethyl acetate) was carried out and the yellowish oil was collected after solvent removal under vacuum (45 % of the total theoretical yield). In figure 5.2 is plotted the NMR and the structure of the synthetized monomer.

^{1}H NMR (400 MHz, cdcl$_3$) δ 8.10 (d, J = 7.9 Hz, 1H), 7.62 (dd, J = 17.8, 7.2 Hz, 2H), 7.50 (d, J = 6.9 Hz, 1H), 5.57 (s, 2H), 3.32 (s, 1H), 2.93 – 2.80 (m, 1H), 2.75 – 2.52 (m, 3H).

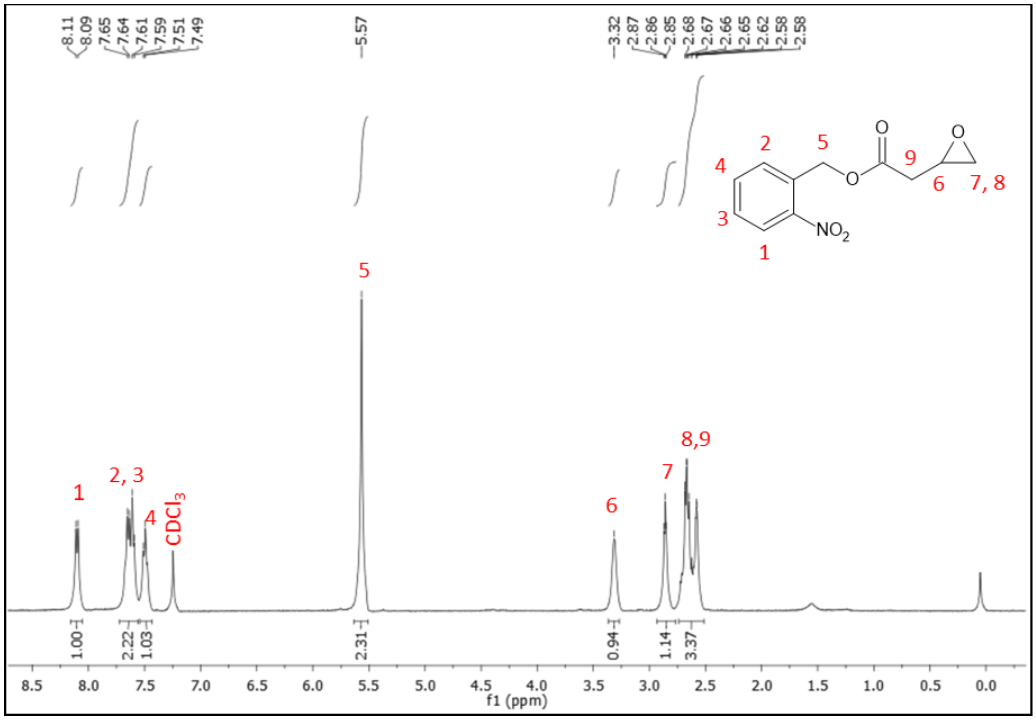

Figure 5.2 H-NMR of the synthetized monofunctional epoxy-NBE

5.2.4 Preparation of photo-responsive silica microparticles

5.2.4.1 Pretreatment of particles

Silica microparticles were cleaned in order to remove any organic contaminants, and to maximize the surface availability of silanol groups (SiOH). In particular, following RCA-SC1 chemical treatment, 1 g of silica particles were first sonicated in 100 ml of deionized water (30 min, 50 °C) and then transferred, adding 100 ml of hydrogen peroxide (30% solution) and 100 ml ammonium hydroxide (30% solution), in an open round-bottom flask. The mixture was then heated at 70 °C and stirred (750 rpm) for 1 hour. The particles were then collected by centrifugation and washed 5 times with absolute ethanol by

centrifugation/redispersion cycles (3 minutes, 3000 rpm). The cleaned particles were finally dried overnight at 100 °C under vacuum, in order to remove water residues.

5.2.4.2 Modification with TMESI²-BAPO

The dried particles (600 mg) were dispersed and sonicated for 30 min in 50 ml of dried acetonitrile (99.98%). The solution was then transferred to a round-bottom flask adding 600 mg of the TMESI²-BAPO (the structure is reported in Figure 5.3). The flask was closed in order to avoid water penetration and the mixture was stirred at 500 rpm and at room temperature for 48 h. Anhydrous conditions were guaranteed in order to avoid any premature condensation among the methoxy groups of the TMESI²-BAPO silane, and the subsequent formation of silane agglomerates. Then, the silanized particles were collected by centrifugation and washed 5 times with acetone by centrifugation/redispersion cycles (3 minutes, 3000 rpm), and finally dried at 60°C under vacuum for 4 hours.

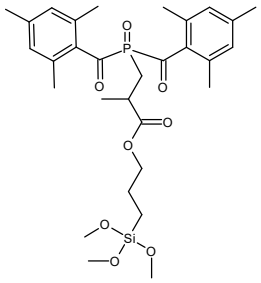

Figure 5.3 Chemical structure of the TMESI²-BAPO

5.2.4.3 Modification with 3-APTMS amino silane

Cleaned and dried particles (600 mg) were dispersed and sonicated for 30 min in 50 ml of dried toluene (99.98%). The solution was then transferred to a tri-round-bottom flask adding 600 mg of 3-APTMS silane (chemical structure is reported in Figure 5.4). The flask was opportunely closed in order to avoid water penetration and then connected to a reflux apparatus, for avoiding solvent evaporation, and to a vacuum/nitrogen line. Additional inert conditions were achieved operating 3 cycles of vacuum/nitrogen atmosphere. The dispersion was heated to 80 °C and stirred at 500 rpm up to 12 h. Inert and dried conditions were adopted in order to avoid any premature condensation among the methoxy groups and the subsequent formation of silane agglomerates. Then, the silanized particles were collected by centrifugation and washed 2 times with toluene and 3 more times with acetone by centrifugation/redispersion cycles (3 minutes, 3000 rpm) and finally dried at 60°C under vacuum for 4 hours.

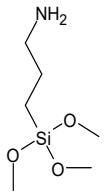

Figure 5.4 Chemical structure of (3-Aminopropyl)trimethoxysilane (3-APTMS)

5.2.4.4 "Photo-grafting from" procedure

For the photo-grafting procedure, 50 mg of the TMESI[2]-BAPO silanized particles were dispersed and sonicated for 30 min in 8 ml of acetonitrile. The solution was then transferred to a round-bottom flask adding 500 mg of the synthetized mono-functional acrylate-NBE. Subsequently, the flask was closed, and inert atmosphere was attained operating 3 cycles of vacuum/nitrogen atmosphere. Inert atmosphere was particularly important in the aim to avoid any oxygen radical inhibition during the photo-grafting process. The mixture was then stirred at 1000 rpm at room temperature and irradiated for 4 hours with a visible light source, in order to prevent a premature cleavage of the o-NBE groups. The visible irradiation was attained using a medium pressure mercury lamp: Omnicure series 1500, equipped with an optical waveguide and interposing an external cut-off (λ<400nm) filter (filter Newport Corporation (UV filter - Color Glass Filter. 25.4 mm DIA, GG400 cut-off λ<400nm), between the lamp fiber and the round flask (visible light intensity, 350 mW/cm^2). The photo-grafted particles were then collected by centrifugation and washed 5 times with acetone by centrifugation/redispersion cycles (3 minutes, 3000 rpm), and finally dried at 60°C under vacuum for 4 hours.

5.2.4.5 Amino epoxy "grafting from" procedure

For the amino-epoxy *"grafting from"* procedure, 125 mg of the 3-APTMS silanized particles with 1.25 g of epoxy-NBE were dispersed and sonicated for 30 min in 20 ml of toluene 99.98%. The solution was then transferred to a round-bottom flask adding 500 mg of the synthetized mono-functional epoxy-NBE. Subsequently, the flask was closed, connected to a reflux apparatus to avoid solvent evaporation, and inert atmosphere was attained operating 3 cycles of vacuum/nitrogen atmosphere. The mixture was then heated up at 65 °C and stirred at 500 rpm at room temperature for several hours in dark condition (up to 24h), and after left overnight (14 h) at room temperature. The grafted particles were then collected by centrifugation and washed 2 times with toluene and 3 times with acetone by centrifugation/redispersion cycles (3 minutes, 3000 rpm), and finally dried at 60°C under vacuum for 4 hours.

5.2.4.6 UV-cleavage

The particles grafted with the two different modalities, photo-grafting and amino-epoxy coupling reaction, were eventually modified by exploiting the

photocleavage of the o-NBE groups. The procedure followed a first dispersion in a Schlenk flask of 50 mg of grafted particles in 14 ml of acetonitrile. Inert atmosphere was attained operating 3 cycles of vacuum/nitrogen atmosphere. The dispersion was then stirred at 1000 rpm at room temperature and irradiated for 2 hours by means of a medium pressure mercury lamp: Omnicure series 1500, equipped with an optical waveguide (intensity : UVA 180 mW/cm^2, UVB 32 mW/cm^2, UVC 19 mW/cm^2, UVV 400 mW/cm^2).

The UV-irradiated particles were then collected by centrifugation and washed 5 times with acetone by centrifugation/redispersion cycles (3 minutes, 3000 rpm), and finally dried at 60°C under vacuum for 4 hours.

In figure 5.5 is sketched the synthesis path of the photo-grafting from and amino-epoxy procedure.

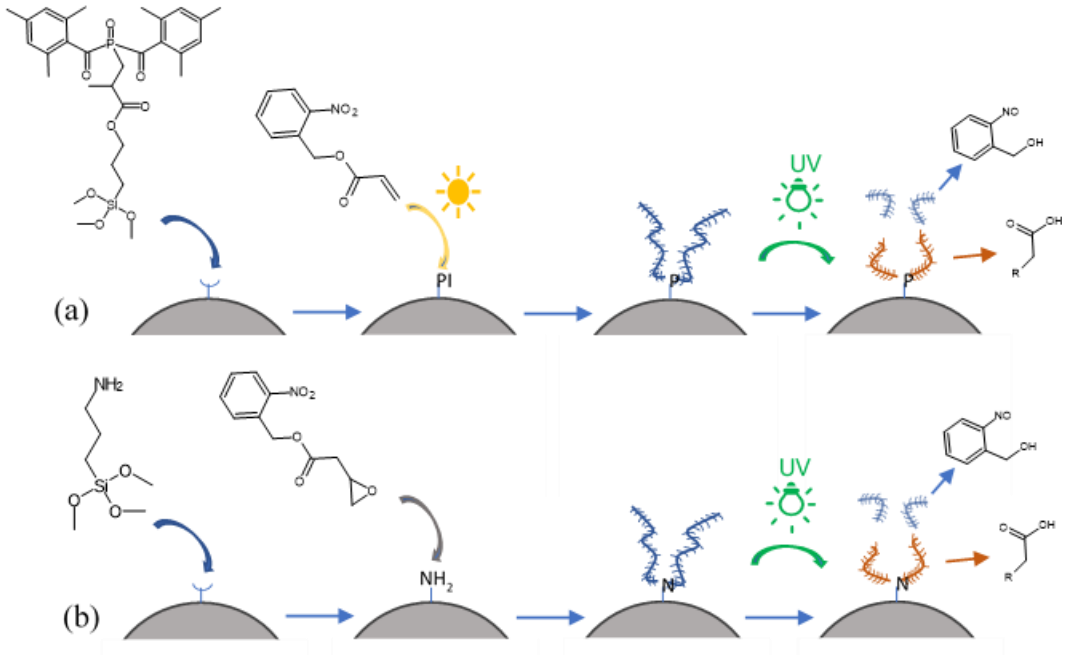

Figure 5.5 Synthetic procedure of: a) photo-grafting from; b) Amino-epoxy grafting from. In both procedures a first step implies the anchoring of silane agents onto the particles surface. In a further step photo-responsive monomer are grown through "photo-grafting from" or amino-epoxy reactions. Eventually the grafted polymer brushes are cleaved upon UV light irradiation leading to carboxylic acids species which stay tether to the surface and nitroso compounds which are released.

5.2.4.7 Surface post-functionalization

To show the potentialities of our light modified silica microparticles, carboxylic acids produced as primary reaction products of the o-NBE isomerization, were used as anchor points for proteins conjugation. In this purpose the carboxylic acids were first "activated" and then conjugated to fluorescent proteins using an EDC/sulfo-

NHS protocol, with a procedure similar to the one used in the previous chapter on planar samples, but opportunely adapted for particles functionalization.
For this purpose, the microparticles were suspended at the concentration of 0.1 mg/mL in 2-(N-morpholino)ethanesulfonic acid (MES 0.1 M, pH 4.7) buffer for 15 minutes to equilibrate the samples with the help of a ultrasonic bath. In a further step, the mixture was centrifugated at 5,000 RCF for 3 minutes and the supernatant was removed; the pelleted microparticles were then resuspended and incubated in a mixture of EDC/sulfo-NHS (4/10 mM) in MES buffer for 15 minutes on an orbital shaker. At the end of the incubation, the samples were centrifugated as previously described, and the supernatant was discarded. The particles were then resuspended in phosphate Buffered Saline (PBS 10 mM, pH 7.3) and put on an orbital shaker for 5 minutes. This procedure was repeated two additional times for a total of three. After the last washing step, the microparticles were resuspended and incubated overnight in a solution of PBS containing 500 mg/mL of Alexa-546 conjugated Protein A on an orbital shaker. Then, the samples were centrifugated and washed as previously described using PBS supplemented with 0.05% Tween-20™. Lastly, the microparticles were resuspended in PBS and stored at 4 °C until their characterization.

5.2.5 Preparation of glass slides with light responsive surface properties

The functionalization of glass slides was carried out to better evaluate and to characterize the surface modification step carried out onto micro-particles. In this aim, 1 cm x 2 cm glass slides were prepared by cutting the glass slides with a cutting diamond pen. The samples were then washed with RCA-SC1 protocol, following the same procedure employed for the particles' cleaning.

5.2.5.1 Surface modification with TMESI^2-BAPO

The silanization of glass slides with TMESI^2-BAPO followed the same procedure adopted for particles, in terms of time and solvent to silane ratio. The cleaned slides were placed in a glass flask with one surface exposed to a solution of 25 ml of acetonitrile (99.99%) and 300 mg of synthetized TMESI^2-BAPO silanes. Subsequently, the flask was closed, and inert atmosphere was attained operating 3 cycles of vacuum/nitrogen atmosphere. The silanization proceeded for 48 h at room temperature and finally, the slides were collected and washed 5 times in acetone in a sonication bath.

5.2.5.2 Surface modification with amino-functional organosilane

The modification of glass slides with 3-APTMS followed the same procedure adopted for particles, in terms of time and solvent to silane ratio. The cleaned slides were placed in a glass flask with one surface exposed to a solution of 25 ml of toluene (99.98%) and 300 mg of 3-APTMS. Subsequently, the flask was closed, and inert atmosphere was attained operating 3 cycles of vacuum/nitrogen atmosphere. The silanization proceeded up to 12 h in oven at 80 °C, and finally the slides were collected and washed 2 times in toluene and 3 times in acetone in a sonication bath.

5.2.5.3 **"Photo-grafting from"** ***procedure***

The "photo-grafting from" protocol followed the same procedure employed for particles in terms of time and solvent to monomer ratio. Particularly, the TMESI[2]-BAPO silanized glass slides were placed in an opened petri dish with the modified surface exposed to a solution of 2 ml of acetonitrile (99.98%) and 125 mg of monofunctional acrylate-NBE. Subsequently, the petri dish was enclosed in an inert atmosphere chamber operating 3 cycles of vacuum/nitrogen atmospheres and further irradiated for 4 hours with a medium pressure mercury lamp: Omnicure series 1500, equipped with an optical waveguide and interposing an external cut-off (λ<400nm) (filter Newport Corporation (UV filter - Color Glass Filter. 25.4 mm DIA, GG400 cut-off λ<400nm) between the lamp fiber and the chamber (Visible light intensity; 350 mW/cm^2). Finally, the slides were collected and washed 5 times in acetone by means of sonification bath.

5.2.5.4 Amino epoxy **"grafting from"** ***procedure***

The *"grafting from"* protocol followed the same procedure employed for particles in terms of time and solvent to monomer ratio. The 3-APTMS silanized slides) were disposed in flask with the modified surface exposed to a solution of 2 ml of toluene (99.98%) and 125 mg of monofunctional epoxy-NBE. Subsequently, the flask was closed and inert atmosphere was attained operating 3 cycles of vacuum/nitrogen atmosphere. The samples were heated up until 65 °C in oven up to 24 h and after left overnight at room temperature (14h). Finally, the slides were collected and washed 2 times in toluene and 3 times in acetone by means of sonification bath.

5.2.5.5 UV-cleavage

The grafted samples were disposed in flask with the grafted surface exposed to a solution of 1,75 ml of acetonitrile (99.98%) and inert atmosphere was attained operating 3 cycles of vacuum/nitrogen atmosphere. The samples were then UV irradiated with a medium pressure mercury lamp: Omnicure series 1500, equipped with an optical waveguide (intensity: UVA 180 mW/cm^2, UVB 32 mW/cm^2, UVC 19 mW/cm^2, UVV 400 mW/cm^2). Finally, the slides were collected and washed 5 times in acetone by means of sonification bath.

5.3 Characterization techniques

5.3.1 Evaluation of polymer grafting yields

Thermogravimetric analyses were performed in order to evaluate the efficiency of the silanization and the grafting reaction, and therefore to measure the grafting yields in terms of mass of grafted polymer per microparticle surface unit. All the experiments were conducted on a thermal analyser Mettler Toledo Tga/DSC 1, loading few grams of dried silica particles in alumina crucible and heating from room temperature up to 900 °C, with a heating rate of 10 K min^{-1} under air atmosphere in order to promote the polymer brush oxidation. The mass loss, along

with the residue at high temperature, were used to evaluate the average polymer per unit area in mg of polymer per m^2 of nanoparticles surface as described elsewhere [272].

5.3.2 Investigation of surface modification

Surface potential measurements

The surface properties of the silica microparticles and glass slides were characterized in terms of zeta potential defined as the electrical potential in the interfacial double layer at the shear plane. Zeta potential measurement for plane surfaces was already described in Appendix A.4. As regards to the particles, the measurement is performed by suspending those in an electrolyte solution which generates ions charge distribution onto the particles surface region. Indeed, when an electric field is applied to the electrolyte solution, charged particles are attracted towards the electrode of opposite charge. The charges flux fluid dynamics is governed by the viscous force, opposed to the particles motion, and the electrochemical forces. Once the equilibrium of these two forces is reached, the particles move with constant velocity and the zeta potential is evaluated by measuring particles velocity and knowing the strength of the applied electric field; the dielectric constant and the viscosity of the medium [273].

In our work, zeta potential measurements were conducted with a "SurPASS II" electrokinetic analyzer (Anton Paar GmbH, Graz, Austria). The experiments were carried out by dispersing and sonicating 12 mg of particles in 15 ml of 1mM KCl electrolyte solution. 5 ml of the stock dispersion was further diluted in 15 ml 1mM KCl and therefore the zeta potential was determined as a function of the pH. The pH value was lowered by adding HCl (30%) to the electrolyte solution. The pH value was instead tuned to higher pH values by adding up to 50 mM of NaOH, in the electrolyte solution. As regards to glass slides, an adjustable gap measuring cell (AGC) was used for performing the experiments. 2 sample size of 1 cm x 2 cm were mounted in the measuring cell in a dark room, in the aim to protect the photo-sensitive surface. The zeta potential was determined as a function of the pH that was changed as previously described.

XPS analysis

The XPS spectra of all the prepared particles were recorded using a Thermo Fisher Scientific Instrument equipped with a monochromatic Al K-Alpha X-ray source (1486.6 eV). For the measurements few milligrams of the synthetized particles were placed on a carbon tip and were analyzed with a spot size of 200 µm. High resolution scans were acquired with a pass energy of 50 eV and a step size of 0.1 eV. Survey scans were acquired with a pass energy of 200 eV and a step size of 1.0 eV. Photo electrons were collected using a take-off of 90˚ relative to the sample surface. Charge compensation was performed with an argon flood gun. All analyses were performed at 20 °C.

5.3.3 Optical characterization

The silica particles silanization with TMESI^2-BAPO was confirmed by means of ultraviolet-visible spectroscopy measurement with a Lambda 950 UV/Vis/NIR Spectrometer. Because of the high light scattering phenomenon in particles in micrometric size, a Labsphere Integrating Sphere, 150 mm was installed in the aim to measure also the diffracted light, and thus reducing the diffraction effect. A wavelength range: 250 nm to 2500 nm, with an interval of 5 nm and a dual beam method were employed for the spectroscopy analysis. The UV-vis measurements were carried out by dispersing the particles in absolute ethanol with a concentration of 0.15 mg ml^{-1}.

5.3.4 Confocal microscopy

The post modified silica surface was finally characterized by a fluorescent confocal spinning disk microscopy, in the aim to proof and map the presence of the bio-conjugate proteins. A microscope (Eclipse Ti2 Nikon, Tokyo, Japan) equipped with a Crest X-Light spinning disk confocal microscope and a Lumencor SPECTRA X light engine was used for the collection of fluorescence images. All images were displayed using the same scaling and were collected using a Plan Apo 20 × 0.75 NA (Nikon, Tokyo, Japan). The fluorescent images were collected on a drop of sample embedded between two cover slip microscope slides (thickness 150 micron).

5.4 Results and discussion

5.4.1 Synthesis of the photoactive microparticles

As described in the experimental part, silica microparticles were first cleaned following an RCA-SC1 protocol in order to remove any organic contaminant and to maximize the availability of surface silanol groups (SiOH). The presence of silanol groups is clearly visible by the peak at 758 nm in the IR spectrum reported in Figure 5.6 a. In a following step, the silanol groups were used as anchor points for the condensation of the synthetized TMESI^2-BAPO or 3-APTMS. The silanization reaction proceeds with a first hydrolysis of silane agents' alkoxy groups, followed by a condensation with the silica surface hydroxyl groups, and therefore obtaining the formation of covalent Si-O-Si bonds between the silane agents and the silica surface (see scheme reported in Figure 5.5). Anhydrous conditions were guaranteed in order to avoid any premature hydrolysis and condensation among the methoxy groups of the TMESI^2-BAPO silane, and therefore preventing the formation of polymer agglomerates. Furthermore, it is also well-known that controlled anhydrous environment favours the formation of surface silane monolayers, which is widely used in many applications (e.g. self-assembled monolayers, SAMs). Thermogravimetric characterization in Figure 5.7 (blue curve) shows an increase of 1.1 % of mass loss percentage for the particles, which have been treated for 48 hours with TMESI^2-BAPO (normalized weight of

0.949) compared to the untreated silica particles (normalized weight value of 0.939).

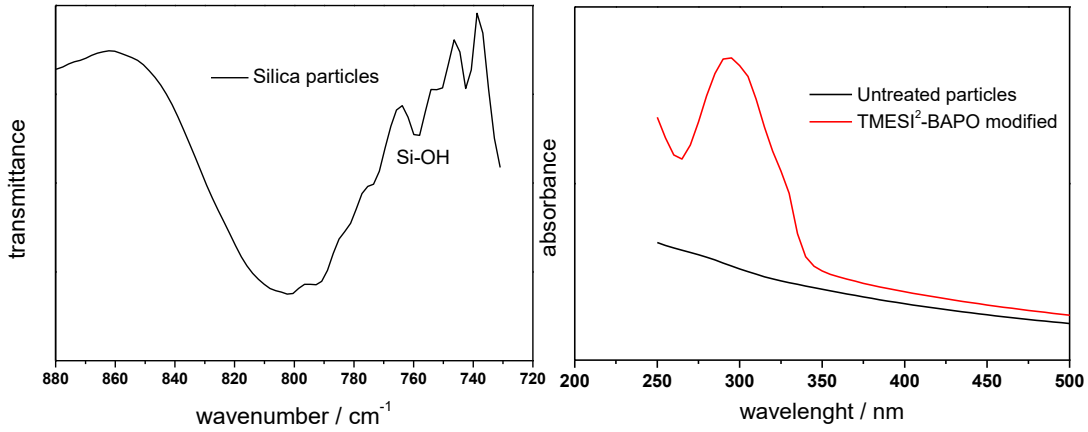

Figure 5.6 a) IR spectra of untreated silica particles (Si-OH peak at 758 cm^{-1}), b) UV-vis spectroscopy of untreated silica particles (black curve) and particles modified with $TMESI^2$-BAPO (red curve), particle concentration amounted to 0.15 mg ml^{-1} in absolute ethanol.

The immobilization of $TMESI^2$-BAPO was further confirmed by UV-vis spectroscopy (Figure 5.6 b) which shows the presence of light-absorbing moieties in particles' dispersion. Longer silanization time (72h) didn't significantly increase the mass loss percentage. The modification with 3-APTMS proceeded also via condensation reaction and grafting yields with an increase of mass loss percentage of 1.05% compared to the untreated silica confirmed the successful silane anchoring (red curve Figure 5.7). An increase of the reaction time up to 12 hours (80 °C) yielded an increase of 0.9% of mass loss percentage, thus reflecting a higher amount of attached silanes (magenta curve, Figure 5.7).

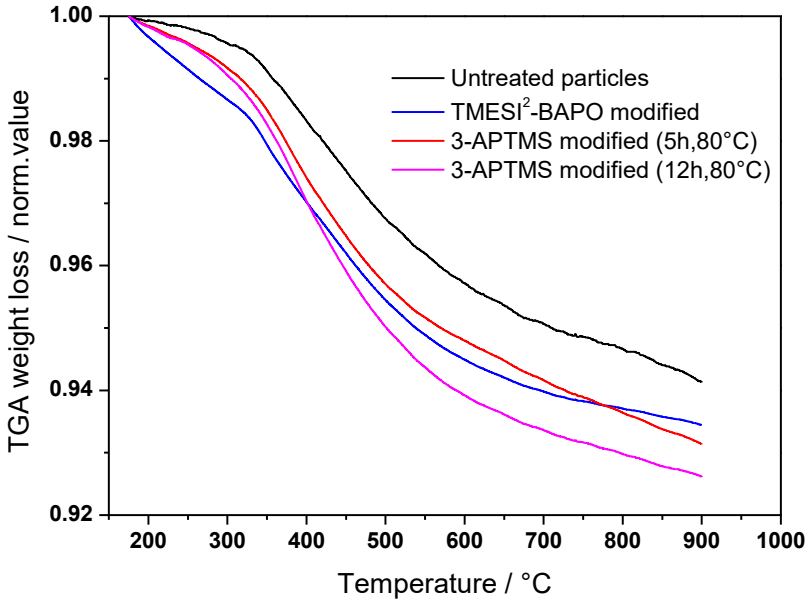

Figure 5.7 TGA of the modified silica particles, in figure: back curve untreated silica, blue curve $TMESI^2$-BAPO modified (48h, room temperature), red curve 3-APTMS amino silanized (5h, 80°C), magenta curve 3-APTMS modified (12h, 80°C).

5.4.2 *"Grafting from"* polymer brushes formation

In a further step, we employed the two modified silica particles (3-APTMS, and TMESI[2]-BAPO modified) following two different *"grafting from"* strategies onto the active silica surface. A first strategy included a visible light promoted formation of polymer brushes, exploiting the TMESI[2]-BAPO surface-bounded photo-initiators. A second mechanism exploited the amino functionalized particles, in the aim to promote an amino-epoxy reaction among the surface primary amines and epoxy groups of the synthetized epoxy-NBE monomers (see scheme reported in Figure 5.5). The "*photo-grafting from"* procedure is of particular interest because it allows a photochemical formation of polymer brushes, taking advantage of the high time-spatial control and mild reaction conditions of the light triggered reactions (reaction scheme in Figure 5.8). As regard to this, bis(acyl)phosphane oxide (BAPO) derivatives were used in literature as anchored photo-initiator molecules for promoting *"Photo-grafting from"* surface modification strategies [269,271] or for the synthesis of nanoparticles photo-initiators [274,275]. BAPO derivatives presents several interesting features as for instances; relatively high thermal stability (> 100 ºC) with long storage stability, and a photolysis which yields a total of up to four radicals, with the phosphinoyl radical about 1000 times more reactive than the acyl radicals. Moreover, in our specific case, BAPO initiator, being active in a range between 360nm and 440nm, doesn't overlap with the o-NBE absorbing window, suiting the requirement to not activate o-NBE cleavage during polymer brushes formation. When a BAPO-derivative is surface-anchored, the above-mentioned advantages apply to the photografting-from process.

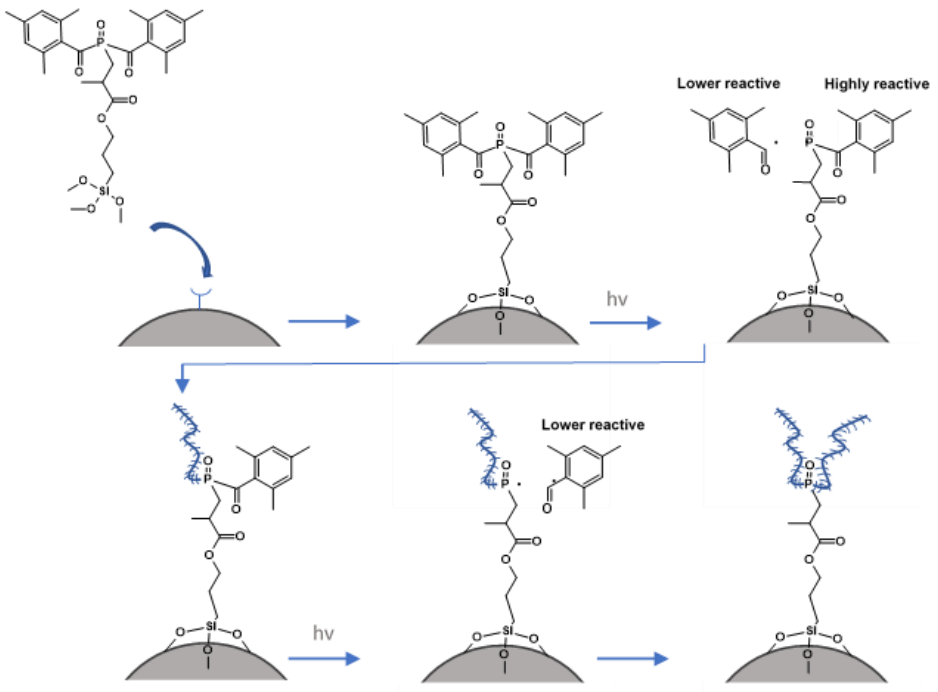

Figure 5.8 TMESI[2]-BAPO surface anchoring and polymer brush formations upon light stimuli.

Upon visible-light irradiation, BAPO photo-cleavage leads to the formation of two phosphinoyl radicals that ideally promote the grown of two polymer chains from a single photoinitiator anchoring site (see scheme in Figure 5.8). Furthermore, this system is ideal for polymer brushes because the acyl radicals which are likewise generated and released in the solvent in each of these steps are significantly less reactive, and the homopolymers generated as side-products by these as initiators, are easily removed [262].

The TGA curve in figure 5.9 shows an increase of the mass loss percentage of 0.6% for the photo-grafted particles (magenta curve) compared to the TMESI^2-BAPO silanized ones (blue curve), confirming that acrylate-NBE monomers were successfully grafted onto the surface anchored TMESI^2-BAPO silanes.

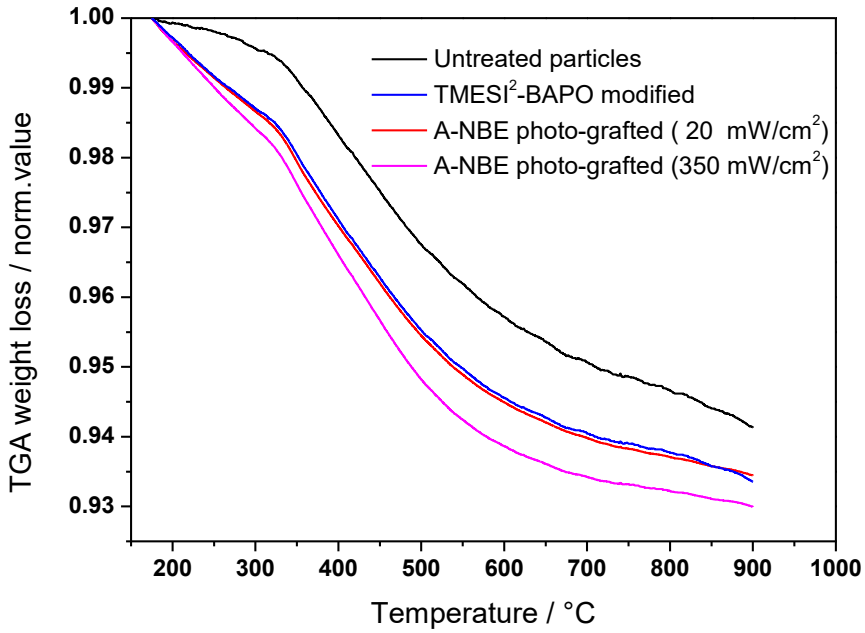

Figure 5.9 Thermogravimetry analysis: black curve untreated silica particles (reference), blue curve TMESI^2-BAPO modified (48h, room temperature), magenta curve Acrylate-NBE photo-grafted (4h, 350 mW/m^2), red curve Acrylate-NBE photo-grafted (4h, 20 mW/m^2);

The absolute value of this mass loss percentage increase (0.6%) might seem irrelevant if we don't take into consideration that we are dealing with polymer brushes of nanometric size, that are grafted onto a silica particle of 1 micrometer. We calculated the polymer grafted per unit area as 3 mg/m^2, which is in good agreement with other "photo-grafted from" polymer brushes reported in literature (7-10 mg/m^2) [269]. However, reducing light intensity to 20 mW/cm^2 (figure 5.9 red curve), the thermogravimetric analysis detected almost no measurable polymer brush presence (except TMESI^2-BAPO silanes), demonstrating high sensitivity of the photo-activated reaction to light irradiation dose. Furthermore, in our specific case the constraint in employing visible light source for the "photo-grafting" reaction in order to avoid premature o-NBE cleavage, reduced also BAPO quantum yields compared to an UV light source because of the narrower photons active

window. Therefore, relatively high light irradiation doses were necessary in order to have good grafting efficiency.

Moreover, the acrylate-NBE monomers showed generally a lower efficiency in terms of grafted monomers compared to other acrylate systems such as PEGMA or acrylic acid. As previously reported, both in radical controlled polymerization and thiol-ene click reactions [112,134], the o-NBE moieties seems to reduce the overall reactivity compared to other acrylate systems.

In an alternative procedure, the formation of "grafting from" polymer brush was carried out exploiting a direct amino-epoxy coupling reaction among the synthetized epoxy-NBE monomers and the activated amino silica particles. Typical amino-epoxy reactions proceed with a step-growth polymerization mechanism through a nucleophilic attack carried by polyamine to the less sterically hindered carbon of an oxirane ring. As depicted in the Figure 5.10, in the case of primary amines, the addition reaction yields a secondary amine and a hydroxyl group [276,277]. The resulting secondary amine, which is more sterically hindered than primary amine, then reacts with another oxirane ring, creating an additional hydroxyl group and a tertiary amine. Eventually, the hydroxyl groups generated by the reaction between the secondary amine and epoxide group will result in the formation of ether linkage. This reaction, generally known as etherification, competes with the epoxy-amine curing reaction (Figure 5.10, step 3).

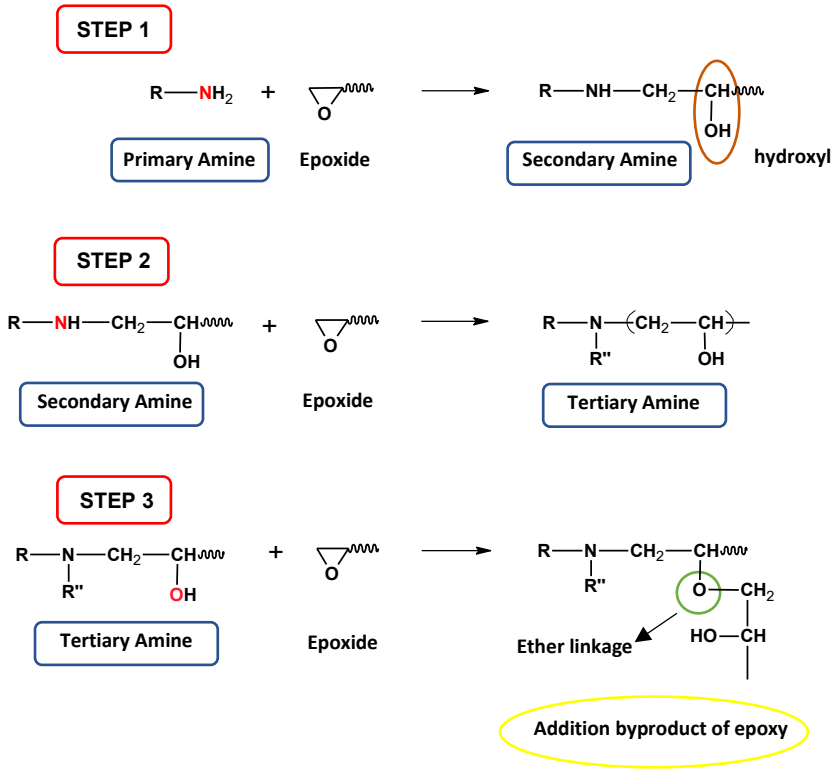

Figure 5.10: Amino-epoxy coupling reaction steps: Step 1) Nucleophilic attack carried by primary amine to the less sterically hindered carbon of an oxirane ring with the formation of a secondary amine and an hydroxyl group. Step 2) Reaction among the formed Secondary Amines and epoxy groups leading the formation of Tertiary Amine and hydroxyl groups. Eventually, the hydroxyl groups generated by the reaction between the secondary amine and epoxide group will result in the formation of ether linkage (Step 3) (etherification).

Etherification reaction might take place after depletion of amine hydrogens if epoxide groups are in excess [277]. The tertiary amine presents no reactivity but has catalytic effect on the amino-epoxy reaction that for this reason can be considered autocatalytic [278]. The polyamine structure affects the overall reaction reactivity with the aliphatic amines that are the most reactive ones followed by cycloaliphatic amines, whereas aromatic amines are much less reactive due to their weaker nucleophilicity which requires long reaction time at higher temperatures [278]. Amino-epoxy reaction mechanism was widely explored in the synthesis of polymer thermosets with elevated temperature performance and outstanding chemical resistance [279]. Amino-epoxy groups were also widely employed for the fabrication of resist with covalent proteins and enzymes immobilization [280].

The thermogravimetric analysis plotted in Figure 5.11a shows the results of the silica particles silanized for 5h at 80 °C, and further grafted for 10 h at 65°C. In thermogravimetric analysis of graph 5.11a, the mass loss percentage of the epoxy-NBE grafted particles (green curve) measured an increase of about +0.6 %, when is compared to the amino silanized particles (red curve).

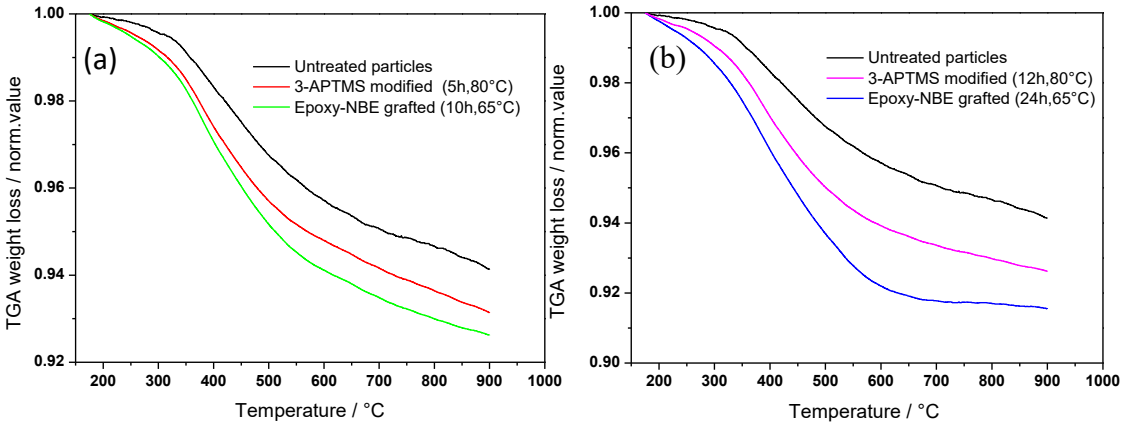

Figure 5.11: a) Thermogravimetric analysis: black curve untreated silica particles (reference), red curve 3-APTMS modified (5h, 80°C), green curve amino-epoxyNBE grafted (10h, 65°C); b) Thermogravimetric analysis: black curve untreated silica particles (reference), magenta curve 3-APTMS modified (12h, 80°C), blue curve amino-epoxy-NBE grafted (24h, 65°C);

This result is almost identical in terms of mass loss percentage measured for the previously described photo-grafted protocol (see figure 5.9). Therefore, in these studied conditions, we may evidence the better performances for the "*photo-grafted"* procedure, which obtained similar grafting efficiency but employing 4 hours of visible light irradiation at room temperature instead of 10 hours at 65 °C.

However, in our experiment conditions, the amino-epoxy reaction resulted more "scalable" in terms of grafted monomers versus reaction time. As depicted in figure 5.11 b, to a silanization and grafting time of respectively 12 hours at 80°C and 24 hours at 65°C (magenta and blue curve), corresponded an almost double amount of mass loss percentage compared to 5 and 10 hours of reaction time in same conditions. As regards to this, despite the "photo-grafted" protocol presents many advantages compared to amino-epoxy reaction, we couldn't increase the

amount of grafted monomer without induce also some reaction drawbacks. For instance, a further increase of the light energy dose, in the aim to enhance the photo-grafting reaction, could also promote a slight cleavage of the o-NBE due to the partial overlapping at the border of the visible light source emission, and o-NBE absorption windows. Furthermore, adopting a higher cut-off filter (i.e. λ<420nm) would reduce the TMESI[2]-BAPO active windows with the subsequent necessity to increase the irradiation time, which would vanish the advantages of light trigger reaction kinetic, that typically proceeds with fast reaction rate. In this aim, a longer wavelength active photo-initiator system would reduce this drawback when is coupled with o-NBE based polymer systems.

5.4.3 UV induced change in surface properties and particles' post-modification

A controlled change of polarity and reactivity of the modified silica particles was carried out by selectively cleaving the o-NBE moieties contained into the grafted polymer brushes upon UV exposure. For this, 50 mg of grafted particles were dispersed in 14 mL of acetonitrile, stirred and simultaneously irradiated under inert atmosphere for 2 hours by means of a UV-light source.

The o-NBE ester isomerization reaction proceeds as previously described, yielding carboxylic acid and nitroso benzaldehyde as primary products (Figure 5.12 a). Therefore, considering the theoretical grafted polymer orientation (see figure 5.5), the o-NBE cleavage would lead to the formation of carboxylic acid species anchored to the particle surface, and nitroso benzaldehyde products that are ideally released in the solvent phase.

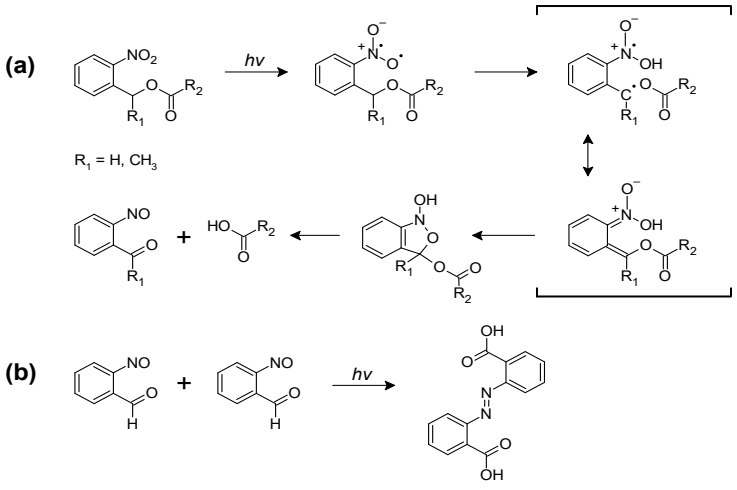

Figure 5.12: (a) Primary and (b) secondary photoreactions during the photoisomerization of *o*-NBE derivatives

In order to characterize the light-induced changes in the surface characteristics, zeta potential measurements and XPS spectroscopy were carried out. The zeta potential results for the two different *"grafting from"* procedures are plotted in figure 5.13 and 5.14. The results related to the "*photo-grafted from*" procedure in figure 5.13b show only slight differences in the zeta potential curves versus pH

values, with similar isoelectric point (IEP) for the non-treated glass surfaces and glass surfaces grafted with the acrylate-NBE monomers prior to (blue curve) and after UV cleavage (red curve). However, whilst the values for the IEP are in a similar range, there is a clear difference in the zeta potential values of the differently treated glass surfaces. Zeta potential values reflect the overall particles charges that depends on both the dissociation of surfaces' functional groups, into cationic or anionic species, and the adsorption of ions onto the particles surface [281].

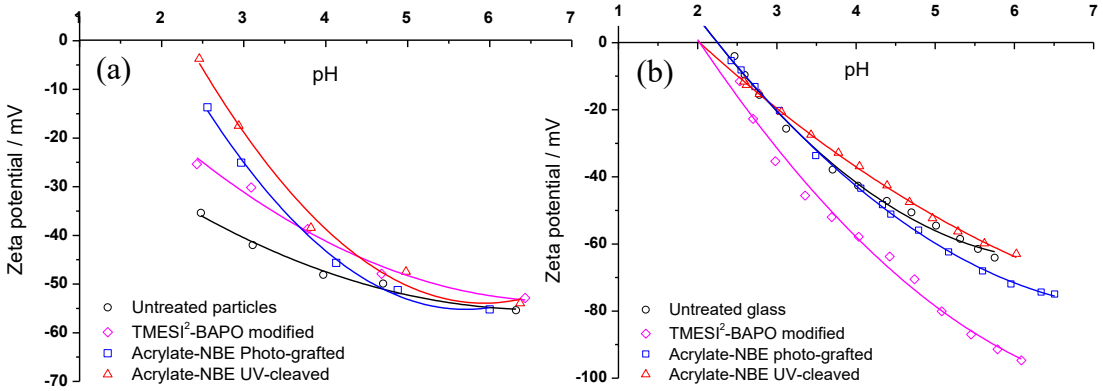

Figure 5.13 a) Zeta potential curves of untreated silica particles (black curve), TMESI^2-BAPO modified (magenta curve), Acrylate-NBE grafted (blue curve), Acrylate-NBE cleaved (red curve). b) Zeta potential curves of an untreated glass surface (black curve), TMESI^2-BAPO modified (magenta curve), Acrylate-NBE grafted (blue curve), Acrylate-NBE cleaved (red curve).

For the untreated glass surface (black curve, Figure 5.13b), the higher negative values at higher pH reflect the particles' silanol groups dissociation into Si-O$^-$ anions, that leads to negative zeta potential values in the range of -40 mV at pH of 4 [282]. The high presence of silanol groups is confirmed by water contact angle measurements of corresponding glass surfaces (Table 1). In the untreated state, the glass slides are well wettable with water and the water contact angle amounts to 23°.

Table 5.1 Water contact angles for the *"photo-grafted from"* modified glass surfaces.

Samples	Water contact angle
Untreated	23° +/- 10°
TMESI^2-BAPO modified	58° +/- 5°
Acrylate-NBE photo-grafted	62° +/- 5°
Acrylate-NBE photo-cleaved	48° +/- 5°

The coupling of TMESI^2-BAPO changes the picture, as the silanol groups of the glass surface are partly occupied by the larger and more hydrophobic photoinitiator molecules. The hydrophobic character of the anchored TMESI^2-BAPO groups causes a preferential adsorption of (OH^{-1}) ions instead of water molecules, which results in a shift of the zeta potential to higher negative values (-60 mV at pH = 4). The higher hydrophobicity is also confirmed by contact angle

measurements (Table 1), showing an increase of the water contact angle from 23 to 58° due to the attachment of TMESI^2-BAPO.

Grafting of acrylate-NBE leads to shift of the zeta potential to lower negative values again. Here it has to be considered that dissociable nitro groups are attached on the surface and at the same time TMESI^2-BAPO is homolytically cleaved during the irradiation step at visible light exposure.

Subsequent cleavage upon UV exposure leads to the formation of free carboxylic acid groups, which are deprotonated at higher pH values. In the deprotonated state, preferentially water molecules adsorb on the silica surface instead of (OH^-) ions, which leads to a further decrease of the zeta potential to lower negative values. The UV induced formation of polar cleavage products is also observed by water contact angle experiments giving rise to a decrease in the water contact angle from 62 to 48° (Table 1).

Along with glass surfaces, the zeta potential was also determined from differently treated silica particles (Figure 5.13a). Whilst the trend of untreated and grafted (prior to and after cleavage) silica surfaces is comparable to the corresponding glass substrates, the attachment of TMESI^2-BAPO onto microsilica particles shifts the zeta potential to lower negative values. This different behaviour may be related to a different degree of surface silanization between particles and the glass slides surface.

In contrast to the photochemical grafting approach, the zeta potential curves of the amino-epoxy modified systems leads to a clear change in the IEP during all modification steps (Figure 5.14). For the sake of clarity, we would like to note that for these characterizations we employed silica particles and glass slides that were treated with an amino-functional silane for 12 h (80 °C), with a further amino-epoxy reaction using an epoxy monomer with an o-NBE group, which was carried out for 24 hours at 65 °C.

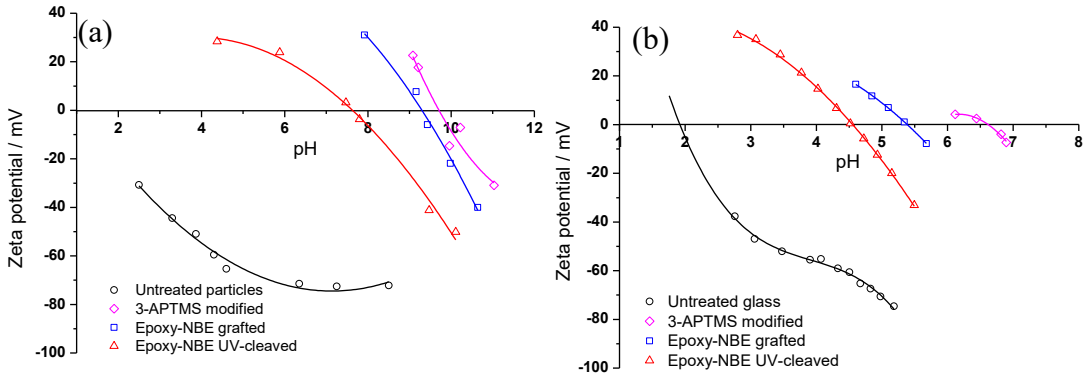

Figure 5.14 a) Zeta potential measurement of untreated silica particles (black curve), magenta curve 3-APTMS modified (12h, 80°C), blue curve Epoxy-NBE grafted (24h, 65°C), Epoxy-NBE cleaved (red curve). b) Zeta potential measurement of untreated glass slides (black curve), magenta curve 3-APTMS modified (12h, 80°C), blue curve Epoxy-NBE grafted (24h, 65°C), Epoxy-NBE cleaved (red curve).

The attachment of the organosilanes leads to a strong shift of the IEP compared to the untreated silica particles reflecting clearly the presence of primary amino groups that in aqueous solution tends to dissociate in -NH_3^+ cations species, leading to positive zeta potential values below pH values of 9.5. The coupling of the amino-functional silane leads to a distinctive increase in the water contact angle from 23 to 50° as the highly polar silanol groups are consumed during the condensation reactions (Table 2).

Subsequent coupling of epoxy-NBE and photocleavage, gradually shifts the IEP to lower pH values, 9 and 7, respectively, reflecting the conversion of the amino groups to the more acidic character of the epoxy-NBE monomers and the cleavage products (e.g. carboxylic acids). The UV induced formation of polar cleavage groups is also evidenced by the distinctive decrease of the water contact angle from 63 to 35° (Table 2).

The zeta potential value of the modified glass slides reflects a similar trend of the modified silica particles but with different IEP values.

Table 5.2 Water contact angles for the "amino-epoxy" modified glass slide

Samples	Water contact angle
Untreated glass slides	23° +/- 10°
Amino-silanized glass slide	50° +/- 5°
Epoxy-NBE grafted	63° +/- 5°
Epoxy-NBE photo-cleaved	35° +/- 5°

A further XPS study was performed in order to characterize the change in the chemical surface composition of the grafted particles prior and after the o-NBE photo cleavage (Figure 5.15 and 5.18). For a clearer interpretation, the C1s magnified region was deconvoluted by fitting the C1s peak (black curve) of the cleaved and un-cleaved particles into three peaks related respectively to: C-C/C-H peak at 284.9 eV (blue curve); C-N/C-O/C-OH peak at 286.3 eV (green curve) and O-C=O ester groups at 288.6 eV (red curve) [153,244]. The relative carbon atomic percentages of each peaks were calculated normalizing the corresponding area to the overall C1s peak ($C1s_{bond}/C1s_{TOT}$) and the results are summarized in table 3. Comparing the photo-grafted particles prior and after UV irradiation (Figure 5.15, a and b), it is visible an increase of the area related to C-OH groups for the cleaved particles (peak at 286.3 eV, red curve) due to the formation of pendant carboxylic acid groups (-COOH). Since consequently to the o-nitrobenzyl ester cleavage, the O-C=O ester groups (288.6 eV) of the acrylate-NBE monomer yields to free carboxylic acid HO-C=O species (289.1 eV), the signal overlapping between the two functional groups makes the curves interpretation difficult for this peak.

However, a slight increase after the UV-cleavage of the ester group (O-C=O) area percentage from 10.7% to 17.7% ($C1s_{(O-C=O)}/C1s_{TOT}$) was calculated in table 3.

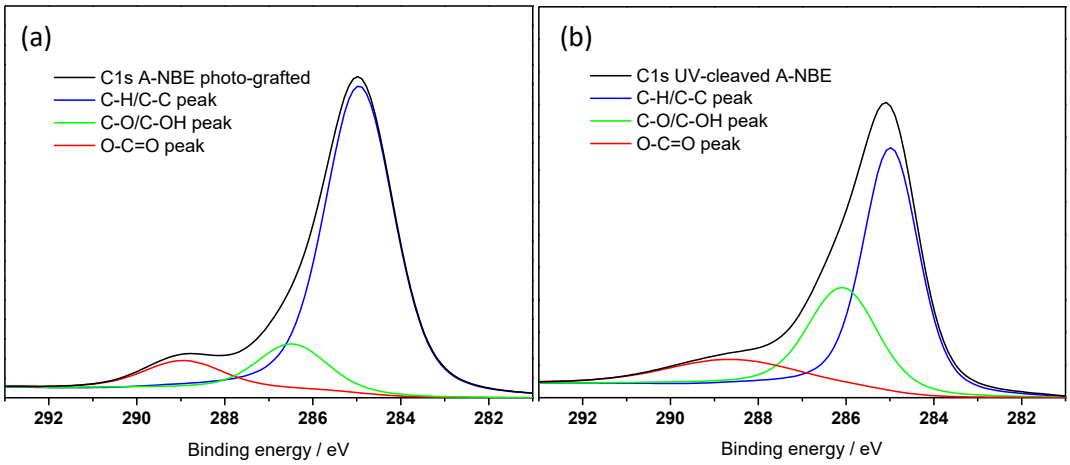

Figure 5.15 C1s magnification of a) Acrylate NBE photo-grafted particles and b) Acrylate NBE UV-cleaved particles. The C1s overall peak (black curve) was deconvoluted in C-C/C-H peak at 284.9 eV (blue curve); C-N/C-O/C-OH peak at 286.3 eV (green curve) and O-C=O ester groups at 288.6 eV (red curve).

Table 5.3 Chemical bonding area percentage prior and after o-NBE cleavage

Binding energy	Chem. bonding	A-NBE photo-graft	A-NBE UV-cleaved	Amino-epoxyNBE grafted	Amino-epoxyNBE UV cleaved
284.9 eV	C-C/C-H	74.9%	56.7%	56.3%	37.9%
286.3 eV	C-O/C-OH/C-N	14.5%	26.2%	34.7%	40.1%
288.6 eV	O-C=O	10.7%	17.7%	9%	22.3%

A clear distinction between the two different particles is instead evident in the magnified N1s region (Figure 5.16). The disappearing of the -NO_2 peak at 406.5 eV in the red curve related to the o-nitrobenzyl ester cleavage, clearly demonstrates that the acrylate-NBE monomer was first successfully grafted onto the silica particles, and subsequently cleaved upon UV light irradiation [153,283].

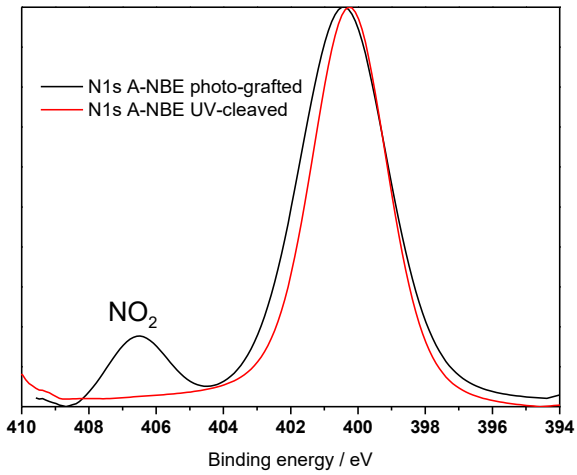

Figure 5.16 N1s magnification of Acrylate NBE photo-grafted particles (black curve), N1s magnification of Acrylate NBE UV-cleaved particles (red curve). NO_2 peak at 406.5 eV.

The XPS survey spectra of the photo-grafted particles (Figure 5.17; a, b) shows a reduction of the overall nitrogen peak passing from the un-cleaved to the cleaved particles, due to the release of the nitroso compounds upon o-NBE cleavage. The atomic percentage in table 4 confirmed the nitrogen reduction from 4.66% to 1.57%, for the cleaved particles.

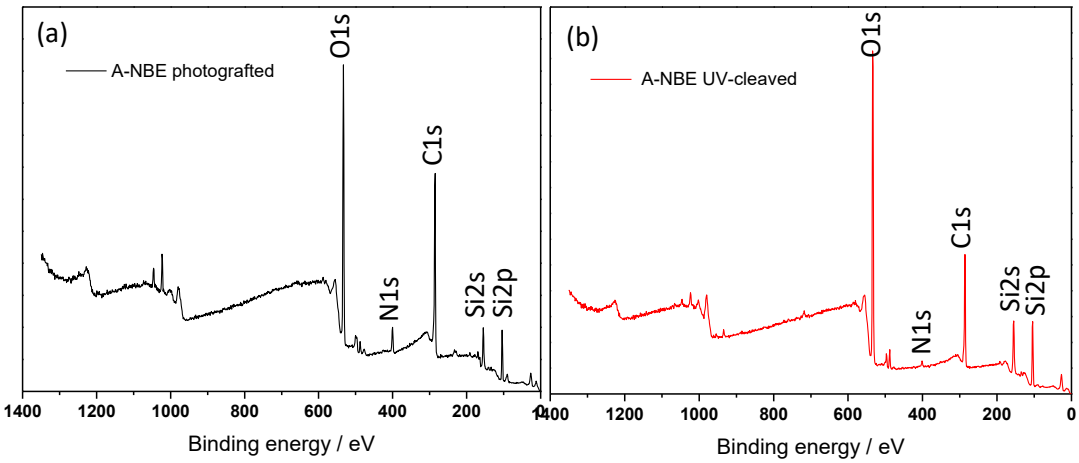

Figure 5.17 XPS survey spectrum of the a) A-NBE photografted particles and b) A-NBE UV-cleaved particles.

Table 5.4 Atomic percentage prior and after UV-cleavage

Particle system	O1s %	C1s %	N1s %	Si2p %
A-NBE photo-grafted	28.32	51.98	4.66	13.39
A-NBE UV-cleaved	38.72	35.91	1.57	22.22
Amino-epoxyNBE grafted	22.69	55.61	6.22	12.05
Amino-epoxyNBE UV-cleaved	19.37	62.68	7.44	7.67

The C1s high resolution peak of the amino-epoxyNBE grafted particles (Figure 5.18, a and b) shows an increase of both the O-C=O (red curve) and the C-OH area (green curve) for the cleaved particles (figure 5.18,b), therefore confirming the carboxylic acid formation upon UV light irradiation. The intense area of the C-N/C-O/C-OH peak (green curve), which appears also for the un-cleaved particles, is due to the presence of amine bonds (C-N) among the 3-APTMS and the Epoxy NBE molecules. The higher increase of O-C=O area for the amino-epoxy cleaved particles compared to the photo-grafted cleaved ones, might be a consequence of the higher amounts of grafted monomers for those particles (compare figure 5.10 and; 5.11b). This result might also depend on the lower overlapping effect of the ester groups for the amino-epoxyNBE grafted particles, because of the absence of ester groups in the 3-APTMS silanes structure that are instead present in the TMESI^2-BAPO molecules (Figure 5.3 and 5.4).

Differently from the photo-grafted particles, for the amino-epoxy grafted particles the survey spectrum of the UV-cleaved particles shows no reduction of the nitrogen peak after the nitroso group release (Figure 19; a and b). The similar percentage amount of nitrogen atom, prior and after the UV irradiation, might be

due to the presence of the amine bond among the 3-APTMS and the Epoxy NBE molecules in both particles.

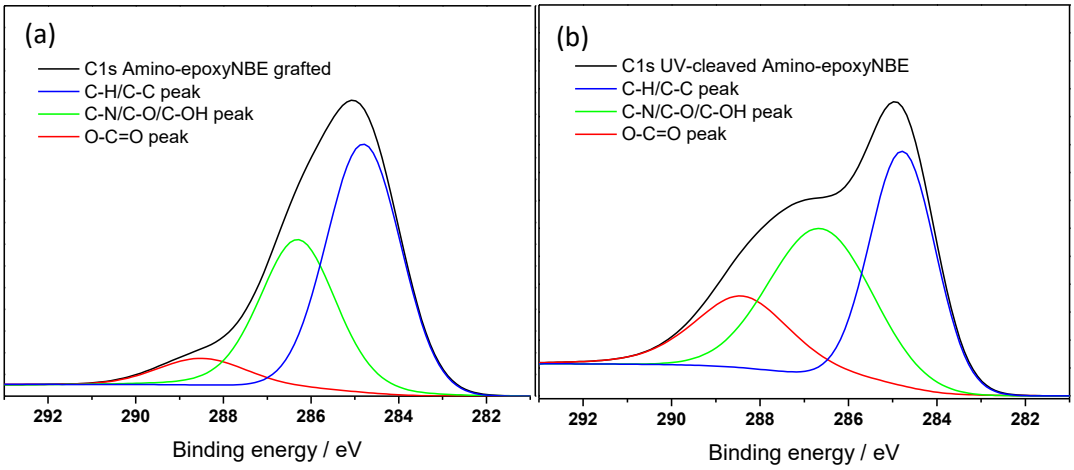

Figure 5.18 C1s magnification of a) Amino-EpoxyNBE grafted particles b) Amino-EpoxyNBE UV-cleaved particles. The C1s overall peak (black curve) was deconvoluted in C-C/C-H peak at 284.9 eV (blue curve); C-N/C-O/C-OH peak at 286.3 eV (green curve) and O-C=O ester groups at 288.6 eV (red curve).

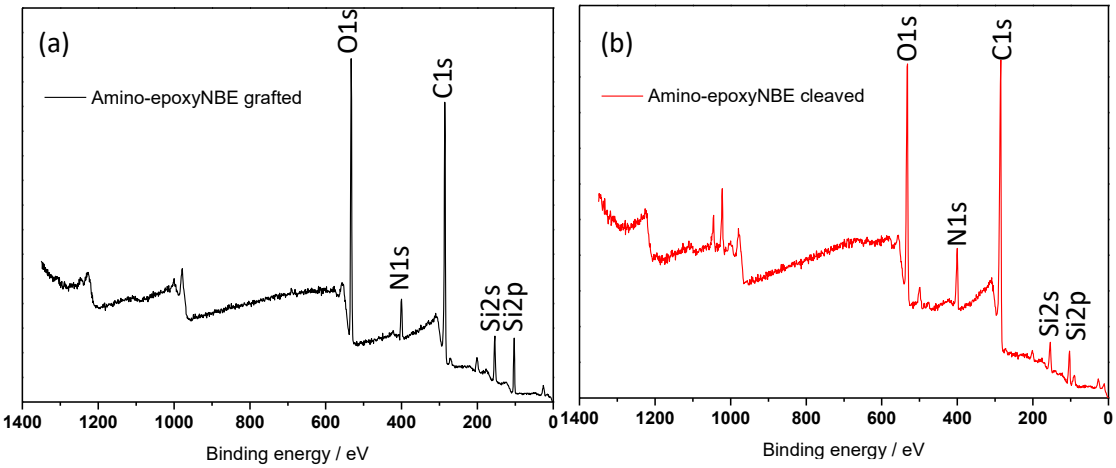

Figure 5.19 XPS survey spectrum of the a) Amino-epoxy NBE grafted particles b) Amino-epoxy NBE cleaved particles

As last evidence, functionalization with labelled protein was performed. Carboxylic groups formed by the photo-cleavage reaction were used as anchor points for attaching an Alexa-546 conjugated fluorescent Protein (see scheme in chapter 4 figure 4.5). This allowed us, not only to evaluate the available surface active moieties, but also to demonstrate that these functional groups can be exploited for the immobilization of biomolecules, such as proteins, which is of primary interest in several applications (e.g. biosensors, microarrays, Lab-On-a-Chip) [239]. The adopted procedure is summarized in paragraph 5.2.4.7 and followed an EDC-NHS protocol (see chapter 4.3.9). For both "grafting from" procedures, the confocal microscopy images in figure 5.20 shows an effective

functionalization of the fluorescent proteins only onto the UV irradiated silica particles, therefore demonstrating the light induce carboxylic acids formation and the active role of the o-NBE chromophores.

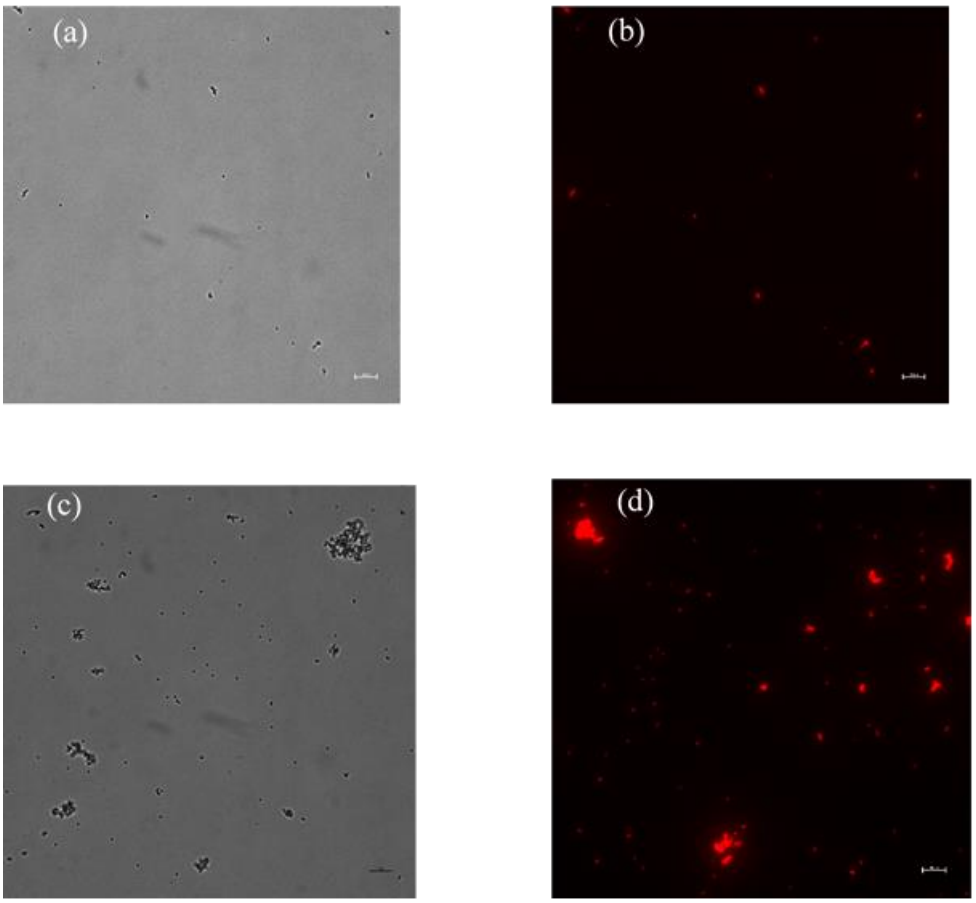

Figure 5.20 Confocal microscopy images: a) Photo-grafted un-cleaved particles, no proteins anchoring and thus no fluorescent signal was detected after EDC-NHS protocols b) Photo-grafted and photo-cleaved particles, fluorescent signal was detected after EDC-NHS protocols and thus protein anchoring c) Amino-epoxy grafted un-cleaved particles, no proteins anchoring was detected after EDC-NHS protocols b) Amino-epoxy grafted and photo-cleaved particles, fluorescent signal was detected after EDC-NHS protocols and thus protein anchoring.

Conclusion

Taking inspiration by previous works, we carried out two different "grafting from" procedures for the synthesis of photo-responsive silica microparticles and glass surfaces. As a first approach, a photochemical synthesis was employed for the formation of photo-responsive polymer brushes, exploiting a radical mediated grafting reaction of acrylate monomers comprising o-NBE chromophores. TMESI^2-BAPO was anchored on the surface of silica particles by condensation reaction and subsequent exposure with visible light lead to the formation of starting radicals for the chain growth reaction of the functional acrylate monomers. The second procedure involved a nucleophilic ring opening reaction of epoxy groups with primary amines to immobilize o-NBE monomers on the surface of silica microparticles. In particular, an amino-functional silane (3-APTMS) was anchored onto the silica surface by condensation reaction and the free amino groups were exploited to covalently attach an epoxy monomer bearing an o-NBE group. In both strategies no toxic substances have been employed and the photochemical synthesis route was carried out at room temperature. Although acrylate-NBE monomers suffer from a low reactivity in radical mediated polymerization, the thermogravimetric analysis showed adequate performance for the photochemical synthesis in terms of grafted-from polymer brush versus reaction time. However, the amino-epoxy reaction appeared instead more "scalable" if higher grafting efficiency was required. Once the polymer brushes were formed, the o-NBE groups of the particles surface were exploited to change the surface properties upon UV light as external trigger. Zeta potential measurements and XPS spectroscopy demonstrated that particles' physical and chemical surface properties were modified through UV light irradiation. Applying a similar synthetic path to glass slides, we further showed that the carboxylic acids, formed as o-NBE cleavage products, can be conveniently employed for changing the water contact angle of the polymer grafted surface. Finally, we showed the possibility to exploit the photo-deprotected carboxylic acid as anchor point for attaching an Alexa-546 conjugated fluorescent Protein A. Confocal microscopy images proved the selective anchoring of the fluorescent protein only onto the UV irradiated particles, therefore demonstrating the potentiality of ortho-nitrobenzyl chemistry for the fabrication of light responsive particles.

General conclusions

Along this thesis, different investigations in which the properties of o-NBE chemistry were exploited for the fabrication of photo-responsive polymer coatings and silica microparticles were presented. For this purpose, monomers containing o-NBE groups and with different end functionalities, such as epoxy, vinyl and acrylate, were first synthesized and then polymerized by means of photo-triggered reaction. Then, the photo-responsive nature of o-NBE moieties was conveniently exploited for changing bulk and surface properties of the synthesized polymers. Taking advantage from the high spatial and temporal control of light triggered reactions, in all the reported works it was demonstrated that light stimulus is a powerful tool for the synthesis and the modification of those polymer networks.

In a first contribution, photocleavable thiol-epoxy networks were prepared by anionic photoinduced ring opening reaction of multi-functional thiols with bi-functional epoxy monomers bearing photo-sensitive o-NBE links. Photo-triggered curing of the UV sensitive epoxy monomer was accomplished with a photo-latent base; ITX was used as light sensitizer to shift the photoinduced curing to the visible light region. Photocuring proceeded rapidly and nearly full conversion of the thiol groups was observed after 8 min of visible light exposure, demonstrating good efficiency for the proposed photo-triggered thiol-epoxy reaction. The subsequent photo-induced network degradation upon UV exposure was conveniently exploited for attaining bulk and surface modifications of the cured thiol-epoxy network.

Positive-tone patterns were successfully inscribed onto the cured networks by photolithography techniques. Despite good resolutions were obtained in surface photo-patterning, typical drawbacks of the adopted photomasking technique consisted in the formation of side reactions that led to a regeneration of covalent crosslinks upon prolonged UV exposure. These side reactions reduced the amount of extractable species, therefore limiting the performance of the synthetized network in photoresist applications. Besides the fabrication of positive-tone photoresist, the surface wettability of these coatings was changed. The photo-induced formation of polar cleavage products, i.e. carboxylic acids, led to a significant increase of the surface polarity and wettability. The results further showed that the decrease of the water contact angle was influenced by both exposure dose as well as the atmosphere in which the UV illumination was carried out. Whilst under nitrogen the decrease in the water contact angle didn't exceed 15°, the surface of the thiol-epoxy networks became fully wettable (<10 C°) if the UV irradiation was performed under air due to additional photo-oxidation of the surface.

In the following investigation, in the aim to overcame to the previously mentioned limitations in photoresists fabrication, it was proposed a novel method for the surface photopatterning which employed a direct laser beam irradiation of the photo-responsive networks. In this research, a photo-triggered thiol-ene click reaction between trifunctional thiols and synthesized bifunctional vinyl monomers

bearing o-NBE groups was carried out for the preparation of the photo-responsive coatings. The curing kinetic and mechanical properties of the obtained coatings matched the features of typical thiol-ene polymer networks, with fast and high conversion rate and with homogeneous mechanical properties. Subsequently, a laser induced writing of o-NBE moieties with UV light was exploited to create a 2.5D positive photoresist with a tunable generation of carboxylic acids as photoreaction products. Compared to the commonly used photomasking techniques, direct laser beam irradiation has given many advantages such as the formation of sharp and defined structures, whose were developed directly through laser surface ablation and without the use of harsh solvents. Moreover, SEM analysis on the sample surface showed that it was possible to inscribe a defined pattern with narrow profile, modulating the z-depth by tuning laser energy dose.

XPS spectroscopy also showed that it was possible to tune the amount of free carboxylic groups as a function of the laser energy dose. These moieties were exploited for a functional immobilization test, by using Alexa-546 conjugated protein A, showing high linearity between laser energy dose and grafting of proteins. This last result proved the possibility to use ortho-nitrobenzyl ester chemistry combined with laser technology for developing 2.5D patterned functional structures, which could be fundamental building blocks for a wide range of bio-applications, such as active sensitive layers of biosensors and/or controlled surfaces for cell growth or Lab-on-Chips.

Finally, passing from planar coatings to particles surface, silica microparticles with light responsive polymer brush were synthetized. The synthesis path followed two different procedures for the polymer brushes formation and respectively a *photo-grafting from* and an amino-epoxy coupling reaction. The photochemical grafting from procedure exploited a radical mediated reaction among TMESI[2]-BAPO surface anchored photo-initiators and a synthesized acrylate-NBE monomer. A second procedure involved an amino-epoxy coupling reaction among the primary amine of a 3-APTMS silanes anchored onto the silica surface, and a photo-responsive epoxy-NBE monomer. Although the low reactivity of acrylate-NBE monomers in radical mediated polymerization, the photochemical synthesis showed better grafting efficiency in terms of polymer grafted (about 3 mg/m^2) versus reaction time (4 hours) compared to the amino epoxy reaction, which for similar grafting yield required instead 10 hours of reaction at 65 degrees. However, the amino-epoxy reaction appeared instead more “scalable” if higher grafting efficiency were required. In a further step, the o-NBE pending groups in the polymer brushes were cleaved in order to change the surface properties upon UV light trigger. Zeta potential measurements and XPS spectroscopy demonstrated that physical and chemical surface properties of the particles were successful modified upon UV light irradiation. Eventually, the presence of photo-deprotected carboxylic acids onto silica particles were confirmed by conjugating an Alexa-546 fluorescent Protein. Confocal microscopy images proved the selective anchoring of the fluorescent protein only onto the UV irradiated particles, therefore demonstrating the potentiality of ortho-nitrobenzyl chemistry for the fabrication of light responsive particles.

Some general conclusions can be made for these class of photoreactions. Although o-nitrobenzyl derivatives were successfully exploited in different applications, some typical drawbacks still need to be fully overcome. For instance, being photo-active in UV wavelength windows limits their applicability in thick coatings or in drug delivery systems, because of UV light low penetration in tissues and its toxicity for living organisms. Some solutions to this drawback rely on the use of photobleaching systems, that basically shift the active light window from UV to IR wavelengths. However, typical problems of these approaches are related to the usual toxicity of the inorganic compounds employed in those systems. In this purpose, two photons emissions source represents a promising technology in order to overcome to this limitation. Other typical drawbacks of o-NB compounds consist in the nitroso byproducts formation that act as an internal filter and that can lead to other even more intensely absorbing materials, such as azo and azoxy compounds.

These byproducts are often reactive with nucleophiles functionalities, such as thiols and amines, and therefore they can be harmful to the living systems. Some possible solutions to this problematic rely on the design of o-nitrobenzyl derivatives that allow to an automatic trap of these compounds. In this aim, Pirrung and co-workers proposed a way of dealing with the nitroso side-products that were trapped in situ by a Diels–Alder reaction with a diene function included at the benzylic site [284].

Azo compounds byproducts reduce also the applicability of o-nitrobenzyl based polymer networks in photoresists applications. In facts, as already discussed in previous chapters, they act as crosslinking points promoting a polymer networks re-formation, and therefore limiting the photoresists fabrication. In this regard, in chapter 4 it was shown that laser beam can overcome to this typical drawback with a direct surface ablation, giving also the opportunity to design 2.5D profile. Finally, it was also mentioned about the low reactivity of monomers containing o-NBE groups in radical mediated polymerization. If a solution to this drawback has still to be found, in chapter 5 it was shown that despite the lower reactivity of acrylate-NBE monomers, it was possible to synthetize polymeric brushes with good efficiencies (3 mg/m^2 of grafted polymer), in a reasonably short time (4h) compared to other “grafting-from” techniques employed in literature.

However, overcoming these listed limitations will provide new opportunities to apply o-nitrobenzyl chemistry in other different areas of polymer science for the next years.

Appendix 1

A1. FTIR

FTIR (Fourier-transform infrared spectroscopy) is a spectroscopic technique used in order to obtain an infrared spectrum of absorption or emission of a solid, liquid or gas and thus information about the chemical bonds of the analysed specimen. The operating principle relies on the selective infrared absorption of covalent bonds inside a molecule, which changes the vibrational energy (stretching or bending) of the atoms in the bond [285]. Since different bonds and functional groups absorb at selective IR radiation, it is possible to record a spectra of the absorbed energy (Y-axis) at different IR wavenumber (X-axis), and therefore study the reaction kinetics comparing the peaks' area related to a certain functional groups at different reaction time [286].

A2. NMR

Solid state NMR is a nuclear magnetic resonance spectroscopy, characterized by the presence of anisotropic (direction dependent) interactions. Compared to common solution NMR, solid state NMR requires additional hardware, such as high-power radio frequency irradiation, and magic-angle spinning in order to overcome the limit of classical NMR spectroscopy [287].

NMR technique is widely adopted in order to study the molecule structures of an analysed sample. The technique bases its operating principle on the fact that protons and neutrons of an atomic nucleus have intrinsic quantum property of spin, and intrinsic angular momentum. The overall spin of the nucleus is determined by the spin combination of its protons and neutrons and an even number of protons and neutrons corresponds to an overall spin quantum number equal to zero and therefore no NMR signal [288].

An applied external magnetic field aligns the magnetic nuclei spin vector in a configuration ranging from a low energy configuration, parallel to the external magnetic field, to a higher energy configuration, anti-parallel to the external magnetic field. In this process the molecule electron clouds participate to the nuclei alignments shielding the external magnetic field, and therefore causing different spin alignment for same atoms that are dislocated in different molecules configurations [289].

Applying a proper oscillating magnetic field, the equilibrium among the atomic nuclei and the external magnetic field may be perturbated due to the nuclei photons absorption with a subsequent increase of the spin energy levels [289].

In NMR measurements, atomic nuclei are placed in a strong magnetic field and then perturbated by an oscillating magnetic field with a specific frequency (Larmor frequency) which is characteristic for each nucleus [288,289]. Upon the applied perturbation, the nuclei undergo a transition in their spin energy levels, passing from a lower energy level to higher energy level, characterized by anti-parallel spin configuration. De-applying the oscillating magnetic field, the spin populations shift again to a lower energy level, emitting photons with a certain frequency and energy which depends on the specific atomic structure of the studied nuclei (relaxation process) [288,289]. By collecting and analysing the emitted photons, it is then possible to create an emission spectrum determining the molecule composition and atomic layout. As also explained above, the interaction among the nuclei spins and the external magnetic field is strongly influenced by the electronic molecule shell, which produce an opposite magnetic field shielding the external magnetic field.

This effect causes a variation of the nuclear magnetic resonance frequency for the same nuclei that present different electronic surrounding, known as chemical shift [288,289].

In a classical liquid-state NMR experiment, the chemical shift generated by the electronic local field is "orientation dependent" because Brownian motion averages the anisotropic interactions to zero, reproducing NMR spectrum with narrow signals [287]. In contrast, the decreased atom mobility in solid state matters generates anisotropic electronic local fields, that have more influence on the nuclear magnetic spin. This anisotropic effect in solid state matter with other interactions, such as dipolar coupling, causes broader signal compared to liquid state NMR spectrum, that especially for polymers becomes even wider due to the high molecular weight [287,290].

In order to distinguish peak in NMR solid state spectra, different technique such as magic angle scattering (MAS) or cross polarization were developed. Magic angle scattering (MAS) reduces the dipolar interaction between hydrogen nuclei and carbon-13, and the anisotropy effect of the chemical shift which specially in polymer material causes broad NMR peaks. Since these two effects are mathematically correlated to the term $3\cos 2\theta - 1$, MAS technique is based in rotating the analysed sample at high rotational speeds in a sample probe angle corresponding to the amount of 54.74°, in order to reduce to zero the $3\cos 2\theta - 1$ term [290].

The cross-polarization technique is instead used in the aim to detect rare nuclei spins (i.e., 13C), which have longer relaxation times, through a polarization transfer process from abundant nucleus spin, such as hydrogen nucleus (^{1}H) [290].

A.3 Confocal microscopy

Confocal microscopy is an optical images technique used in order to overcome the limit of traditional microscopy in the resolution and contrast of a micrograph [291,292]. In a conventional microscopy technique, the entire specimen is illuminated at the same time and the resulting images is then viewed on the

microscope ocular lens or on a camera[293]. Since the image is collected using a specific focal plane, the light captured from the un-focused planes reduce the depth resolution of a 3D specimen [293]. In contrast, in confocal microscopy the specimen is illuminated by a focus beam of light point by point, and a pinhole in an optically conjugate plane in front of the detector eliminates the out of focus signal [291]. The light collected from a detector is then processed and the 3D image is rebuilt. Since only the light coming by the part of the specimen very close to the focal plane can be detected, the optical resolution, particularly on the z-axis, is higher compared to traditional microscopy [291].

A.4 Zeta potential

Zeta Potential is the electric potential at the shear plane of a solid surrounded by a liquid [294,295]. The interaction of solid surface functional groups with its surrounding medium causes a dissociation of ionogenic groups in the solid surface, and the differential adsorption of solution ions into the surface region. The net charge that is established at the particle surface affects the ion distribution in the nearby region, increasing the concentration of counterions close to the surface. The created electrical potential in this region decays with increasing of distance from the surface, reaching a plateau value in the bulk solution that is conventionally taken as zero [294].

The charge distribution could be further divided into a first region of counterions bound relatively tightly to the surface by electrostatic forces, known as stern layer, and an outer region in which the ions motion is caused by electrostatic interactions and thermal motions. The zeta potential is then defined as the electrical potential at the surface (shear surface) which divided the stationary to the diffusion ions layer [294,296].

Another perspective for studying the same property is to measure the isoelectric point defined as the pH value of the surrounding medium in which a molecule (functional group) carries no net electrical charge or is electrically neutral in the statistical mean [273].

A common technique adopted in order to determine the zeta potential of macroscopic solid surfaces in a liquid medium is the streaming potential method. The measurement consists in flowing an aqueous solution across the solid surface, which is analysed, under defined pressure conditions [296]. The fluid which flows through the solid surface produces a pressure gradient, considering the fluid dynamic aspect, as well as a charges motion at the solid/liquid interface along the liquid direction. The charges motion causes an electrical potential difference, called streaming potential, that with the applied pressure is at the end proportional to the zeta potential value [294,296].

A.5 XPS

X-ray photoelectron spectroscopy (XPS) technique gives information to the orbital energetic and therefore to the molecular structure of the analysed specimen [297].

The working principle relies on the electrons photo-emission mechanism of atoms or molecules after a monochromatic X-ray beam radiation. As a consequence of the X-ray absorption, the sample emits electrons of a specific energy level which depends on the X-ray energetic and therefore wavelength. The photo-emitted electrons are collected by an electron collected lens, and their binding energy is calculated by subtracting the measured kinetic energy from the absorbed X-ray [298].

Since the photo-emitted electrons, in their path, can undergo through inelastic collisions, recombination, excitation of the sample, recapture or trapping in various excited states within the material, the effective number which leave the sample, and are detected, is exponential attenuated by the sample depth. For this reason, XPS measurements are surface sensitive, measuring the chemical properties of the first atomic layers of the specimen surface [299].

The result of this acquisition process is a spectrum reporting on the Y-axis the number of electrons detected (counts) for a specific binding energy (X-axis). Each element generates a characteristic peak with a specific binding energy which depends on the atomic or molecular orbitals (i.e. 1s, 2s, 3p, 3s, etc.). Since the configuration of a given element, meaning the local bonding environment of an atomic species, produces a shift in the electronic binding energy (chemical shift), XPS is a powerful tool for providing chemical state information of a specimen surface [244].

A.6 SEM

A scanning electron microscope (SEM) is a type of electron microscopy which is mostly used in order to overcome the diffraction limits of optical microscopy, and therefore capturing high resolution images on nanometric scale [300]. SEM microscopy provides topographical images of the sample surface, through the signals generated by the interaction between a scanning focused electron beam and the analysed specimen. When the focused primary beam penetrates the specimen surface, produces different kinds of interactions, and therefore measurable signals, such as the electron scattering at different specimen depths [301]. Some scattered electrons that are created by inelastic collisions, known as secondary electrons, escape close to the surface because of their low kinetic energy (less than 50 eV) which limits their mean free path in solid matter. Because of their low energetic, secondary electrons can only escape from the top surface nanometers, and can be detected and converted to photons (generally by means of scintillator or a photomultiplier) in order to reproduce the topographical image of the specimen

surface [301,302]. X-rays are instead emitted when the electron primary beam removes an inner shell electron from the sample, causing an electron from the outer shell to fill the vacancy and therefore releasing energy by means of X-ray emissions.

The energy or wavelength of these characteristic X-rays can be measured by Energy-dispersive X-ray spectroscopy or Wavelength-dispersive X-ray spectroscopy and used to identify and measure the abundance of elements in the sample, mapping also their distribution throughout the surface [303].

A.7 Confocal microscopy spinning disk

As deeply described in the Appendix A.4, in a confocal microscopy measurement, a specimen is illuminated by a focus laser beam point by point, and a pinhole in an optically conjugate plane in front of the detector eliminates the out of focus signals [291]. Despite the high image resolution and sharp contrast, a typical drawback of this technique includes the low acquisition speed of the overall image [304]. The image acquisition time may be reduced increasing the laser beam speed on the sample surface, but thus reducing the pixel dwell time. As a result of the limited pixel dwell time, a higher laser illumination strength would be necessary in order to excite the fluorophore, which eventually may induce photo-bleaching and, in same case, cause photo-toxicity for live cells [292].

In order overcome these limitations, a spinning disk confocal microscopy uses multiple pinholes mounted on a rotating disk which allows a parallel-spots scanning of the specimen surface, therefore reducing the acquisition time of the overall image. Furthermore, because of multiple light beams operating in parallel through the spinning disk, the pixel dwell time can be increased without reducing considerably the overall acquisition speed, and thus limiting the photobleaching and photo-toxicity [305].

By choosing appropriate dimensions and distance among the disk pinholes as well as the rotating velocity and the exposure time (pixel dwell time), it is possible to acquire sharp images at much higher frame, reducing photobleaching and photo-toxicity [305,306]. These peculiar characteristics make spinning disk confocal microscopy a suitable technique for studying live cells dynamic.

Appendix 2

List of Figures.

Introduction:

Chapter 2:

Figure 2.9 Photo-induced formation and light triggered cleavage of thiol-ene networks for the design of switchable polymer patterns. (Adapted from reference [134] published by the Royal Society of Chemistry).

Figure 2.10 Schematic illustration of (a) photopolymerization of the thiol-yne network at long wavelength. (b) Patterned and asymmetrical UV exposure to realize (c) a wedge-shaped surface area with a lengthwise wettability gradient, which is surrounded by the hydrophobic (not exposed and thus, not-cleaved) thiol-yne network. (d) Water contact angle and droplet movement on the irradiated surface (Adapted from reference [106] published by the Royal Society of Chemistry).

Figure 2.11 Schematic illustration of (a,b) Patterned and asymmetrical UV exposure on NIL thiol-acrylate structure. (c) SEM micrographs of the topography of needle-like micropatterns inscribed by visible light assisted NIL (d) Surface structures of the photocured photopolymer after 1500 s of UV exposure (269 mW/cm^2) under air (Adapted from reference [107] published by the Royal Society of Chemistry).

Figure 2.12 Schematic representation of the process for generation of multifunctional pattern on silicon wafer (Reprinted with the permission from reference [139] Copyright 2014 American Chemical Society).

Figure 2.13 Schematic representation of the methacrylate o-nitrobenzyl thioether synthesis and subsequent UV deprotection process (Reprinted with the permission of The Royal Society of Chemistry from reference [129])

Figure 2.14 Positive-type photoresists and storage modulus variation of epoxy-NBE network upon UV exposure (Reprinted from reference [141] with the permission of Elsevier).

Figure 2.15 Schematic representation of the formation of a positive-tone resist and (a) subsequent removal of the resist by hydrolytic degradation of the PDMS network. (b and c) Confocal micrographs of positive-tone relief structures (100 μm lines and spaces) inscribed into PDMS-1 by photolithography after the development in chloroform. (d) Schematic representation of the formation of a negative-tone resist. (e and f) Confocal micrographs of negative-tone relief structures (50 and 100 μm lines and spaces) inscribed into polymer network by photolithography after the development in 1 M aqueous NaOH (Reprinted with permission from reference [151]).

Figure 2.16 Synthetic route of light-responsive silica nanoparticles (Reprinted with permission of Elsevier from reference [153]).

Figure 2.17 Schematic Illustration of the Photo-Induced Shape Transformation of PS-b-P2VP Particles Enabled by Light-Active 5-Hexyloxy-2-nitrobenzyl-16-N,N,N-trimethylhexadecan-1-ammonium Bromide (N-CTAB) Surfactants (Reprinted with permission from reference [157] Copyright 2019 American Chemical Society).

Figure 2.18 Schematic representation of the preparation and light-induced degradation of silica nanoparticles. (Reprinted with permission from reference [158] Copyright 2020 American Chemical Society).

Figure 2.19 Synthetic pathway used in the preparation of the NIR light responsive drug delivery system. (Reprinted with permission from reference [168] Copyright 2015 American Chemical Society).

Figure 2.20 Degradation mechanism through oxidation and UV-illumination of bicompartmental microparticles. The particles were incubated in 30% v/v hydrogen peroxide

for 1 hour, followed by UV illumination at 365 nm for 30 min. The SEM images on the right visualize the degradation of the particles (Reprinted with permission from reference [177],Copyright 2015 American Chemical Society).

Figure 2.21 Chemical structures of the (a) BTA- and (b) UPy- derivatives. Schematic representation of the behavior of (c) BTA- and (d) UPy-colloids. Upon UV-irradiation, the labile o-nitrobenzyl group is cleaved of and the H-bonds become active, triggering colloidal clustering. Confocal images of an equal mixture of BTA-colloids (green) and UPy-colloids (red) (e) before and (f) afer 30min of irradiation (λmax=354mm). (Reprinted with permission from reference [189]).

Chapter 3:

Figure 3.1 Reaction mechanism of the base-catalyzed nucleophilic addition reaction between thiol and epoxy groups. Homopolymerization of the epoxy groups does not occur due to the thermodynamically favored protonation step [194].

Figure 3.2 Components used in photo-responsive thiol-epoxy resin formulations.

Figure 3.3 Thermally and photochemically triggered base-catalyzed curing of photo-responsive thiol-epoxy networks in the presence of a photolatent base and ITX as photosensitizer, which shifts the spectral sensitivity of the photolatent base towards the visible light region [215].

Figure 3.4 (a) FT-IR spectra of PI4 (1) prior to and (2) after photo-curing (1.8 J/cm^2, $\lambda > 400$ nm, air). Inserts show the IR bands of the characteristic (I) OH, (II) SH and (III) epoxy groups magnified out of the FT-IR spectra. Normalized depletion of (b) the thiol absorption band (2580 cm^{-1}) versus illumination time (1.8 J/cm^2, $\lambda > 400$ nm, air). Resin formulations contained varying amounts of photolatent base and ITX: Pl2 (solid circles); Pl3 (solid diamonds); Pl4 (solid squares) and Pl5 (solid triangles). (c) Normalized depletion of the thiol absorption band (2580 cm^{-1}) of non-illuminated resin formulation PI4 versus reaction time. The reaction temperature amounted to 23 (open diamonds), 50 (open squares) and 70 °C (half open diamonds).

Figure 3.5 Normalized depletion of the thiol absorption band (2580 cm^{-1}) versus illumination time (4 J/cm^2, $\lambda > 400$ nm, air). Resin formulations contained varying amounts of epoxy-GME at a given PLB and ITX level of 4 wt%: Pl4 (solid squares); PI4-G5 (open diamonds) and PI4-G7 (open triangles).

Figure 3.6 (a) Primary and (b) secondary photoreactions during the photoisomerization of *o*-NBE derivatives [36,57,226].

Figure 3.7 (a) FT-IR spectra of cured **PI4** (1) prior to and (2) after photo-induced cleavage of the *o*-NBE links (85 J/cm^2, $\lambda < 400$ nm, N_2). (b) Following the photocleavage kinetics of the *o*-NBE links by FT-IR spectroscopy upon prolonged UV exposure: Decrease of the normalized intensity of the nitro band at 1537 cm^{-1} in **PI4** (*solid squares*), **PI4-G5** (*open diamonds*) and **PI4-G7** (*open triangles*).

Figure 3.8 (a) Gel fraction of **PI4**, **PI4-G5** and **PI4-G7** versus exposure dose (75 mW/cm^2, $\lambda < 400$ nm, N_2) as obtained from FT-IR measurements. (b) Confocal micrograph of positive-tone relief structures (100 and 50 µm lines and spaces) inscribed into **PI4-G5** by photolithography after the development in tetrahydrofuran.

Figure 3.9 ^{13}C CP/MAS solid state NMR of crosslinked Pl4-G5 acquired on 600 MHz solid state NMR. Sample was spun at 10 kHz. Chemical shift of signals belonging to the formulation components are marked in blue, spinning side bands are marked in grey.

Figure 3.10 ^{13}C CP/MAS solid state NMR of crosslinked Pl4-G5 illuminated with a low UV exposure dose (100 J/cm^2) acquired on 600 MHz solid state NMR. Sample was spun at 16 kHz. UV irradiation were carried under (a) air or (b) nitrogen.

Figure 3.11 ^{13}C CP/MAS solid state NMR of crosslinked Pl4-G5 illuminated with a high UV exposure dose (300 J/cm^2) acquired on 600 MHz solid state NMR. Sample was spun at 16 kHz. UV irradiation were carried under (a) air or (b) nitrogen. Chemical shift of signals belonging to the network and cleavage products are marked in blue, spinning side bands are marked in grey.

Figure 3.12 (a) Water contact angle of cured **PI4-G5** versus exposure dose (138 mW/cm^2, $\lambda < 400$ nm). UV exposure was carried out either in air (*open circles*) or nitrogen (*open squares*). (b) Zeta potential as a function of the pH value of cured **PI4-G5** versus exposure dose (138 mW/cm^2, $\lambda < 400$ nm) and atmosphere (nitrogen *versus* air).

Chapter 4:

Figure 4.1 (a) Typical ortho-nitrobenzyl cleavage kinetic in thiol-click network. (b) Thiol-ene network's normalized gel fraction after o-NBE photo-cleavage (Adapted from reference [134] published by the Royal Society of Chemistry)

Figure 4.2 Comparison between photolithography and direct laser writing for the introduction of micropatterns in photo-sensitive thiol-ene networks.

Figure 4.3 Monomers and photoinitiations used for the preparation of thiol-ene photo-responsive network

Figure 4.4 EDC (carbodiimide) reactions with carboxylic acid. The conjugation proceeds through a first reaction between the carbodiimide (EDC) and the carboxylic acid, with the formation of O-acylisourea reactive intermediates. O-acylisourea intermediates may then react with a primary amine, through nucleophilic attack, with the formation of an amide bond and isourea by-product.

Figure 4.5 EDC/-sulfo NHS reaction scheme. The o-Acylisourea unstable intermediate may undergo through tree different reaction paths (a, b, c). The Sulfo-NHS ester (path c) reacting with a primary amine groups (reaction path d) leads to the formation of amide bonds as final product.

Figure 4.6 Radical mediated mechanism of the thiol-ene click reaction [128].

Figure 4.7 a) FT-IR spectra of TMPMP/vinyl-NBE formulation prior (black) to and after (blue) photo-curing (3.6 J/cm^2, $\lambda > 400$ nm, air). Inserts show the IR bands of the characteristic (I) SH (2569 cm^{-1}) and (II) C=C (1640 cm^{-1}) groups magnified out of the FT-IR spectra. b) Normalized depletion of the thiol absorption band (2580 cm^{-1}) solid square and double carbon bonds absorption band (1640 cm^{-1}) (open circles) versus illumination time (8 mW/cm^2, $\lambda > 400$ nm, air).

Figure 4.8 a) DMA measurement of TMPMP/vinyl-NBE sample with storage modulus (black) and tanδ (blue) of the crosslinked polymer b) heat flow/temperature curve according to DSC measurement of the TMPMP/vinyl-NBE formulation with insert of first derivate of the heat flow; $\Delta W/\Delta T$ in the glass transition interval.

Figure 4.9 a) Profilometer of visible light cured TMPMP/vinyl-NBE samples, cleaved at different energy doses (70%, 80%, 90% and 100%). b) Depth profile/laser energy dose (in %) of visible light cured TMPMP/vinyl-NBE samples, cleaved at different energy doses. c)

profilometry of patterns obtained at different laser doses. d) SEM of a 2.5D pattern generated with different energy doses.

Figure 4.10 C1s HR XPS spectra of visible-light cured TMPMP/vinyl-NBE samples, which were then cleaved upon exposure to a laser beam with varying exposure dose. The inset graph shows a magnification of the carboxylic chemical shift, with the peaks located between 288.6 and 288.8 eV. In the Table, UV laser energy dose vs –COOH/CTOT peak area, calculated from HR XPS spectra by a deconvolution procedure applied to C1s peaks, are listed.

Figure 4.11 High Resolution C1s XPS peaks for the blank sample and the samples irradiated with different laser energy doses.

Figure 4.12 (a) Spinning Disk confocal Microscope of the TMPMP/vinyl-NBE sample (each square is 50 x 50 microns) patterned at different laser UV irradiation dose, functionalized with Alexa-546 conjugated Protein A. (b) Plot profile of the average signal (average of 10 profiles) along the yellow line in image (a) for the three replicates of each laser UV irradiation dose.

Chapter 5:

Figure 5.1 H-NMR of the synthetized monofunctional acrylate-NBE.

Figure 5.2 H-NMR of the synthetized monofunctional epoxy-NBE.

Figure 5.3 Chemical structure of the TMESI^2-BAPO.

Figure 5.4 Chemical structure of (3-Aminopropyl)trimethoxysilane (3-APTMS)

Figure 5.5 Synthetic procedure of: a) photo-grafting from; b) Amino-epoxy grafting from. In both procedures a first step implies the anchoring of silane agents onto the particles surface. In a further step photo-responsive monomer are grown through “photo-grafting from” or amino-epoxy reactions. Eventually the grafted polymer brushes are cleaved upon UV light irradiation leading to carboxylic acids species which stay tether to the surface and nitroso compounds which are released.

Figure 5.6 a) IR spectra of untreated silica particles (Si-OH peak at 758 cm^{-1}), b) UV-vis spectroscopy of untreated silica particles (black curve) and particles modified with TMESI^2-BAPO (red curve), particle concentration amounted to 0.15 mg ml^{-1} in absolute ethanol.

Figure 5.7 TGA of the modified silica particles, in figure: back curve untreated silica, blue curve TMESI^2-BAPO modified (48h, room temperature), red curve 3-APTMS amino silanized (5h, 80°C), magenta curve 3-APTMS modified (12h, 80°C).

Figure 5.8 TMESI^2-BAPO surface anchoring and polymer brush formations upon light stimuli.

Figure 5.9 Thermogravimetry analysis: black curve untreated silica particles (reference), blue curve TMESI^2-BAPO modified (48h, room temperature), magenta curve Acrylate-NBE photo-grafted (4h, 350 mW/m^2), red curve Acrylate-NBE photo-grafted (4h, 20 mW/m^2);

Figure 5.10 Amino-epoxy coupling reaction steps: Step 1) Nucleophilic attack carried by primary amine to the less sterically hindered carbon of an oxirane ring with the formation of a secondary amine and an hydroxyl group. Step 2) Reaction among the formed Secondary Amines and epoxy groups leading the formation of Tertiary Amine and hydroxyl groups. Eventually, the hydroxyl groups generated by the reaction between the secondary amine and epoxide group will result in the formation of ether linkage (Step 3) (etherification)

List of tables.

Chapter 3:

Chapter 5:

References

1. Kuang, X.; Roach, D.J.; Wu, J.; Hamel, C.M.; Ding, Z.; Wang, T.; Dunn, M.L.; Qi, H.J. Advances in 4D Printing: Materials and Applications. *Adv. Funct. Mater.*, **2019**, *29*, 1–23.

2. Jeong, B.; Gutowska, A. Lessons from Nature: Stimuli-Responsive Polymers and Their Biomedical Applications. *Trends Biotechnol.*, **2002**, *20*, 305–311.

3. Stuart, M.A.C.; Huck, W.T.S.; Genzer, J.; Müller, M.; Ober, C.; Stamm, M.; Sukhorukov, G.B.; Szleifer, I.; Tsukruk, V. V.; Urban, M.; Winnik, F.; Zauscher, S.; Luzinov, I.; Minko, S. Emerging Applications of Stimuli-Responsive Polymer Materials. *Nat. Mater.*, **2010**, *9*, 101–113.

4. Ikeda, M. Stimuli-Responsive Supramolecular Systems Guided by Chemical Reactions. *Polym. J.*, **2019**, *51*, 371–380.

5. Wei, M.; Gao, Y.; Li, X.; Serpe, M.J. Stimuli-Responsive Polymers and Their Applications. *Polym. Chem.*, **2017**, *8*, 127–143.

6. Montero De Espinosa, L.; Meesorn, W.; Moatsou, D.; Weder, C. Bioinspired Polymer Systems with Stimuli-Responsive Mechanical Properties. *Chem. Rev.*, **2017**, *117*, 12851–12892.

7. Liu, Z.; Calvert, P. Multilayer Hydrogels as Muscle-like Actuators. *Adv. Mater.*, **2000**, *12*, 288–291.

8. Oliveira, J.; Correia, V.; Castro, H.; Martins, P.; Lanceros-Mendez, S. Polymer-Based Smart Materials by Printing Technologies: Improving Application and Integration. *Addit. Manuf.*, **2018**, *21*, 269–283.

9. Guo, Z.; Liu, H.; Dai, W.; Lei, Y. Responsive Principles and Applications of Smart Materials in Biosensing. *Smart Mater. Med.*, **2020**, *1*, 54–65.

10. Cabane, E.; Zhang, X.; Langowska, K.; Palivan, C.G.; Meier, W. Stimuli-Responsive Polymers and Their Applications in Nanomedicine. *Biointerphases*, **2012**, *7*, 1–27.

11. Roy, D.; Cambre, J.N.; Sumerlin, B.S. Future Perspectives and Recent Advances in Stimuli-Responsive Materials. *Prog. Polym. Sci.*, **2010**, *35*, 278–301.

12. Li, Y.C.; Zhang, Y.S.; Akpek, A.; Shin, S.R.; Khademhosseini, A. 4D Bioprinting: The next-Generation Technology for Biofabrication Enabled by Stimuli-Responsive Materials. *Biofabrication*, **2017**, *9*, 1–16.

13. Jochum, F.D.; Theato, P. Temperature- and Light-Responsive Smart Polymer Materials. *Chem. Soc. Rev.*, **2013**, *42*, 7468–7483.

14. Theato, P.; Sumerlin, B.S.; O'reilly, R.K.; Epp, T.H. Stimuli Responsive

Materials. *Chem. Soc. Rev.*, **2013**, *42*, 7055–7056.

15. Gao, S.; Tang, G.; Hua, D.; Xiong, R.; Han, J.; Jiang, S.; Zhang, Q.; Huang, C. Stimuli-Responsive Bio-Based Polymeric Systems and Their Applications. *J. Mater. Chem. B*, **2019**, *7*, 709–729.

16. Roth, P.J.; Lowe, A.B. Stimulus-Responsive Polymers. *Polym. Chem.*, **2017**, *8*, 10–11.

17. Bertrand, O.; Gohy, J.F. Photo-Responsive Polymers: Synthesis and Applications. *Polym. Chem.*, **2017**, *8*, 52–73.

18. Klán, P.; Šolomek, T.; Bochet, C.G.; Blanc, A.; Givens, R.; Rubina, M.; Popik, V.; Kostikov, A.; Wirz, J. Photoremovable Protecting Groups in Chemistry and Biology: Reaction Mechanisms and Efficacy. *Chem. Rev.*, **2013**, *113*, 119–191.

19. Roth, H.D. The Beginnings of Organic Photochemistry. *Angew. Chemie Int. Ed. English*, **1989**, *28*, 1193–1207.

20. Heath, H. A New Sensitive Chemical Actinometer - II. Potassium Ferrioxalate as a Standard Chemical Actinometer. *Proc. R. Soc. London. Ser. A. Math. Phys. Sci.*, **1956**, *235*, 518–536.

21. Parker, C.A.; A, P.R.S.L. A New Sensitive Chemical Actinometer. I. Some Trials with Potassium Ferrioxalate. *Proc. R. Soc. London. Ser. A. Math. Phys. Sci.*, **1953**, *220*, 104–116.

22. Roth, H.D. A Tribute to Stanislao Cannizzaro, Chemical Informationist and Photochemist. *Photochem. Photobiol. Sci.*, **2011**, *10*, 1849–1853.

23. Heines, S.V. Peter Griess—Discoverer of Diazo Compounds. *J. Chem. Educ.*, **1958**, *35*, 187.

24. Ciamician, G.; Silber, P. Chemische Lichtwirkungen. *Berichte der Dtsch. Chem. Gesellschaft*, **1901**, *34*, 2040–2046.

25. Ciamician, G.; Silber, P. Chemische Lichtwirkungen. *Berichte der Dtsch. Chem. Gesellschaft*, **1902**, *35*, 4128–4131.

26. Ciamician, G. THE PHOTOCHEMISTRY OF THE FUTURE. *Science (80-.).*, **1912**, *36*, 385–394.

27. Chatani, S.; Kloxin, C.J.; Bowman, C.N. The Power of Light in Polymer Science: Photochemical Processes to Manipulate Polymer Formation, Structure, and Properties. *Polym. Chem.*, **2014**, *5*, 2187–2201.

28. Hansen, M.J.; Velema, W.A.; Lerch, M.M.; Szymanski, W.; Feringa, B.L. Wavelength-Selective Cleavage of Photoprotecting Groups: Strategies and Applications in Dynamic Systems. *Chem. Soc. Rev.*, **2015**, *44*, 3358–3377.

29. Russew, M.M.; Hecht, S. Photoswitches: From Molecules to Materials. *Adv. Mater.*, **2010**, *22*, 3348–3360.

30. Habault, D.; Zhang, H.; Zhao, Y. Light-Triggered Self-Healing and Shape-Memory Polymers. *Chem. Soc. Rev.*, **2013**, *42*, 7244–7256.

31. Trenor, S.R.; Shultz, A.R.; Love, B.J.; Long, T.E. Coumarins in Polymers: From Light Harvesting to Photo-Cross-Linkable Tissue Scaffolds. *Chem. Rev.*, **2004**, *104*, 3059–3077.

32. Il'ichev, Y. V.; Schwörer, M.A.; Wirz, J. Photochemical Reaction Mechanisms of 2-Nitrobenzyl Compounds: Methyl Ethers and Caged ATP. *J. Am. Chem. Soc.*, **2004**, *126*, 4581–4595.

33. Guillier, F.; Orain, D.; Bradley, M. Linkers and Cleavage Strategies in Solid-Phase Organic Synthesis and Combinatorial Chemistry. *Chem. Rev.*, **2000**, *100*, 2091–2157.

34. Pelliccioli, A.P.; Wirz, J. Photoremovable Protecting Groups: Reaction Mechanisms and Applications. *Photochem. Photobiol. Sci.*, **2002**, *1*, 441–458.

35. Bochet, C.G. Photolabile Protecting Groups and Linkers. *J. Chem. Soc. Perkin 1*, **2002**, *2*, 125–142.

36. V. N. Rajasekharan Pillai. Photoremovable Protecting Groups in Organic Synthesis. *Synthesis (Stuttg).*, **1980**, *1*, 1–26.

37. Barltrop, J.A.; Plant, P.J.; Schofield, P. Photosensitive Protective Groups. *Chem. Commun.*, **1966**, 822–823.

38. Romano, A.; Roppolo, I.; Giebler, M.; Dietliker, K.; Možina; Šket, P.; Mühlbacher, I.; Schlögl, S.; Sangermano, M. Stimuli-Responsive Thiol-Epoxy Networks with Photo-Switchable Bulk and Surface Properties. *RSC Adv.*, **2018**, *8*, 41904–41914.

39. Cameron, J.F.; Fréchet, J.M.J. Photogeneration of Organic Bases from O-Nitrobenzyl-Derived Carbamates. *J. Am. Chem. Soc.*, **1991**, *113*, 4303–4313.

40. Wang, P. Photolabile Protecting Groups: Structure and Reactivity. *Asian J. Org. Chem.*, **2013**, *2*, 452–464.

41. Amit, B.; Zehavi, U.; Patchornik, A. Photosensitive Protecting Groups — A Review. *Isr. J. Chem.*, **1974**, *12*, 103–113.

42. Rich, D.H.; Gurwara, S.K. Removal of Protected Peptides from an Ortho-Nitrobenzyl Resin by Photolysis. *J. Chem. Soc. Chem. Commun.*, **1973**, *17*, 610–611.

43. Zhao, H.; Sterner, E.S.; Coughlin, E.B.; Theato, P. O-Nitrobenzyl Alcohol Derivatives: Opportunities in Polymer and Materials Science. *Macromolecules*, **2012**, *45*, 1723–1736.

44. Zhang, X.; Xi, W.; Gao, G.; Wang, X.; Stansbury, J.W.; Bowman, C.N. O-Nitrobenzyl-Based Photobase Generators: Efficient Photoinitiators for Visible-Light Induced Thiol-Michael Addition Photopolymerization. *ACS*

Macro Lett., **2018**, *7*, 852–857.

45. Kretschy, N.; Holik, A.K.; Somoza, V.; Stengele, K.P.; Somoza, M.M. Next-Generation o-Nitrobenzyl Photolabile Groups for Light-Directed Chemistry and Microarray Synthesis. *Angew. Chemie - Int. Ed.*, **2015**, *54*, 8555–8559.

46. Holmes, C.P. Model Studies for New O-Nitrobenzyl Photolabile Linkers: Substituent Effects on the Rates of Photochemical Cleavage. *J. Org. Chem.*, **1997**, *62*, 2370–2380.

47. Bley, F.; Schaper, K.; Görner, H. Photoprocesses of Molecules with 2-Nitrobenzyl Protecting Groups and Caged Organic Acids. *Photochem. Photobiol.*, **2008**, *84*, 162–171.

48. Wöll, D.; Smirnova, J.; Galetskaya, M.; Prykota, T.; Bühler, J.; Stengele, K.P.; Pfleiderer, W.; Steiner, U.E. Intramolecular Sensitization of Photocleavage of the Photolabile 2-(2-Nitrophenyl)Propoxycarbonyl (NPPOC) Protecting Group: Photoproducts and Photokinetics of the Release of Nucleosides. *Chem. - A Eur. J.*, **2008**, *14*, 6490–6497.

49. Wöll, D.; Laimgruber, S.; Galetskaya, M.; Smirnova, J.; Pfleiderer, W.; Heinz, B.; Gilch, P.; Steiner, U.E. On the Mechanism of Intramolecular Sensitization of Photocleavage of the 2-(2-Nitrophenyl)Propoxycarbonyl (NPPOC) Protecting Group. *J. Am. Chem. Soc.*, **2007**, *129*, 12148–12158.

50. Zeng, X.; Zhou, X.; Wu, S. Red and Near-Infrared Light-Cleavable Polymers. *Macromol. Rapid Commun.*, **2018**, *39*, 1–16.

51. Lunzer, M.; Shi, L.; Andriotis, O.G.; Gruber, P.; Markovic, M.; Thurner, P.J.; Ossipov, D.; Liska, R.; Ovsianikov, A. A Modular Approach to Sensitized Two-Photon Patterning of Photodegradable Hydrogels. *Angew. Chemie*, **2018**, *130*, 15342–15347.

52. Lee, G.; Park, Y. Il. Lanthanide-Doped Upconversion Nanocarriers for Drug and Gene Delivery. *Nanomaterials*, **2018**, *8*, 511.

53. Petropoulos, C.C. SYNTHESIS OF NOVEL PHOTODEGRADABLE POLY(o-NITROBENZALDEHYDE ACETAL) POLYMERS. *J Polym Sci Polym Chem Ed*, **1977**, *15*, 1637–1644.

54. Zhu, C.; Bettinger, C.J. Photoreconfigurable Physically Cross-Linked Triblock Copolymer Hydrogels: Photodisintegration Kinetics and Structure-Property Relationships. *Macromolecules*, **2015**, *48*, 1563–1572.

55. Zhao, H.; Gu, W.; Sterner, E.; Russell, T.P.; Coughlin, E.B.; Theato, P. Highly Ordered Nanoporous Thin Films from Photocleavable Block Copolymers. *Macromolecules*, **2011**, *44*, 6433–6440.

56. Bertrand, O.; Poggi, E.; Gohy, J.F.; Fustin, C.A. Functionalized Stimuli-Responsive Nanocages from Photocleavable Block Copolymers. *Macromolecules*, **2014**, *47*, 183–190.

57. Reichmanis, E.; Smith, B.C.; Gooden, R. Omicron -NITROBENZYL

PHOTOCHEMISTRY: SOLUTION VS. SOLID-STATE BEHAVIOR. *J. Polym. Sci. A1.*, **1985**, *23*, 1–8.

58. Kloxin, A.M.; Kasko, A.M.; Salinas, C.N.; Anseth, K.S. Photodegradable Hydrogels for Dynamic Tuning of Physical and Chemical Properties. *Science (80-.).*, **2009**, *324*, 59–63.

59. Zhao, H.; Gu, W.; Kakuchi, R.; Sun, Z.; Sterner, E.; Russell, T.P.; Coughlin, E.B.; Theato, P. Photocleavable Triblock Copolymers Featuring an Activated Ester Middle Block: "One-Step" Synthesis and Application as Locally Reactive Nanoporous Thin Films. *ACS Macro Lett.*, **2013**, *2*, 966–969.

60. Mo, B.; Liu, H.; Zhou, X.; Zhao, Y. Facile Synthesis of Photolabile Dendritic-Unit-Bridged Hyperbranched Graft Copolymers for Stimuli-Triggered Topological Transition and Controlled Release of Nile Red. *Polym. Chem.*, **2015**, *6*, 3489–3501.

61. Liu, C.; Ewert, K.K.; Yao, W.; Wang, N.; Li, Y.; Safinya, C.R.; Qiao, W. A Multifunctional Lipid Incorporating Active Targeting and Dual-Control Release Capabilities for Precision Drug Delivery. *ACS Appl. Mater. Interfaces*, **2020**, *12*, 70–85.

62. Li, W.; He, Y.G.; Shi, S.Y.; Liu, N.; Zhu, Y.Y.; Ding, Y.S.; Yin, J.; Wu, Z.Q. Fabrication of a Multi-Charge Generable Poly(Phenyl Isocyanide)-Block-Poly(3-Hexylthiophene) Rod-Rod Conjugated Copolymer. *Polym. Chem.*, **2015**, *6*, 2348–2355.

63. Li, L.; Scheiger, J.M.; Levkin, P.A. Design and Applications of Photoresponsive Hydrogels. *Adv. Mater.*, **2019**, *31*, 1807333.

64. Hegazy, M.; Zhou, P.; Rahoui, N.; Wu, G.; Taloub, N.; Lin, Y.; Huang, X.; Huang, Y. A Facile Design of Smart Silica Nanocarriers via Surface-Initiated RAFT Polymerization as a Dual-Stimuli Drug Release Platform. *Colloids Surfaces A Physicochem. Eng. Asp.*, **2019**, *581*, 123797.

65. Han, D.; Tong, X.; Zhao, Y. Block Copolymer Micelles with a Dual-Stimuli-Responsive Core for Fast or Slow Degradation. *Langmuir*, **2012**, *28*, 2327–2331.

66. Cao, Z.; Li, Q.; Wang, G. Photodegradable Polymer Nanocapsules Fabricated from Dimethyldiethoxysilane Emulsion Templates for Controlled Release. *Polym. Chem.*, **2017**, *8*, 6817–6823.

67. Wang, Y.Z.; Li, L.; Du, F.S.; Li, Z.C. A Facile Approach to Catechol Containing UV Dismantlable Adhesives. *Polymer (Guildf).*, **2015**, *68*, 270–278.

68. Del Campo, A.; Boos, D.; Spiess, H.W.; Jonas, U. Surface Modification with Orthogonal Photosensitive Silanes for Sequential Chemical Lithography and Site-Selective Particle Deposition. *Angew. Chemie - Int. Ed.*, **2005**, *44*, 4707–4712.

69. Cordonier, C.E.J.; Nakamura, A.; Shimada, K.; Fujishima, A. Metallic Film Formation Using Direct Micropatterning with Photoreactive Metal Complexes. *Langmuir*, **2012**, *28*, 13542–13548.

70. Shadish, J.A.; Benuska, G.M.; DeForest, C.A. Bioactive Site-Specifically Modified Proteins for 4D Patterning of Gel Biomaterials. *Nat. Mater.*, **2019**, *18*, 1005–1014.

71. Katz, J.S.; Doh, J.; Irvine, D.J. Composition-Tunable Properties of Amphiphilic Comb Copolymers Containing Protected Methacrylic Acid Groups for Multicomponent Protein Patterning. *Langmuir*, **2006**, *22*, 353–359.

72. Gumbley, P.; Koylu, D.; Pawle, R.H.; Umezuruike, B.; Spedden, E.; Staii, C.; Thomas, S.W. Wavelength-Selective Disruption and Triggered Release with Photolabile Polyelectrolyte Multilayers. *Chem. Mater.*, **2014**, *26*, 1450–1456.

73. Hu, X.; Qureishi, Z.; Thomas, S.W. Light-Controlled Selective Disruption, Multilevel Patterning, and Sequential Release with Polyelectrolyte Multilayer Films Incorporating Four Photocleavable Chromophores. *Chem. Mater.*, **2017**, *29*, 2951–2960.

74. Konishi, T.; Hashimoto, T.; Sato, N.; Nakajima, K.; Yamaguchi, K. Substituent Effects at the Benzyl Position and Aromatic Ring of Silane-Coupling Agents Containing 2-Nitrobenzyl Esters on Photosensitivity and Hydrophobic Surface of a Self-Assembled Monolayer (SAM). *Bull. Chem. Soc. Jpn.*, **2016**, *89*, 125–134.

75. Bardecker, J.A.; Afzali, A.; Tulevski, G.S.; Graham, T.; Hannon, J.B.; Jen, A.K.Y. UV-Sensitive Self-Assembled Monolayer Photoresist for the Selective Deposition of Carbon Nanotubes. *Chem. Mater.*, **2012**, *24*, 2017–2021.

76. Wei, P.; Li, B.; De Leon, A.; Pentzer, E. Beyond Binary: Optical Data Storage with 0, 1, 2, and 3 in Polymer Films. *J. Mater. Chem. C*, **2017**, *5*, 5780–5786.

77. Edler, M.; Mayrbrugger, S.; Fian, A.; Trimmel, G.; Radl, S.; Kern, W.; Griesser, T. Wavelength Selective Refractive Index Modulation in a ROMP Derived Polymer Bearing Phenyl- and Ortho-Nitrobenzyl Ester Groups. *J. Mater. Chem. C*, **2013**, *1*, 3931–3938.

78. Romano, A.; Roppolo, I.; Rossegger, E.; Schlögl, S.; Sangermano, M. Recent Trends in Applying Ortho-Nitrobenzyl Esters for the Design of Photo-Responsive Polymer Networks. *Materials (Basel).*, **2020**, *13*, 1–26.

79. Konuray, O.; Fernández-Francos, X.; Ramis, X.; Serra, À. State of the Art in Dual-Curing Acrylate Systems. *Polymers (Basel).*, **2018**, *10*, 178.

80. Bland, M.H.; Peppas, N.A. Photopolymerized Multifunctional (Meth)Acrylates as Model Polymers for Dental Applications. *Biomaterials*, **1996**, *17*, 1109–1114.

81. Fertier, L.; Koleilat, H.; Stemmelen, M.; Giani, O.; Joly-Duhamel, C.; Lapinte, V.; Robin, J.J. The Use of Renewable Feedstock in UV-Curable Materials-A New Age for Polymers and Green Chemistry. *Prog. Polym. Sci.*, **2013**, *38*, 932–962.

82. Ebe, K.; Seno, H.; Horigome, K. UV Curable Pressure-Sensitive Adhesives for Fabricating Semiconductors. I. Development of Easily Peelable Dicing Tapes. *J. Appl. Polym. Sci.*, **2003**, *90*, 436–441.

83. Nguyen, L.H.; Straub, M.; Gu, M. Acrylate-Based Photopolymer for Two-Photon Microfabrication and Photonic Applications. *Adv. Funct. Mater.*, **2005**, *15*, 209–216.

84. Gonzalez, G.; Chiappone, A.; Roppolo, I.; Fantino, E.; Bertana, V.; Perrucci, F.; Scaltrito, L.; Pirri, F.; Sangermano, M. Development of 3D Printable Formulations Containing CNT with Enhanced Electrical Properties. *Polymer (Guildf).*, **2017**, *109*, 246–253.

85. Ligon, S.C.; Liska, R.; Stampfl, J.; Gurr, M.; Mülhaupt, R. Polymers for 3D Printing and Customized Additive Manufacturing. *Chem. Rev.*, **2017**, *117*, 10212–10290.

86. del Barrio, J.; Sánchez-Somolinos, C. Light to Shape the Future: From Photolithography to 4D Printing. *Adv. Opt. Mater.*, **2019**, *7*, 1900598.

87. del Campo, A.; Arzt, E. Fabrication Approaches for Generating Complex Micro- and Nanopatterns on Polymeric Surfaces. *Chem. Rev.*, **2008**, *108*, 911–945.

88. Franssila, S. Introduction to Microfabrication. *Introd. to Microfabr.*, **2010**, *321*, 5–15.

89. Reichmanis, E.; Gooden, R.; Wilkins, C.W.; Schonhorn, H. STUDY OF THE PHOTOCHEMICAL RESPONSE OF O-NITROBENZYL CHOLATE DERIVATIVES IN P(MMA-MAA) MATRICES. *J. Polym. Sci. A1.*, **1983**, *21*, 1075–1083.

90. Schwalm, R. Lithographic Evaluation of One-Component Deep-UV Resists Containing o-Nitrobenzyl Ester Moieties. *J. Electrochem. Soc.*, **1989**, *136*, 3471.

91. J. E. Guillet, S.-K. L. Li, and H.C.N. Photochemistry of Ketone Polymers in the Solid Phase: A Review. *Mater. Microlithogr.*, **1985**, *6*, 165–177.

92. Willson, C.G. Approaches to the Design of Radiation-Sensitive Polymeric Imaging Systems with Improved Sensitivity and Resolution. *J. Electrochem. Soc.*, **1986**, *133*, 181.

93. Wilkins, C.W. Lithographic Evaluation of an O-Nitrobenzyl Ester Based Deep U.V. Resist System. *J. Electrochem. Soc.*, **1982**, *129*, 2552.

94. Bargon, J. Lithographic Materials BT - Methods and Materials in Microelectronic Technology. In; Bargon, J., Ed.; Springer US: Boston, MA,

1984; pp. 181–241.

95. Burn Jeng Lin. Deep Uv Lithography. *J Vac Sci Technol*, **1975**, *12*, 1317–1320.

96. Taylor, P.G.; Lee, J.K.; Zakhidov, A.A.; Chatzichristidi, M.; Fong, H.H.; DeFranco, J.A.; Malliaras, G.G.; Ober, C.K. Orthogonal Patterning of PEDOT:PSS for Organic Electronics Using Hydrofluoroether Solvents. *Adv. Mater.*, **2009**, *21*, 2314–2317.

97. Doh, J.; Irvine, D.J. Photogenerated Polyelectrolyte Bilayers from an Aqueous-Processible Photoresist for Multicomponent Protein Patterning. *J. Am. Chem. Soc.*, **2004**, *126*, 9170–9171.

98. Kim, M.; Choi, J.C.; Jung, H.R.; Katz, J.S.; Kim, M.G.; Doh, J. Addressable Micropatterning of Multiple Proteins and Cells by Microscope Projection Photolithography Based on a Protein Friendly Photoresist. *Langmuir*, **2010**, *26*, 12112–12118.

99. Kwon, K.W.; Choi, J.C.; Suh, K.Y.; Doh, J. Multiscale Fabrication of Multiple Proteins and Topographical Structures by Combining Capillary Force Lithography and Microscope Projection Photolithography. *Langmuir*, **2011**, *27*, 3238–3243.

100. Jiang, X.; Zheng, H.; Gourdin, S.; Hammond, P.T. Polymer-on-Polymer Stamping: Universal Approaches to Chemically Patterned Surfaces. *Langmuir*, **2002**, *18*, 2607–2615.

101. Ariga, K.; Hill, J.P.; Ji, Q. Layer-by-Layer Assembly as a Versatile Bottom-up Nanofabrication Technique for Exploratory Research and Realistic Application. *Phys. Chem. Chem. Phys.*, **2007**, *9*, 2319–2340.

102. Laugel, N.; Betscha, C.; Winterhalter, M.; Voegel, J.C.; Schaaf, P.; Ball, V. Relationship between the Growth Regime of Polyelectrolyte Multilayers and the Polyanion/Polycation Complexation Enthalpy. *J. Phys. Chem. B*, **2006**, *110*, 19443–19449.

103. Abu-Thabit, N.Y.; Hamdy, A.S. Stimuli-Responsive Polyelectrolyte Multilayers for Fabrication of Self-Healing Coatings – A Review. *Surf. Coatings Technol.*, **2016**, *303*, 406–424.

104. Harriott, L.R. Limits of Lithography. *Proc. IEEE*, **2001**, *89*, 366–374.

105. Batchelor, R.; Messer, T.; Hippler, M.; Wegener, M.; Barner-Kowollik, C.; Blasco, E. Two in One: Light as a Tool for 3D Printing and Erasing at the Microscale. *Adv. Mater.*, **2019**, *31*, 1904085.

106. Rossegger, E.; Hennen, D.; Griesser, T.; Roppolo, I.; Schlögl, S. Directed Motion of Water Droplets on Multi-Gradient Photopolymer Surfaces. *Polym. Chem.*, **2019**, *10*, 1882–1893.

107. Rossegger, E.; Nees, D.; Turisser, S.; Radl, S.; Griesser, T.; Schlögl, S. Photo-Switching of Surface Wettability on Micropatterned Photopolymers

for Fast Transport of Water Droplets over a Long-Distance. *Polym. Chem.*, **2020**, *11*, 3125–3135.

108. Kim, M.; Chung, H. Photo-Responsive Bio-Inspired Adhesives: Facile Control of Adhesion Strength: Via a Photocleavable Crosslinker. *Polym. Chem.*, **2017**, *8*, 6300–6308.

109. Xue, L.; Xiong, X.; Krishnan, B.P.; Puza, F.; Wang, S.; Zheng, Y.; Cui, J. Light-Regulated Growth from Dynamic Swollen Substrates for Making Rough Surfaces. *Nat. Commun.*, **2020**, *11*, 1–9.

110. Schumers, J.M.; Bertrand, O.; Fustin, C.A.; Gohy, J.F. Synthesis and Self-Assembly of Diblock Copolymers Bearing 2-Nitrobenzyl Photocleavable Side Groups. *J. Polym. Sci. Part A Polym. Chem.*, **2012**, *50*, 599–608.

111. Jiang, J.; Tong, X.; Morris, D.; Zhao, Y. Toward Photocontrolled Release Using Light-Dissociable Block Copolymer Micelles. *Macromolecules*, **2006**, *39*, 4633–4640.

112. Jean-Marc Schumers, Charles-Andrè Fustin, Aydin Can, Richard Hoogenboom, Ulrich S. Schubert, J.-F.G. Are O-Nitrobenzyl (Meth)Acrylate Monomers Polymerizable by Controlled-Radical Polymerization? *J. Polym. Sci. Part A Polym. Chem.*, **2009**, *47*, 6504–6513.

113. Soliman, S.M.A.; Nouvel, C.; Babin, J.; Six, J.L. O-Nitrobenzyl Acrylate Is Polymerizable by Single Electron Transfer-Living Radical Polymerization. *J. Polym. Sci. Part A Polym. Chem.*, **2014**, *52*, 2192–2201.

114. Liu, Y.; Wang, L.; Pan, C. Synthesis of Block Copoly(Styrene-o-p-Nitrophenyl Methacrylate) and Its Derivatives by Atom Transfer Radical Polymerization. *Macromolecules*, **1999**, *32*, 8301–8305.

115. Yang, F.; Cao, Z.; Wang, G. Micellar Assembly of a Photo- and Temperature-Responsive Amphiphilic Block Copolymer for Controlled Release. *Polym. Chem.*, **2015**, *6*, 7995–8002.

116. Bates, F.S.; Fredrickson, G.H. Block Copolymers-Designer Soft Materials. *Phys. Today*, **1999**, *52*, 32–38.

117. Klok, H.A.; Lecommandoux, S. Supramolecular Materials via Block Copolymer Self-Assembly. *Adv. Mater.*, **2001**, *13*, 1217–1229.

118. Letchford, K.; Burt, H. A Review of the Formation and Classification of Amphiphilic Block Copolymer Nanoparticulate Structures: Micelles, Nanospheres, Nanocapsules and Polymersomes. *Eur. J. Pharm. Biopharm.*, **2007**, *65*, 259–269.

119. Albert, J.N.L.; Epps, T.H. Self-Assembly of Block Copolymer Thin Films. *Mater. Today*, **2010**, *13*, 24–33.

120. Altinpinar, S.; Zhao, H.; Ali, W.; Kappes, R.S.; Schuchardt, P.; Salehi, S.; Santoro, G.; Theato, P.; Roth, S. V.; Gutmann, J.S. Distortion of Ultrathin Photocleavable Block Copolymer Films during Photocleavage and

Nanopore Formation. *Langmuir*, **2015**, *31*, 8947–8952.

121. Segalman, R.A. Patterning with Block Copolymer Thin Films. *Mater. Sci. Eng. R Reports*, **2005**, *48*, 191–226.

122. Cheng, J.Y.; Ross, C.A.; Thomas, E.L.; Smith, H.I.; Vancso, G.J. Templated Self-Assembly of Block Copolymers: Effect of Substrate Topography. *Adv. Mater.*, **2003**, *15*, 1599–1602.

123. An, S.; Kim, H.; Kim, M.; Kim, S. Photoinduced Modulation of Polymeric Interfacial Behavior Controlling Thin-Film Block Copolymer Wetting. *Langmuir*, **2020**, *36*, 3046–3056.

124. Klinger, D.; Landfester, K. Dual Stimuli-Responsive Poly(2-Hydroxyethyl Methacrylate-Co-Methacrylic Acid) Microgels Based on Photo-Cleavable Cross-Linkers: PH-Dependent Swelling and Light-Induced Degradation. *Macromolecules*, **2011**, *44*, 9758–9772.

125. Yin, J.; Hu, H.; Wu, Y.; Liu, S. Thermo- and Light-Regulated Fluorescence Resonance Energy Transfer Processes within Dually Responsive Microgels. *Polym. Chem.*, **2011**, *2*, 363–371.

126. Ionov, L.; Diez, S. Environment-Friendly Photolithography Using Poly(N-Isopropylacrylamide)- Based Thermoresponsive Photoresists. *J. Am. Chem. Soc.*, **2009**, *131*, 13315–13319.

127. Kolb, H.C.; Finn, M.G.; Sharpless, K.B. Click Chemistry: Diverse Chemical Function from a Few Good Reactions. *Angew. Chemie - Int. Ed.*, **2001**, *40*, 2004–2021.

128. Hoyle, C.E.; Lowe, A.B.; Bowman, C.N. Thiol-Click Chemistry: A Multifaceted Toolbox for Small Molecule and Polymer Synthesis. *Chem. Soc. Rev.*, **2010**, *39*, 1355–1387.

129. Pauloehrl, T.; Delaittre, G.; Bastmeyer, M.; Barner-Kowollik, C. Ambient Temperature Polymer Modification by in Situ Phototriggered Deprotection and Thiol-Ene Chemistry. *Polym. Chem.*, **2012**, *3*, 1740–1749.

130. Lowe, A.B. Thiol-Ene “Click” Reactions and Recent Applications in Polymer and Materials Synthesis. *Polym. Chem.*, **2010**, *1*, 17–36.

131. Hoyle, C.E.; Lee, T.Y.; Roper, T. Thiol-Enes: Chemistry of the Past with Promise for the Future. *J. Polym. Sci. Part A Polym. Chem.*, **2004**, *42*, 5301–5338.

132. Marx, P.; Romano, A.; Roppolo, I.; Chemelli, A.; Mühlbacher, I.; Kern, W.; Chaudhary, S.; Andritsch, T.; Sangermano, M.; Wiesbrock, F. 3D-Printing of High-κ Thiol-Ene Resins with Spiro-Orthoesters as Anti-Shrinkage Additive. *Macromol. Mater. Eng.*, **2019**, *304*, 1–10.

133. Marx, P.; Romano, A.; Fischer, R.; Roppolo, I.; Sangermano, M.; Wiesbrock, F. Dual-Cure Coatings: Spiroorthoesters as Volume-Controlling Additives in Thiol–Ene Reactions. *Macromol. Mater. Eng.*, **2019**, *304*, 1–5.

134. Radl, S. V.; Schipfer, C.; Kaiser, S.; Moser, A.; Kaynak, B.; Kern, W.; Schlögl, S. Photo-Responsive Thiol-Ene Networks for the Design of Switchable Polymer Patterns. *Polym. Chem.*, **2017**, *8*, 1562–1572.

135. Wenzel, R.N. Resistance of Solid Surfaces to Wetting by Water. *Ind. Eng. Chem.*, **1936**, *28*, 988–994.

136. Kim, D.; Pugno, N.M.; Ryu, S. Wetting Theory for Small Droplets on Textured Solid Surfaces. *Sci. Rep.*, **2016**, *6*, 1–8.

137. Rosario, R.; Gust, D.; Garcia, A.A.; Hayes, M.; Taraci, J.L.; Clement, T.; Dailey, J.W.; Picraux, S.T. Lotus Effect Amplifies Light-Induced Contact Angle Switching. *J. Phys. Chem. B*, **2004**, *108*, 12640–12642.

138. Razza, N.; Castellino, M.; Sangermano, M. Fabrication of Janus Particles via a "Photografting-from" Method and Gold Photoreduction. *J. Mater. Sci.*, **2017**, *52*, 13444–13454.

139. Li, L.; Deng, X.X.; Li, Z.L.; Du, F.S.; Li, Z.C. Multifunctional Photodegradable Polymers for Reactive Micropatterns. *Macromolecules*, **2014**, *47*, 4660–4667.

140. Giebler, M.; Radl, S.; Ules, T.; Griesser, T.; Schlögl, S. Photopatternable Epoxy-Based Thermosets. *Materials (Basel).*, **2019**, *12*, 2350.

141. Radl, S.; Kreimer, M.; Manhart, J.; Griesser, T.; Moser, A.; Pinter, G.; Kalinka, G.; Kern, W.; Schlögl, S. Photocleavable Epoxy Based Materials. *Polymer (Guildf).*, **2015**, *69*, 159–168.

142. Radl, S.; Roppolo, I.; Pölzl, K.; Ast, M.; Spreitz, J.; Griesser, T.; Kern, W.; Schlögl, S.; Sangermano, M. Light Triggered Formation of Photo-Responsive Epoxy Based Networks. *Polymer (Guildf).*, **2017**, *109*, 349–357.

143. Sangermano, M.; Razza, N.; Crivello, J.V. Cationic UV-Curing: Technology and Applications. *Macromol. Mater. Eng.*, **2014**, *299*, 775–793.

144. Vidil, T.; Tournilhac, F.; Musso, S.; Robisson, A.; Leibler, L. Control of Reactions and Network Structures of Epoxy Thermosets. *Prog. Polym. Sci.*, **2016**, *62*, 126–179.

145. Crivello, J.V.; Liu, S. Photoinitiated Cationic Polymerization of Epoxy Alcohol Monomers. *J. Polym. Sci. part a Polym. Chem.*, **2000**, *38*, 389–401.

146. Crivello, J. V.; Sangermano, M. Visible and Long-Wavelength Photoinitiated Cationic Polymerization. *J. Polym. Sci. Part A Polym. Chem.*, **2001**, *39*, 343–356.

147. Eduok, U.; Faye, O.; Szpunar, J. Recent Developments and Applications of Protective Silicone Coatings: A Review of PDMS Functional Materials. *Prog. Org. Coatings*, **2017**, *111*, 124–163.

148. Wolf, M.P.; Salieb-Beugelaar, G.B.; Hunziker, P. PDMS with Designer Functionalities—Properties, Modifications Strategies, and Applications.

Prog. Polym. Sci., **2018**, *83*, 97–134.

149. Chen, J.; Zheng, J.; Gao, Q.; Zhang, J.; Zhang, J.; Omisore, O.M.; Wang, L.; Li, H. Polydimethylsiloxane (PDMS)-Based Flexible Resistive Strain Sensors for Wearable Applications. *Appl. Sci.*, **2018**, *8*, 345.

150. Fujii, T. PDMS-Based Microfluidic Devices for Biomedical Applications. *Microelectron. Eng.*, **2002**, *61–62*, 907–914.

151. Giebler, M.; Radl, S.V.; Ast, M.; Kaiser, S.; Griesser, T.; Kern, W.; Schlögl, S. Dual-Responsive Polydimethylsiloxane Networks. *J. Polym. Sci. Part A Polym. Chem.*, **2018**, *56*, 2319–2329.

152. Shafranek, R.T.; Millik, S.C.; Smith, P.T.; Lee, C.; Boydston, A.J.; Nelson, A. Progress in Polymer Science Stimuli-Responsive Materials in Additive Manufacturing. *Prog. Polym. Sci.*, **2019**, *93*, 36–67.

153. Lin, B.; Zhou, S. Light-Responsive Nanoparticles with Wettability Changing from Hydrophobicity to Hydrophilicity and Their Application towards Highly Hydrophilic Fluorocarbon Coatings. *Appl. Surf. Sci.*, **2015**, *359*, 380–387.

154. Pham, S.H.; Choi, Y.; Choi, J. Stimuli-Responsive Nanomaterials for Application in Antitumor Therapy and Drug Delivery. *Pharmaceutics*, **2020**, *12*, 630.

155. Cheng, H.; Guan, Q.; Villalobos, L.F.; Peinemann, K.V.; Pain, A.; Hong, P.Y. Understanding the Antifouling Mechanisms Related to Copper Oxide and Zinc Oxide Nanoparticles in Anaerobic Membrane Bioreactors. *Environ. Sci. Nano*, **2019**, *6*, 3467–3479.

156. Zahid, M.; Rashid, A.; Akram, S.; Rehan, Z.A.; Razzaq, W. A Comprehensive Review on Polymeric Nano-Composite Membranes for Water Treatment. *J. Membr. Sci. Technol.*, **2018**, *08*, 1–20.

157. Lee, J.; Ku, K.H.; Kim, J.; Lee, Y.J.; Jang, S.G.; Kim, B.J. Light-Responsive, Shape-Switchable Block Copolymer Particles. *J. Am. Chem. Soc.*, **2019**, *141*, 15348–15355.

158. Picchetti, P.; Dimarco, B.N.; Travaglini, L.; Zhang, Y.; Ortega-Liebana, M.C.; De Cola, L. Breaking with Light: Stimuli-Responsive Mesoporous Organosilica Particles. *Chem. Mater.*, **2020**, *32*, 392–399.

159. Li, L.; Yang, W.W.; Xu, D.G. Stimuli-Responsive Nanoscale Drug Delivery Systems for Cancer Therapy. *Journal of Drug Targeting*, **2019**, *27*, 423–433.

160. Raza, A.; Rasheed, T.; Nabeel, F.; Hayat, U.; Bilal, M.; Iqbal, H.M.N. Endogenous and Exogenous Stimuli-Responsive Drug Delivery Systems for Programmed Site-Specific Release. *Molecules*, **2019**, *24*, 1117.

161. McMillan, J.; Batrakova, E.; Gendelman, H.E. Cell Delivery of Therapeutic Nanoparticles. In *Progress in Molecular Biology and Translational Science*; Elsevier Inc., **2011**; Vol. 104, pp. 563–601.

162. Serrano-Ruiz, D.; Laurenti, M.; Ruiz-Cabello, J.; Lopez-Cabarcos, E.; Rubio-Retama, J. Hybrid Microparticles for Drug Delivery and Magnetic Resonance Imaging. *J. Biomed. Mater. Res. - Part B Appl. Biomater.*, **2013**, *101*, 498–505.

163. Ruiz-Hernández, E.; Baeza, A.; Vallet-Regí, M. Smart Drug Delivery through DNA/Magnetic Nanoparticle Gates. *ACS Nano*, **2011**, *5*, 1259–1266.

164. Weaver, C.L.; Larosa, J.M.; Luo, X.; Cui, X.T. Electrically Controlled Drug Delivery from Graphene Oxide Nanocomposite Films. *ACS Nano*, **2014**, *8*, 1834–1843.

165. Patra, J.K.; Das, G.; Fraceto, L.F.; Campos, E.V.R.; Rodriguez-Torres, M.D.P.; Acosta-Torres, L.S.; Diaz-Torres, L.A.; Grillo, R.; Swamy, M.K.; Sharma, S.; Habtemariam, S.; Shin, H.S. Nano Based Drug Delivery Systems: Recent Developments and Future Prospects. *J. Nanobiotechnology*, **2018**, *16*.

166. Chen, G.; Cao, Y.; Tang, Y.; Yang, X.; Liu, Y.; Huang, D.; Zhang, Y.; Li, C.; Wang, Q. Advanced Near-Infrared Light for Monitoring and Modulating the Spatiotemporal Dynamics of Cell Functions in Living Systems. *Adv. Sci.*, **2020**, *7*, 1903783.

167. Luo, Y.L.; Shiao, Y.S.; Huang, Y.F. Release of Photoactivatable Drugs from Plasmonic Nanoparticles for Targeted Cancer Therapy. *ACS Nano*, **2011**, *5*, 7796–7804.

168. Alonso-Cristobal, P.; Oton-Fernandez, O.; Mendez-Gonzalez, D.; Díaz, J.F.; Lopez-Cabarcos, E.; Barasoain, I.; Rubio-Retama, J. Synthesis, Characterization, and Application in HeLa Cells of an NIR Light Responsive Doxorubicin Delivery System Based on NaYF4:Yb,Tm@SiO2-PEG Nanoparticles. *ACS Appl. Mater. Interfaces*, **2015**, *7*, 14992–14999.

169. Xin, F.; Wei, M.; Jiang, S.; Gao, Y.; Nie, J.; Wu, Y.; Sun, F. Design of Hydrophilic Photocleavage O-Nitrobenzyl Acrylate-Modified Nanogels with Outstanding Biocompatibility Prepared by RAFT Polymerization for Drug Carrier. *Eur. Polym. J.*, **2020**, *122*, 109364.

170. Pasparakis, G.; Vamvakaki, M. Multiresponsive Polymers: Nano-Sized Assemblies, Stimuli-Sensitive Gels and Smart Surfaces. *Polym. Chem.*, **2011**, *2*, 1234–1248.

171. Colson, Y.L.; Grinstaff, M.W. Biologically Responsive Polymeric Nanoparticles for Drug Delivery. *Adv. Mater.*, **2012**, *24*, 3878–3886.

172. Gao, W.; Chan, J.M.; Farokhzad, O.C. PH-Responsive Nanoparticles for Drug Delivery. *Mol. Pharm.*, **2010**, *7*, 1913–1920.

173. Uttara, B.; Singh, A. V.; Zamboni, P.; Mahajan, R.T. Oxidative Stress and Neurodegenerative Diseases: A Review of Upstream and Downstream Antioxidant Therapeutic Options. *Curr Neuropharmacol*, **2009**, *7*, 65–74.

174. Thanan, R.; Oikawa, S.; Hiraku, Y.; Ohnishi, S.; Ma, N.; Pinlaor, S.; Yongvanit, P.; Kawanishi, S.; Murata, M. Oxidative Stress and Its Significant Roles in Neurodegenerative Diseases and Cancer. *Int. J. Mol. Sci.*, **2015**, *16*, 193–217.

175. Barnham, K.J.; Masters, C.L.; Bush, A.I. Neurodegenerative Diseases and Oxidatives Stress. *Nat. Rev. Drug Discov.*, **2004**, *3*, 205–214.

176. Tsutsui, H.; Kinugawa, S.; Matsushima, S. Oxidative Stress and Heart Failure. *Am. J. Physiol. - Hear. Circ. Physiol.*, **2011**, *301*, 2181–2190.

177. Sokolovskaya, E.; Rahmani, S.; Misra, A.C.; Bräse, S.; Lahann, J. Dual-Stimuli-Responsive Microparticles. *ACS Appl. Mater. Interfaces*, **2015**, *7*, 9744–9751.

178. Li, H.; Zheng, H.; Zhang, Y.; Zhang, W.; Tong, W.; Gao, C. Preparation of Photo-Responsive Poly(Ethylene Glycol) Microparticles and Their Influence on Cell Viability. *J. Colloid Interface Sci.*, **2018**, *514*, 182–189.

179. Whitesides, G.M.; Mathias, J.P.; Seto, C.T. Molecular Self-Assembly and Nanochemistry: A Chemical Strategy for the Synthesis of Nanostructures. *Science (80-.).*, **1991**, *254*, 1312–1319.

180. Klajn, R.; Bishop, K.J.M.; Grzybowski, B.A. Light-Controlled Self-Assembly of Reversible and Irreversible Nanoparticle Suprastructures. *Proc. Natl. Acad. Sci. U. S. A.*, **2007**, *104*, 10305–10309.

181. Wang, Y.; Hollingsworth, A.D.; Yang, S.K.; Patel, S.; Pine, D.J.; Weck, M. Patchy Particle Self-Assembly via Metal Coordination. *J. Am. Chem. Soc.*, **2013**, *135*, 14064–14067.

182. Chen, Q.; Bae, S.C.; Granick, S. Directed Self-Assembly of a Colloidal Kagome Lattice. *Nature*, **2011**, *469*, 381–384.

183. De Feijter, I.; Albertazzi, L.; Palmans, A.R.A.; Voets, I.K. Stimuli-Responsive Colloidal Assembly Driven by Surface-Grafted Supramolecular Moieties. *Langmuir*, **2015**, *31*, 57–64.

184. Cantekin, S.; de Greef, T.F.A.; Palmans, A.R.A. Benzene-1,3,5-Tricarboxamide: A Versatile Ordering Moiety for Supramolecular Chemistry. *Chem. Soc. Rev.*, **2012**, *41*, 6125–6137.

185. Harada, A.; Kobayashi, R.; Takashima, Y.; Hashidzume, A.; Yamaguchi, H. Macroscopic Self-Assembly through Molecular Recognition. *Nat. Chem.*, **2011**, *3*, 34–37.

186. Hu, C.; West, K.R.; Scherman, O.A. Hollow Mesoporous Raspberry-like Colloids with Removable Caps as Photoresponsive Nanocontainers. *Nanoscale*, **2016**, *8*, 7840–7844.

187. Di Michele, L.; Fiocco, D.; Varrato, F.; Sastry, S.; Eiser, E.; Foffi, G. Aggregation Dynamics, Structure, and Mechanical Properties of Bigels. *Soft Matter*, **2014**, *10*, 3633–3648.

188. Chen, Z.; Zhou, L.; Bing, W.; Zhang, Z.; Li, Z.; Ren, J.; Qu, X. Light Controlled Reversible Inversion of Nanophosphor-Stabilized Pickering Emulsions for Biphasic Enantioselective Biocatalysis. *J. Am. Chem. Soc.*, **2014**, *136*, 7498–7504.

189. Vilanova, N.; De Feijter, I.; Teunissen, A.J.P.; Voets, I.K. Light Induced Assembly and Self-Sorting of Silica Microparticles. *Sci. Rep.*, **2018**, *8*, 1–9.

190. Sentürk, O.I.; Chervyachkova, E.; Ji, Y.; Wegner, S. V. Independent Blue and Red Light Triggered Narcissistic Self-Sorting Self-Assembly of Colloidal Particles. *Small*, **2019**, *15*, 1–6.

191. Dietliker, K.; Hüsler, R.; Birbaum, J.L.; Ilg, S.; Villeneuve, S.; Studer, K.; Jung, T.; Benkhoff, J.; Kura, H.; Matsumoto, A.; Oka, H. Advancements in Photoinitiators-Opening up New Applications for Radiation Curing. *Prog. Org. Coatings*, **2007**, *58*, 146–157.

192. Fringuelli, F.; Pizzo, F.; Tortoioli, S.; Vaccaro, L. Thiolysis of 1,2-Epoxides under Environmentally Friendly Conditions. In *TARGETS IN HETEROCYCLIC SYSTEMS Chemistry and Properties*; **2004**; Vol. 8, pp. 146–161.

193. Konuray, A.O.; Fernández-Francos, X.; Ramis, X. Analysis of the Reaction Mechanism of the Thiol-Epoxy Addition Initiated by Nucleophilic Tertiary Amines. *Polym. Chem.*, **2017**, *8*, 5934–5947.

194. Stuparu, M.C.; Khan, A. Thiol-Epoxy "Click" Chemistry: Application in Preparation and Postpolymerization Modification of Polymers. *J. Polym. Sci. Part A Polym. Chem.*, **2016**, *54*, 3057–3070.

195. Fernández-Francos, X.; Konuray, A.O.; Belmonte, A.; De La Flor, S.; Serra, À.; Ramis, X. Sequential Curing of Off-Stoichiometric Thiol-Epoxy Thermosets with a Custom-Tailored Structure. *Polym. Chem.*, **2016**, *7*, 2280–2290.

196. Sangermano, M.; Cerrone, M.; Colucci, G.; Roppolo, I.; Ortiz, R.A. Preparation and Fcharacterization of Hybrid Thiol-Ene/Epoxy UV-Thermal Dual-Cured Systems. *Polym. Int.*, **2010**, *59*, 1046–1051.

197. Isarn, I.; Ramis, X.; Ferrando, F.; Serra, A. Thermoconductive Thermosetting Composites Based on Boron Nitride Fillers and Thiol-Epoxy Matrices. *Polymers (Basel).*, **2018**, *10*, 277.

198. Binder, S.; Gadwal, I.; Bielmann, A.; Khan, A. Thiol-Epoxy Polymerization via an AB Monomer: Synthetic Access to High Molecular Weight Poly(β-Hydroxythio-Ether)S. *J. Polym. Sci. Part A Polym. Chem.*, **2014**, *52*, 2040–2046.

199. Gadwal, I.; Khan, A. Multiply Functionalized Dendrimers: Protective-Group-Free Synthesis through Sequential Thiol-Epoxy "click" Chemistry and Esterification Reaction. *RSC Adv.*, **2015**, *5*, 43961–43964.

200. Iwata, R.; Satoh, R.; Iwasaki, Y.; Akiyoshi, K. Covalent Immobilization of

Antibody Fragments on Well-Defined Polymer Brushes via Site-Directed Method. *Colloids Surfaces B Biointerfaces*, **2008**, *62*, 288–298.

201. Rahane, S.B.; Hensarling, R.M.; Sparks, B.J.; Stafford, C.M.; Patton, D.L. Synthesis of Multifunctional Polymer Brush Surfaces via Sequential and Orthogonal Thiol-Click Reactions. *J. Mater. Chem.*, **2012**, *22*, 932–943.

202. Yang, W.J.; Neoh, K.-G.; Kang, E.-T.; Teo, S.L.-M.; Rittschof, D. Stainless Steel Surfaces with Thiol-Terminated Hyperbranched Polymers for Functionalization via Thiol-Based Chemistry. *Polym. Chem.*, **2013**, *4*, 3105–3115.

203. Muzammil, E.M.; Khan, A.; Stuparu, M.C. Post-Polymerization Modification Reactions of Poly(Glycidyl Methacrylate)S. *RSC Adv.*, **2017**, *7*, 55874–55884.

204. Benaglia, M.; Alberti, A.; Giorgini, L.; Magnoni, F.; Tozzi, S. Poly(Glycidyl Methacrylate): A Highly Versatile Polymeric Building Block for Post-Polymerization Modifications. *Polym. Chem.*, **2013**, *4*, 124–132.

205. Günay, K.A.; Theato, P.; Klok, H.A. Standing on the Shoulders of Hermann Staudinger: Post-Polymerization Modification from Past to Present. *J. Polym. Sci. Part A Polym. Chem.*, **2013**, *51*, 1–28.

206. Cengiz, N.; Rao, J.; Sanyal, A.; Khan, A. Designing Functionalizable Hydrogels through Thiol-Epoxy Coupling Chemistry. *Chem. Commun.*, **2013**, *49*, 11191–11193.

207. Carioscia, J.A.; Stansbury, J.W.; Bowman, C.N. Evaluation and Control of Thiol-Ene/Thiol-Epoxy Hybrid Networks. *Polymer (Guildf).*, **2007**, *48*, 1526–1532.

208. Carlborg, C.F.; Vastesson, A.; Liu, Y.; Van Der Wijngaart, W.; Johansson, M.; Haraldsson, T. Functional Off-Stoichiometry Thiol-Ene-Epoxy Thermosets Featuring Temporally Controlled Curing Stages via an UV/UV Dual Cure Process. *J. Polym. Sci. Part A Polym. Chem.*, **2014**, *52*, 2604–2615.

209. Korychenska, O.; Acebo, C.; Bezuglyi, M.; Serra, A.; Grazulevicius, J. V. Epoxy-Thiol Thermosets Modified by Carbazole Decorated Hyperbranched Poly(Ethyleneimine) for Optical Applications. *React. Funct. Polym.*, **2016**, *106*, 86–92.

210. Guzmán, D.; Ramis, X.; Fernández-Francos, X.; Serra, A. Preparation of Click Thiol-Ene/Thiol-Epoxy Thermosets by Controlled Photo/Thermal Dual Curing Sequence. *RSC Adv.*, **2015**, *5*, 101623–101633.

211. Loureiro, R.M.; Amarelo, T.C.; Abuin, S.P.; Soulé, E.R.; Williams, R.J.J. Kinetics of the Epoxy-Thiol Click Reaction Initiated by a Tertiary Amine: Calorimetric Study Using Monofunctional Components. *Thermochim. Acta*, **2015**, *616*, 79–86.

212. Konuray, A.O.; Fernández-Francos, X.; Ramis, X. Curing Kinetics and

Characterization of Dual-Curable Thiol-Acrylate-Epoxy Thermosets with Latent Reactivity. *React. Funct. Polym.*, **2018**, *122*, 60–67.

213. Dietliker, K.; Jung, T.; Studer, K.; Benkhoff, J. Photolatent Tertiary Amines – A New Technology Platform for Radiation Curing. *Chimia (Aarau).*, **2007**, *61*, 655–660.

214. Arimitsu, K.; Endo, R. Application to Photoreactive Materials of Photochemical Generation of Superbases with High Efficiency Based on Photodecarboxylation Reactions. *Chem. Mater.*, **2013**, *25*, 4461–4463.

215. Sangermano, M.; Vitale, A.; Dietliker, K. Photolatent Amines Producing a Strong Base as Photocatalyst for the In-Situ Preparation of Organic-Inorganic Hybrid Coatings. *Polymer (Guildf).*, **2014**, *55*, 1628–1635.

216. Salmi, H.; Allonas, X.; Ley, C.; Defoin, A.; Ak, A. Quaternary Ammonium Salts of Phenylglyoxylic Acid as Photobase Generators for Thiol-Promoted Epoxide Photopolymerization. *Polym. Chem.*, **2014**, *5*, 6577–6583.

217. Griffin, D.R.; Kasko, A.M. Photoselective Delivery of Model Therapeutics from Hydrogels. *ACS Macro Lett.*, **2012**, *1*, 1330–1334.

218. Yesilyurt, V.; Ramireddy, R.; Thayumanavan, S. Photoregulated Release of Noncovalent Guests from Dendritic Amphiphilic Nanocontainers. *Angew. Chemie*, **2011**, *123*, 3094–3098.

219. Pasparakis, G.; Manouras, T.; Argitis, P.; Vamvakaki, M. Photodegradable Polymers for Biotechnological Applications. *Macromol. Rapid Commun.*, **2012**, *33*, 183–198.

220. Tibbitt, M.W.; Kloxin, A.M.; Sawicki, L.A.; Anseth, K.S. Mechanical Properties and Degradation of Chain and Step-Polymerized Photodegradable Hydrogels. *Macromolecules*, **2013**, *46*, 2785–2792.

221. Giebler, M.; Radl, S.; Ules, T.; Griesser, T.; Schlögl, S. Photopatternable Epoxy-Based Thermosets. *Materials (Basel).*, **2019**, *12(15)*, 2350.

222. Wagner, N.; Theato, P. Light-Induced Wettability Changes on Polymer Surfaces. *Polymer (Guildf).*, **2014**, *55*, 3436–3453.

223. Mann, A. Nanoindentation. In *Surfaces and Interfaces for Biomaterials*; **2005**; pp. 225–247.

224. Munoz-Paniagua, D.J.; McDermott, M.T.; Norton, P.R.; Tadayyon, S.M. Direct Tip Shape Determination of a Berkovich Indenter: Effect on Nanomechanical Property Measurement and Description of a Worn Indenter. *IEEE Trans. Nanotechnol.*, **2010**, *9*, 487–493.

225. Zhao, Y.H.; Vuluga, D.; Lecamp, L.; Burel, F. Photoinitiated Thiol-Epoxy Addition for the Preparation of Photoinduced Self-Healing Fatty Coatings. *RSC Adv.*, **2016**, *6*, 32098–32105.

226. Barzynski, H.; Sänger, D. Zur Photolyse von Makromolekularen O-

Nitrobenzylderivaten. *Die Angew. Makromol. Chemie*, **1981**, *93*, 131–141.

227. Oliver, W.C.; Pharr, G.M. An Improved Technique for Determining Hardness and Elastic Modulus Using Load and Displacement Sensing Indentation Experiments. *J. Mater. Res.*, **1992**, *7*, 1564–1583.

228. Park, S.J.; Jin, F.L.; Lee, C. Preparation and Physical Properties of Hollow Glass Microspheres-Reinforced Epoxy Matrix Resins. *Mater. Sci. Eng. A*, **2005**, *402*, 335–340.

229. Kuo, C.H.; Liu, C.P.; Lee, S.H.; Chang, H.Y.; Lin, W.C.; You, Y.W.; Liao, H.Y.; Shyue, J.J. Effect of Surface Chemical Composition on the Work Function of Silicon Substrates Modified by Binary Self-Assembled Monolayers. *Phys. Chem. Chem. Phys.*, **2011**, *13*, 15122–15126.

230. Manhart, J.; Hausberger, A.; Mühlbacher, I.; Schaller, R.; Holzner, A.; Kern, W.; Schlögl, S. UV-Induced Modulation of Tribological Characteristics: Elastomeric Materials Featuring Controlled Anisotropic Friction Properties. *AIP Conf. Proc.*, **2016**, *1779*.

231. Romano, A.; Angelini, A.; Rossegger, E.; Palmara, G.; Castellino, M.; Frascella, F.; Chiappone, A.; Chiadò, A.; Sangermano, M.; Schlögl, S.; Roppolo, I. Laser-Triggered Writing and Biofunctionalization of Thiol-Ene Networks. **2020**, *2000084*, 1–7.

232. Hermanson, G.T. *Bioconjugate Techniques*; **2013**.

233. Sheehan, J.; Cruickshank, P.; Boshart, G. Notes- A Convenient Synthesis of Water-Soluble Carbodiimides. *J. Org. Chem.*, **1961**, *26*, 2525–2528.

234. Wang, C.; Yan, Q.; Liu, H.B.; Zhou, X.H.; Xiao, S.J. Different EDC/NHS Activation Mechanisms between PAA and PMAA Brushes and the Following Amidation Reactions. *Langmuir*, **2011**, *27*, 12058–12068.

235. Nakajima, N.; Ikada, Y. Mechanism of Amide Formation by Carbodiimide for Bioconjugation in Aqueous Media. *Bioconjug. Chem.*, **1995**, *6*, 123–130.

236. James V. Staros. N-Hydroxysulfosuccinimide Active Esters : Bis (N-Hydroxysulfosuccinimide) Esters of Two Dicarboxylic Acids Are Hydrophilic, Membrane-Impermeant, Protein Cross-Linkers. *Biochemistry*, **1982**, *21*, 3950–3955.

237. Hoare, D.G.; Koshland, D.E. A Method for the Quantitative Modification and Estimation of Carboxylic Acid Groups in Proteins. *J. Biol. Chem.*, **1967**, *242*, 2447–2453.

238. Staros, J. V.; Wright, R.W.; Swingle, D.M. Enhancement by N-Hydroxysulfosuccinimide of Water-Soluble Carbodiimide-Mediated Coupling Reactions. *Anal. Biochem.*, **1986**, *156*, 220–222.

239. Chiadò, A.; Palmara, G.; Ricciardi, S.; Frascella, F.; Castellino, M.; Tortello, M.; Ricciardi, C.; Rivolo, P. Optimization and Characterization of a Homogeneous Carboxylic Surface Functionalization for Silicon-Based

Biosensing. *Colloids Surfaces B Biointerfaces*, **2016**, *143*, 252–259.

240. Cramer, N.B.; Couch, C.L.; Schreck, K.M.; Boulden, J.E.; Wydra, R.; Stansbury, J.W.; Bowman, C.N. Properties of Methacrylate-Thiol-Ene Formulations as Dental Restorative Materials. *Dent. Mater.*, **2010**, *26*, 799–806.

241. Kade, M.J.; Burke, D.J.; Hawker, C.J. The Power of Thiol-Ene Chemistry. *J. Polym. Sci. Part A Polym. Chem.*, **2010**, *48*, 743–750.

242. Beigi, S.; Yeganeh, H.; Atai, M. Evaluation of Fracture Toughness and Mechanical Properties of Ternary Thiol-Ene-Methacrylate Systems as Resin Matrix for Dental Restorative Composites. *Dent. Mater.*, **2013**, *29*, 777–787.

243. Garino, N.; Castellino, M.; Sacco, A.; Risplendi, F.; Munoz-Tabares, J.A.; Armandi, M.; Chiodoni, A.; Salomon, D.; Quaglio, M.; Pirri, C.F.; Cicero, G. Proving the Existence of Mn Porphyrin-like Complexes Hosted in Reduced Graphene Oxide with Outstanding Performance as Oxygen Reduction Reaction Catalysts. *2D Mater.*, **2019**, *6*, 045001.

244. Briggs, D.; Beamson, G. Primary and Secondary Oxygen-Induced C1s Binding Energy Shifts in X-Ray Photoelectron Spectroscopy of Polymers. *Anal. Chem.*, **1992**, *64*, 1729–1736.

245. Guimond, S.; Wertheimer, M.R. Surface Degradation and Hydrophobic Recovery of Polyolefins Treated by Air Corona and Nitrogen Atmospheric Pressure Glow Discharge. *J. Appl. Polym. Sci.*, **2004**, *94*, 1291–1303.

246. Wong, L.S.; Khan, F.; Micklefield, J. Selective Covalent Protein Immobilization: Strategies and Applications. *Chem Rev.*, **2009**, *109*, 4025–4053.

247. Chan, C.M.; Weng, L.T. Surface Characterization of Polymer Blends by XPS and ToF-SIMS. *Materials (Basel).*, **2016**, *9*, 655.

248. Zhou, J.; Ellis, A.V.; Voelcker, N.H. Recent Developments in PDMS Surface Modification for Microfluidic Devices. *Electrophoresis*, **2010**, *31*, 2–16.

249. Joye, I.J.; McClements, D.J. Biopolymer-Based Nanoparticles and Microparticles: Fabrication, Characterization, and Application. *Curr. Opin. Colloid Interface Sci.*, **2014**, *19*, 417–427.

250. Khan, I.; Saeed, K.; Khan, I. Nanoparticles: Properties, Applications and Toxicities. *Arab. J. Chem.*, **2019**, *12*, 908–931.

251. Dechézelles, J.F.; Ciotonea, C.; Catrinescu, C.; Ungureanu, A.; Royer, S.; Nardello-Rataj, V. Emulsions Stabilized with Alumina-Functionalized Mesoporous Silica Particles. *Langmuir*, **2020**, *36*, 3212–3220.

252. Kango, S.; Kalia, S.; Celli, A.; Njuguna, J.; Habibi, Y.; Kumar, R. Surface Modification of Inorganic Nanoparticles for Development of Organic-Inorganic Nanocomposites - A Review. *Prog. Polym. Sci.*, **2013**, *38*, 1232–

1261.

253. Sakazaki, Y.; Schmitt, V.; Olsson, U. Particles with Tunable Wettability for Solid-Stabilized Emulsions. *J. Dispers. Sci. Technol.*, **2019**, *40*, 219–230.

254. Puretskiy, N.; Ionov, L. Synthesis of Robust Raspberry-like Particles Using Polymer Brushes. *Langmuir*, **2011**, *27*, 3006–3011.

255. Kawaguchi, H. Functional Polymer Microspheres. *Prog. Polym. Sci.*, **2000**, *25*, 1171–1210.

256. Vlassopoulos, D.; Fytas, G. From Polymers to Colloids: Engineering the Dynamic Properties of Hairy Particles. In *High Solid Dispersions. Advances in Polymer Science*; **2009**; pp. 1–54.

257. Li, C.Y.; Zhao, B.; Zhu, L. Hairy Particles: Theory, Synthesis, Behavior, and Applications. *J. Polym. Sci. Part B Polym. Phys.*, **2014**, *52*, 1581–1582.

258. Levental, I.; Georges, P.C.; Janmey, P.A. Soft Biological Materials and Their Impact on Cell Function. *Soft Matter*, **2007**, *3*, 299–306.

259. Wang, X.; Foltz, V.J.; Rackaitis, M.; Bo, G.G.A. Dispersing Hairy Nanoparticles in Polymer Melts. *Polymer (Guildf).*, **2008**, *49*, 5683–5691.

260. Nakayama, S.; Yusa, S.; Nakamura, Y.; Fujii, S. Aqueous Foams Stabilized by Temperature-Sensitive Hairy Polymer Particles. *Soft Matter*, **2015**, *11*, 9099–9106.

261. Minko, S.; Department. Grafting on Solid Surfaces: "Grafting to" and "Grafting from" Methods. In *Polymer Surfaces and Interfaces*; **2008**; pp. 215–234.

262. Sangermano, M.; Razza, N. Light Induced Grafting-from Strategies as Powerful Tool for Surface Modification. *Express Polym. Lett.*, **2019**, *13*, 135–145.

263. Gonçalves, J.L.M.; Castanheira, E.J.; Alves, S.P.C.; Baleizão, C.; Farinha, J.P. Grafting with RAFT-GRAFT Strategies to Prepare Hybrid Nanocarriers with Core-Shell Architecture. *Polymers (Basel).*, **2020**, *12*, 2175.

264. Tsuji, S.; Kawaguchi, H. Temperature-Sensitive Hairy Particles Prepared by Living Radical Graft Polymerization. *Langmuir*, **2004**, *20*, 2449–2455.

265. Roy, D.; Guthrie, J.T.; Perrier, S. Graft Polymerization: Grafting Poly(Styrene) from Cellulose via Reversible Addition-Fragmentation Chain Transfer (RAFT) Polymerization. *Macromolecules*, **2005**, *38*, 10363–10372.

266. Le-Masurier, S.P.; Gody, G.; Perrier, S.; Granville, A.M. One-Pot Polymer Brush Synthesis via Simultaneous Isocyanate Coupling Chemistry and "Grafting from" RAFT Polymerization. *Polym. Chem.*, **2014**, *5*, 2816–2823.

267. Shu, T.; Shen, Q.; Zhang, X.; Serpe, M.J. Stimuli-Responsive Polymer/Nanomaterial Hybrids for Sensing Applications. *Analyst*, **2020**,

145, 5713–5724.

268. Motornov, M.; Roiter, Y.; Tokarev, I.; Minko, S. Stimuli-Responsive Nanoparticles, Nanogels and Capsules for Integrated Multifunctional Intelligent Systems. *Prog. Polym. Sci.*, **2010**, *35*, 174–211.

269. Razza, N.; Rizza, G.; Coulon, P.E.; Didier, L.; Fadda, G.C.; Voit, B.; Synytska, A.; Grützmacher, H.; Sangermano, M. Enabling the Synthesis of Homogeneous or Janus Hairy Nanoparticles through Surface Photoactivation. *Nanoscale*, **2018**, *10*, 14492–14498.

270. Sangermano, M.; Periolatto, M.; Castellino, M.; Wang, J.; Dietliker, K.; Grützmacher, J.L.; Grützmacher, H. A Simple Preparation of Photoactive Glass Surfaces Allowing Coatings via the "Grafting-from" Method. *ACS Appl. Mater. Interfaces*, **2016**, *8*, 19764–19771.

271. Huber, A.; Kuschel, A.; Ott, T.; Santiso-Quinones, G.; Stein, D.; Bräuer, J.; Kissner, R.; Krumeich, F.; Schönberg, H.; Levalois-Grützmacher, J.; Grützmacher, H. Phosphorous-Functionalized Bis(Acyl)Phosphane Oxides for Surface Modification. *Angew. Chemie - Int. Ed.*, **2012**, *51*, 4648–4652.

272. Gann, J.P.; Yan, M. A Versatile Method for Grafting Polymers on Nanoparticles. *Langmuir*, **2008**, *24*, 5319–5323.

273. HUNTER, R.J. *Zeta Potential in Colloid Science Principles and Applications*; **2013**.

274. Sahin, M.; Krawczyk, K.K.; Roszkowski, P.; Wang, J.; Kaynak, B.; Kern, W.; Schlögl, S.; Grützmacher, H. Photoactive Silica Nanoparticles: Influence of Surface Functionalization on Migration and Kinetics of Radical-Induced Photopolymerization Reactions. *Eur. Polym. J.*, **2018**, *98*, 430–438.

275. Sahin, M.; Schlögl, S.; Kaiser, S.; Kern, W.; Wang, J.; Grützmacher, H. Efficient Initiation of Radical-Mediated Thiol-Ene Chemistry with Photoactive Silica Particles. *J. Polym. Sci. Part A Polym. Chem.*, **2017**, *55*, 894–902.

276. Muzammil, E.M.; Khan, A.; Stuparu, M.C. Post-Polymerization Modification Reactions of Poly(Glycidyl Methacrylate)S. *RSC Adv.*, **2017**, *7*, 55874–55884.

277. Singh, A.K.; Panda, B.P.; Mohanty, S.; Nayak, S.K.; Gupta, M.K. Thermokinetics Behavior of Epoxy Adhesive Reinforced with Low Viscous Aliphatic Reactive Diluent and Nano-Fillers. *Korean J. Chem. Eng.*, **2017**, *34*, 3028–3040.

278. Wang, R.; Schuman, T. Towards Green: A Review of Recent Developments in Bio-Renewable Epoxy Resins from Vegetable Oils. In *Green Materials from Plant Oils*; **2015**; pp. 202–241.

279. Fernández-Francos, X.; Santiago, D.; Ferrando, F.; Ramis, X.; Salla, J.M.; Serra, À.; Sangermano, M. Network Structure and Thermomechanical Properties of Hybrid DGEBA Networks Cured with 1-Methylimidazole and

Hyperbranched Poly(Ethyleneimine)S. *J. Polym. Sci. Part B Polym. Phys.*, **2012**, *50*, 1489–1503.

280. Mateo, C.; Torres, R.; Fernández-Lorente, G.; Ortiz, C.; Fuentes, M.; Hidalgo, A.; López-Gallego, F.; Abian, O.; Palomo, J.M.; Betancor, L.; Pessela, B.C.C.; Guisan, J.M.; Fernández-Lafuente, R. Epoxy-Amino Groups: A New Tool for Improved Immobilization of Proteins by the Epoxy Method. *Biomacromolecules*, **2003**, *4*, 772–777.

281. Jacobasch, H.-J.; Schurz, J. Characterization of Polymer Surfaces by Means of Electrokinetic Measurements. *Dispersed Syst.*, **2007**, *48*, 40–48.

282. Xu, P.; Wang, H.; Tong, R.; Du, Q.; Zhong, W. Preparation and Morphology of SiO2/PMMA Nanohybrids by Microemulsion Polymerization. *Colloid Polym. Sci.*, **2006**, *284*, 755–762.

283. Luo, C.; Ji, X.; Hou, S.; Eidson, N.; Fan, X.; Liang, Y.; Deng, T.; Jiang, J.; Wang, C. Azo Compounds Derived from Electrochemical Reduction of Nitro Compounds for High Performance Li-Ion Batteries. *Adv. Mater.*, **2018**, *30*, 1–9.

284. Pirrung, M.C.; Lee, Y.R.; Park, K.; Springer, J.B. Pentadienylnitrobenzyl and Pentadienylnitropiperonyl Photochemically Removable Protecting Groups. *J. Org. Chem.*, **1999**, *64*, 5042–5047.

285. Schmitt, J.; Flemming, H. FTIR-Spectroscopy in Microbial and Material Analysis. *Microbially Influ. Corros. Mater.*, **1996**.

286. Parikh, S.J.; Lafferty, B.J.; Sparks, D.L. An ATR-FTIR Spectroscopic Approach for Measuring Rapid Kinetics at the Mineral/Water Interface. *J. Colloid Interface Sci.*, **2008**, *320*, 177–185.

287. Duer, M.J. *Solid State NMR Spectroscopy: Principles and Applications*; **2001**.

288. Diehl, B. *Principles in NMR Spectroscopy*; **2008**.

289. Hammerath, F. Magnetism and Superconductivity in Iron-Based Superconductors as Probed by Nuclear Magnetic Resonance. In *Magnetism and Superconductivity in Iron-Based Superconductors as Probed by Nuclear Magnetic Resonance*; **2012**; pp. 1–172.

290. Tavares, M.I.B. Solid State NMR. In *Spectroscopic Analyses - Developments and Applications*; IntechOpen: Rijeka, **2017**.

291. Merchant, F.A.; Bartels, K.A.; Bovik, A.C.; Diller, K.R. Confocal Microscopy. In *Handbook of Image and Video Processing*; Elsevier Inc., **2005**; pp. 1291–1309.

292. St. Croix, C.M.; Shand, S.H.; Watkins, S.C. Confocal Microscopy: Comparisons, Applications, and Problems. *Biotechniques*, **2005**, *39*, S2–S5.

293. Ebnesajjad, S. Surface and Material Characterization Techniques. In *Surface*

Treatment of Materials for Adhesive Bonding; **2014**; pp. 39–75.

294. Ferraris, S.; Cazzola, M.; Peretti, V.; Stella, B.; Spriano, S. Zeta Potential Measurements on Solid Surfaces for in Vitro Biomaterials Testing: Surface Charge, Reactivity upon Contact with Fluids and Protein Absorption. *Front. Bioeng. Biotechnol.*, **2018**, *6*, 1–7.

295. Jacobasch, H.J.; Grundke, K.; Schneider, S.; Simon, F. Surface Characterization of Polymers by Physico-Chemical Measurements. *J. Adhes.*, **1995**, *48*, 57–73.

296. Tandon, V.; Bhagavatula, S.K.; Nelson, W.C.; Kirby, B.J. Zeta Potential and Electroosmotic Mobility in Microfluidic Devices Fabricated from Hydrophobic Polymers: 1. The Origins of Charge. *Electrophoresis*, **2008**, *29*, 1092–1101.

297. Bagus, P.S.; Ilton, E.; Nelin, C.J. Extracting Chemical Information from XPS Spectra: A Perspective. *Catal. Letters*, **2018**, *148*, 1785–1802.

298. Aziz, M.; Ismail, A.F. *X-Ray Photoelectron Spectroscopy (XPS)*; Elsevier B.V., **2017**.

299. Andrade, J.D. X-Ray Photoelectron Spectroscopy (XPS). In *Surface and Interfacial Aspects of Biomedical Polymers*; **1985**; pp. 105–195.

300. Van Meerbeek, B.; Vargas, M.; Inoue, S.; Yoshida, Y.; Perdigão, J.; Lambrechts, P.; Vanherle, G. Microscopy Investigations. Techniques, Results, Limitations. *Am. J. Dent.*, **2000**, *13*.

301. Goldstein, J.I.; Newbury, D.E.; Michael, J.R.; Ritchie, N.W.M.; Scott, J.H.J.; Joy, D.C. *Scanning Electron Microscopy and X-Ray Microanalysis*; **2017**.

302. Suzuki, E. High-Resolution Scanning Electron Microscopy of Immunogold-Labelled Cells by the Use of Thin Plasma Coating of Osmium. *J. Microsc.*, **2002**, *208*, 153–157.

303. Khan, M.S.I.; Oh, S.W.; Kim, Y.J. Power of Scanning Electron Microscopy and Energy Dispersive X-Ray Analysis in Rapid Microbial Detection and Identification at the Single Cell Level. *Sci. Rep.*, **2020**, *10*, 1–10.

304. Van Meerbeek, B.; Vargas, M.; Inoue, S.; Yoshida, Y.; Perdigão, J.; Lambrechts, P.; Vanherle, G. Microscopy Investigations. Techniques, Results, Limitations. *Am. J. Dent.*, **2000**, *13*, 3D-18D.

305. Paddock, S.W. Principles and Practices of Laser Scanning Confocal Microscopy. *Appl. Biochem. Biotechnol. - Part B Mol. Biotechnol.*, **2000**, *16*, 127–149.

306. Ghosh, S.; Saha, S.; Goswami, D.; Bilgrami, S.; Mayor, S. Dynamic Imaging of Homo-FRET in Live Cells by Fluorescence Anisotropy Microscopy. *Methods Enzymol.*, **2012**, *505*, 291–327.